

Large-scale machine learning-based phenotyping significantly improves genomic discovery for optic nerve head morphology

Babak Alipanahi^{1,†,*}, Farhad Hormozdiari^{2,†}, Babak Behsaz^{2,†}, Justin Cosentino^{1,†}, Zachary R. McCaw^{1,†}, Emanuel Schorsch¹, D Sculley², Elizabeth H. Dorfman¹, Sonia Phene¹, Naama Hammel¹, Andrew Carroll¹, Anthony P. Khawaja^{3,4,‡}, Cory Y. McLean^{2,‡,*}

¹Google, Health, Palo Alto, CA

²Google, Health, Cambridge, MA

³NIHR Biomedical Research Centre at Moorfields Eye Hospital & UCL Institute of Ophthalmology, London, UK

⁴Department of Public Health & Primary Care, University of Cambridge, Cambridge, UK

[†]These authors contributed equally to this work.

[‡]These authors contributed equally to this work.

^{*}To whom correspondence should be addressed: cym@google.com or babaka@google.com.

Abstract

Genome-wide association studies (GWAS) require accurate cohort phenotyping, but expert labeling can be costly, time-intensive, and variable. Here we develop a machine learning (ML) model to predict glaucomatous optic nerve head features from color fundus photographs. We used the model to predict vertical cup-to-disc ratio (VCDR), a diagnostic parameter and cardinal endophenotype for glaucoma, in 65,680 Europeans in the UK Biobank (UKB). A GWAS of ML-based VCDR identified 299 independent genome-wide significant (GWS; $P \leq 5 \times 10^{-8}$) hits in 156 loci. The ML-based GWAS replicated 62 of 65 GWS loci from a recent VCDR GWAS in the UKB for which two ophthalmologists manually labeled images for 67,040 Europeans. The ML-based GWAS also identified 92 novel loci, significantly expanding our understanding of the genetic etiologies of glaucoma and VCDR. Pathway analyses support the biological significance of the novel hits to VCDR, with select loci near genes involved in neuronal and synaptic biology or known to cause severe Mendelian ophthalmic disease. Finally, the ML-based GWAS results significantly improve polygenic prediction of VCDR and primary open-angle glaucoma in the independent EPIC-Norfolk cohort.

Introduction

Genome-wide association studies (GWAS) require accurate phenotyping of large cohorts, but expert phenotyping can be costly and time-intensive. On the other hand, self-reported phenotyping, while cost-effective and often insightful (Tung et al. 2011), can be inaccurate for nuanced phenotypes such as osteoarthritis (Deveza et al. 2017) or infeasible to obtain for complex quantitative phenotypes. Population-scale biobanks, such as the UK Biobank (UKB) (Sudlow et al. 2015) and Biobank Japan (Nagai et al. 2017) that contain genomics, biomedical data, and health records for hundreds of thousands of individuals provide opportunities to study complex disorders and traits (DeBoever et al. 2020). GWAS of individual blood- and urine-based biomarkers, which can be assayed accurately with high throughput, have shed light on disease etiology (Wheeler et al. 2017; Sinnott-Armstrong et al. 2019).

Advances in deep learning have enabled the extraction of medically relevant features from high-dimensional data, such as using cardiac magnetic resonance imaging to infer cardiac and aortic dimensions (Bai et al. 2020), color fundus photographs to detect glaucoma risk (Phene et al. 2019), and optical coherence tomography images to predict age-related macular degeneration progression (Yim et al. 2020). Using medically relevant features extracted from biobank data by machine learning (ML) models as GWAS phenotypes provides an opportunity to identify genetic signals influencing these traits.

Here we propose training an ML model to automatically phenotype a large cohort for genomic discovery. The proposed paradigm has two phases: in the "model training" phase, a database of expert-labeled samples (for which genomics data are not required) is used to train and validate a phenotype prediction model (Fig. 1a). In the "model application" phase, the model is applied to biobank data to predict phenotypes of interest, which are then analyzed for genomic associations (Fig. 1b). This paradigm has several advantages: first, model application is scalable and efficient. Second, a single model can predict multiple phenotypes simultaneously. Third, the model can be applied retrospectively to existing data, resulting in new phenotypes or more accurate predictions for the existing phenotypes. Fourth, multiple lines of evidence can be integrated to predict a single phenotype, which would be prohibitively expensive if performed manually.

As a proof of concept, we investigate predicting glaucoma-related features from fundus images and performing genomic discovery on the predicted features. Glaucoma is an optic neuropathy that results from progressive retinal ganglion cell degeneration (Jonas et al. 2017) and is the leading cause of irreversible blindness globally (Pascolini and Mariotti 2012), affecting more than 80 million people worldwide (Tham et al. 2014). Moreover, glaucoma is one of the most heritable common human diseases, with heritability estimates of 70% (K. Wang et al. 2017), and there is evidence for effective genomic risk prediction (Khawaja et al. 2018; Craig et al. 2020).

The hallmark diagnostic feature of glaucoma is optic disc cupping (Jonas et al. 2017). The vertical cup-to-disc ratio (VCDR; Fig. 1c), a quantitative indicator for optic nerve head morphology and a frequently reported quantitative measure of cupping, is an important endophenotype of glaucoma (Foster et al. 2002; Gordon et al. 2002; Czudowska et al. 2010; Springelkamp et al. 2017). With the advent of very large biobank studies and routine retinal

imaging in community optometric practices, there is huge potential for furthering our understanding of glaucoma through population-level analysis of VCDR; however, human grading of optic disc images to ascertain VCDR is costly and infeasible at large scale.

Here we developed an ML model using 81,830 non-UKB, ophthalmologist-labeled fundus images to predict image gradability, VCDR, and referable glaucoma risk. We used the model to predict VCDR in 65,680 UKB participants of European ancestry from 175,337 fundus images. We then performed a GWAS on the ML-based VCDR phenotype (hereafter, “ML-based GWAS”) and compared the results to prior VCDR GWAS, including a recent VCDR GWAS using phenotypes derived from expert-labeled UKB fundus images (Craig et al. 2020). We show that ML-based phenotypes are accurate and substantially more efficient to obtain than expert-phenotyped VCDR measurements, identify novel genetic associations with plausible links to known VCDR biology, and produce more accurate polygenic risk scores for predicting VCDR in an independent population.

Results

Overview of the ML-based phenotyping method

We used 81,830 fundus images graded by a panel of experts that passed our labeling guideline assessment (Supplementary Note) to train a phenotype prediction model that jointly predicts image gradability, VCDR, and referable glaucoma risk (Fig. 1d). We split these images into *train*, *tune*, and *test* sets; training images were graded by 1–2 eye care providers with varied expertise, while images in the two latter sets were each graded by three glaucoma specialist experts. We benchmarked model performance on all data splits (Fig. 1e–g; Supplementary Table 1). On the test set of 1,076 test images, the model achieved a Pearson's correlation of $R=0.91$ between predicted and graded VCDR (95% confidence interval [CI]=0.90–0.92) and root mean square error (RMSE) of 0.079 (95% CI=0.074–0.085). Additionally, we validated model generalizability on 2,115 UKB fundus images each graded by 2–3 experts (hereafter, “UKB test set”), which achieved similar predictive performance to the test set (Fig. 1h; $R=0.89$, 95% CI=0.88–0.90; RMSE=0.092, 95% CI=0.088–0.096; Supplementary Table 1).

ML-based GWAS replicates a manual phenotyping VCDR GWAS and discovers 92 additional novel loci

We applied the VCDR prediction model to the entire set of 175,337 UKB fundus images. After removing 21,400 images predicted to be ungradable (e.g. under- or over-exposed, or out of focus), aggregating predicted VCDR values across left and right eyes and the first and second visits for each individual, subsetting the cohort to individuals of European ancestry, and performing cohort quality control, a cohort of 65,680 individuals with VCDR phenotype remained for further analysis (Supplementary Note and Supplementary Fig. 1). To control for confounding factors (e.g., population structure) and increase power, we added age at the time of visit, sex, average image gradability, number of fundus images used in VCDR calculation, normalized refractive error, genotyping array type, and the top 15 genetic principal components as covariates.

We performed the ML-based GWAS using BOLT-LMM (Supplementary Note). While genomic inflation λ_{GC} was 1.20 (Supplementary Fig. 2), the stratified linkage disequilibrium score regression-based (S-LDSC) intercept (Bulik-Sullivan et al. 2015) was 1.06 (s.e.m=0.02), indicating that most test statistic inflation can be attributed to polygenicity rather than population structure. The SNP-based heritability in the ML-based GWAS was 0.43 (s.e.m=0.03), a majority of the 56% heritability estimated for VCDR by twin and family-based studies (Asefa et al. 2019). The ML-based GWAS identified 299 independent genome-wide significant (GWS) hits ($R^2 \leq 0.1$, $P \leq 5 \times 10^{-8}$) at 156 independent GWS loci after merging hits within 250kb together (Fig. 2a, Supplementary Tables 2 and 3). Based on Sum of Single Effects Regression (G. Wang et al. 2020), the number of causal variants within the 156 independent GWS loci was conservatively estimated at 813 (Supplementary Note; Supplementary Tables 4 and 5).

To understand the influence of training dataset size on model performance and GWAS results, we retrained the ML model with as little as 10% of the full training set. Performance curves indicate that using fewer than 8,000 training images achieved a Pearson's correlation $R=0.83$ (95% CI=0.81–0.84) on the UKB test set, identified 131 GWS loci, and replicated 123 of the 156 loci identified in the full model (Supplementary Figs. 3 and 4). An analysis of the implications of phenotyping accuracy on genomic discovery suggested that the difference in power for the model trained with 10% of the training data and the model trained with all data would maximally reach 15% (Supplementary Fig. 5).

Next, we compared the ML-based GWAS results with those from the two largest existing VCDR GWAS. First, we compared with the VCDR meta-analysis from the International Glaucoma Genetics Consortium (IGGC) in 23,899 Europeans (Springelkamp et al. 2017), for which all summary statistics are publicly available (see URLs). The ML-based GWAS replicated all 22 GWS loci, exhibited strong genetic correlation (0.95, s.e.m=0.03, $P=2.1 \times 10^{-167}$) with the IGGC GWAS (Fig. 2b; Table 1), and effect size regression analysis showed a slope significantly different from zero (slope=0.983, s.e.m.=0.041, $P=1 \times 10^{-61}$) and indistinguishable from one ($P=0.67$; Supplementary Fig. S7; Supplementary Note). Second, we compared with a GWAS on 67,040 manually-phenotyped UKB fundus images (Craig et al. 2020), for which only the independent genome-wide significant SNPs are publicly available. The ML-based GWAS replicated 62 out of 65 GWS loci with very similar estimated effect sizes (Fig. 2b,c; Table 1) and more significant P -values (Supplementary Fig. 6). The three loci not replicated at the GWS level in the ML-based GWAS were all Bonferroni-replicated (adjusting for 65 tests), with P -values ranging from 5.5×10^{-8} to 6.6×10^{-5} . Third, we compared our results with a meta-analysis of the Craig *et al.* and IGGC VCDR GWAS (Craig et al. 2020). The ML-based GWAS replicated 82 of the 90 loci at GWS level, with the remaining eight loci Bonferroni-replicated with P -values ranging from 1.4×10^{-7} to 6.6×10^{-5} (Table 1).

Finally, we performed a meta-analysis of our ML-based GWAS with the IGGC VCDR GWAS, which resulted in 189 GWS loci (Supplementary Note; Table 1 and Supplementary Tables 6 and 7). This ML-based meta-analysis replicated 63 out of 65 of Craig *et al.*'s discovery GWAS and 85 out of 90 Craig *et al.*'s meta-analysis at GWS level (Table 1). Taken together, these comparisons demonstrate that the ML-based GWAS accurately identifies known VCDR associations and additionally identifies over 90 novel loci (Fig. 2b), substantially increasing our

understanding of the genetic underpinnings of this complex trait.

To assess the biological plausibility of the novel loci identified in the ML-based GWAS, we compared gene set enrichment analyses of the 156 ML-based loci to those of the 65 Craig *et al.* loci using FUMA (Watanabe *et al.* 2017). Nine eye-related gene sets were significantly enriched in both sets of loci. The enrichment odds ratios (ML-based enrichment over Craig *et al.* enrichment) of all nine gene sets were greater than one, suggesting improved identification of functionally relevant pathways in the ML-based loci (Supplementary Fig. 8). To assess effects of distal *cis*-regulatory interactions, we also performed enrichment analyses for the two sets of loci using GREAT (McLean *et al.* 2010). Consistent with the FUMA results, the ML-based loci were more significantly enriched than the Craig *et al.* loci across all tested ontologies (Supplementary Fig. 9). The ML-based loci were significantly enriched for 22 gene sets, the majority of which are developmental and seven of which are eye-related (Supplementary Table 8). In contrast, the Craig *et al.* loci were significantly enriched for only three gene sets; two of these are eye-related sets that were also enriched in the ML-based results (Supplementary Table 8).

Biological significance of select novel VCDR-associated loci

Several of the VCDR-associated loci discovered in this study are known to be associated with intraocular pressure (IOP), including rs1361108 near *CENPW* (Gao *et al.* 2018), rs2570981 in *SNCAIP* (Gao *et al.* 2018), rs6999835 near *PKIA* (Khawaja *et al.* 2018), and rs351364 in *WNT2B* (Khawaja *et al.* 2018). This suggests that a proportion of the genetic variation in VCDR is mediated via IOP and pathophysiological processes affecting the anterior segment of the eye, consistent with IOP being a strong risk factor for glaucoma (Chan *et al.* 2017). Indeed, we observed that 13% (14 of 107) of the GWS loci from the latest IOP meta-analysis (Khawaja *et al.* 2018) were GWS in the ML-based VCDR GWAS. In addition, the overall genetic correlation between our ML-based VCDR GWAS and the IOP GWAS meta-analysis is 0.19 (s.e.m.=0.02, $P=5.5 \times 10^{-15}$), indicating that VCDR is partially explained by IOP. Moreover, a Mendelian randomization (MR) analysis followed by Egger regression (Egger *et al.* 1997) suggests that IOP has a strong directional association with ML-based VCDR (Intercept=0.001, SE=0.002, $P=0.7$; Slope=0.072, SE=0.020, $P=4 \times 10^{-4}$), whereas the reverse analysis provided no evidence for a directional association between ML-based VCDR and IOP (Supplementary Note; Supplementary Fig. 10).

VCDR is an objective quantification of the proportion of neuronal tissue at the head of the optic nerve (Fig. 1c). Interestingly, several VCDR-associated loci discovered in this study encompass genes involved in neuronal and synaptic biology, and thus may influence VCDR via direct effects on the retina and optic nerve rather than via IOP. *NCKIPSD* (rs7633840) is involved in the formation and maintenance of dendritic spines, and modulates synaptic activity in neurons (Lee *et al.* 2006). *CPLX4* (rs77759734) is required for the maintenance of synaptic ultrastructure in the adult retina (Reim *et al.* 2009). *MARK2* (rs199826712) has roles in neuronal cell polarity and the regulation of neuronal migration (Sapir *et al.* 2008). These loci complement additional neuronal loci also discovered by Craig *et al.*; some notable examples include *MYO16* (rs10162202), *TRIM71* (rs56131903), and *FLRT2* (rs1289426). An increase in VCDR may be due not only to loss of retinal ganglion cell neurons, but also loss of neural supporting tissue,

such as glial cells. One of our novel VCDR-associated loci is an indel on chromosome 8 (8:131606303_CTGTT_C), near *ASAP1*; this locus has been associated with glioma (Melin et al. 2017), suggesting glial cells as potential mediators of the VCDR association.

Several genes at the novel VCDR-associated loci harbor mutations that cause severe Mendelian ophthalmic disease. Here, for the first time, we report common variants at these genes that are associated with VCDR variation at a population level. Three of our novel loci are at *ADAMTSL3* (rs59199978), *PITX2* (rs2661764) and *FOXC1* (rs2745572), all of which are associated with syndromic ocular anterior segment dysgenesis, which in turn causes raised IOP and secondary glaucoma. *ADAMTSL3* is an important paralog of *ADAMTSL1* — which itself is also associated with VCDR in our GWAS. A mutation in *ADAMTSL1* has been reported to cause inherited anterior segment dysgenesis and secondary congenital glaucoma (Hendee et al. 2017). Mutations in *PITX2* and *FOXC1* cause Axenfeld-Rieger syndrome (Seifi and Walter 2018). Common variants at these loci may mark more subtle effects on ocular anterior segment development, resulting in subclinical changes in IOP and VCDR that are apparent on a population level. While *FOXC1* variants have been previously associated with glaucoma (Bailey et al. 2016), this is the first time they have been associated with population-variation in VCDR. Mutations in *PRSS56*, a gene at one of our novel VCDR-associated loci, cause microphthalmia in humans (Gal et al. 2011). Another two of our VCDR-associated loci are at *EYA1* and *EYA2* (eyes absent homologs 1 and 2), genes that are important for eye development in *Drosophila*. *EYA1* has been implicated in ocular anterior segment anomalies and cataract (Azuma et al. 2000). We also replicate some of the loci identified by Craig *et al.* such as *ELP4*, which has been associated with aniridia (Wawrocka and Krawczynski 2018), a condition characterized by the absence of an iris and that can predispose patients to glaucoma (D’Elia et al. 2007; Wawrocka and Krawczynski 2018).

ML-based GWAS improves VCDR polygenic risk scores

We developed two polygenic risk scores (PRS) from the ML-based VCDR GWAS using pruning and thresholding (P+T) (Chatterjee, Shi, and García-Closas 2016) and Elastic Net (Zou and Hastie 2005) methods. These PRS were evaluated in two test sets: A holdout set of 2,076 subjects from UKB with VCDR measured by 2–3 experts, and a set of 5,868 subjects from the European Prospective Investigation into Cancer Norfolk (EPIC-Norfolk) cohort with VCDR measured by scanning laser ophthalmoscopy (HRT) (Hayat et al. 2014). Since the EPIC-Norfolk imputation was done using the HRC v1 (Haplotype Reference Consortium) panel, which excludes indels (McCarthy et al. 2016), we subset the ML-based GWAS summary statistics to HRC v1.

For the P+T model, subsetting to HRC v1 results in 282 hits, down from 299 original hits. Using the effect sizes from the ML-based GWAS, this model achieves a Pearson's correlation $R=0.37$ (95% CI=0.33–40) in the UKB adjudicated cohort. The P+T model from Craig *et al.* GWAS does not include 18 out of 76 SNPs (absent in HRC v1) and achieves a Pearson's correlation $R=0.29$ (95% CI=0.25–0.33). The performance metrics of the ML-based Craig *et al.* P+T models when not subset to HRC v1 are shown in Supplementary Fig. 11. Performance in the EPIC-Norfolk set was slightly lower but the P+T model still explained 9.6% of the total variance (Fig. 3a). In both

sets, the ML-based P+T model outperformed the Craig *et al.* P+T model (UKB: $\Delta R=0.079$, $P < 0.031$, $n=2,076$; EPIC: $\Delta R=0.082$, $P < 5.9 \times 10^{-4}$, $n=5,868$, permutation test).

We then used the ML-based VCDR values from UKB to train Elastic Net models; after removing all images used in building the adjudicated test set, the training set contained 62,969 samples. In contrast to the P+T model in which GWAS marginal effect sizes are used as PRS weights, Elastic Net jointly learns all weights in a supervised manner. To make up for the 18 missing Craig *et al.* SNPs, we identified linkage disequilibrium-based proxies for all of the missing hits in HRC v1 and included them in training the Elastic Net model. The ML-based Elastic Net model numerically improved upon the P+T model in both UKB ($R=0.38$, 95% CI=0.34–0.41) and EPIC ($R=0.33$, 95% CI=0.30–0.35) sets (Fig. 3b). The Elastic Net model explains 14.2% and 10.6% of total VCDR variation in the UKB and EPIC-Norfolk sets, respectively. The Craig *et al.* Elastic Net model has a more pronounced improvement — probably due to the addition of proxy SNPs — but the ML-based model still significantly outperforms it (UKB: $\Delta R=0.064$, $P < 9.6 \times 10^{-3}$, $n=2,076$; EPIC: $\Delta R=0.053$, $P < 6.8 \times 10^{-4}$, $n=5,868$, permutation test).

Relationship of primary open-angle glaucoma and VCDR

To study the relationship between primary open-angle glaucoma (POAG) and VCDR, we defined POAG status in UKB using a combination of self-report and hospital episode ICD 9/10 codes (Supplementary Note). ML-based VCDR has moderate predictive power for POAG, with an area under the ROC curve (AUC) of 0.76 ($n=65,193$, 95% CI=0.74–0.78, POAG prevalence=1.9%) and area under the precision-recall curve (AUPRC) of 0.14 (95% CI=0.12–0.16). After binning individuals by ML-based VCDR, we computed odds ratios (ORs) in each bin versus the bottom bin (Fig. 4a). The most extreme bin (VCDR>0.7, $n=385$), which corresponds to a diagnostic criterion for glaucoma (Foster *et al.* 2002), has an OR of 74.3 (95% CI=57.0–94.3) versus the bottom bin (VCDR<0.3, $n=30,752$).

We then performed mediation analysis (MA) to study the association of VCDR with glaucoma. Similar to MR, MA evaluates the association between an intermediary or mediating phenotype (here, VCDR) and an outcome phenotype (here, glaucoma). However, whereas in MR the SNP set is selected based on association with the mediator, due to the limited availability of glaucoma summary statistics from the study by (Gharahkhani *et al.* 2020), the SNP set for MA was selected based on association with the outcome. Since, contrary to MR's exclusion restriction, the included SNPs may have affected glaucoma through a pathway other than VCDR (e.g. IOP), the per-SNP estimates of association were meta-analyzed using Egger regression (Egger *et al.* 1997), which is robust to this assumption (Bowden *et al.* 2017). The Egger slope of 5.7 (SE=1.8, $P=3 \times 10^{-3}$) differs significantly from zero, providing evidence that VCDR, as ascertained by our ML-based models, is strongly associated with the odds of glaucoma (Supplementary Fig. 12). We note that the Egger intercept of 0.04 also differs significantly from zero ($P=7 \times 10^{-7}$), indicating the presence of directional pleiotropy; that is, variants included in the analysis, on average, were associated with an increase in the odds of POAG through a pathway other than VCDR.

As shown above, VCDR is an informative endophenotype for glaucoma and we hypothesize

that its PRS should also be predictive of POAG. Indeed, 32 out of 118 loci previously associated with POAG (Gharahkhani et al. 2020) were significantly associated with ML-based VCDR in this study. We applied the ML-based Elastic Net model to the UKB individuals of European ancestry that do not have fundus images ($n=98,151$) to estimate their genetic VCDR. As expected, this genetic model performs noticeably worse than the model using a direct measurement of the VCDR phenotype (AUC=0.56, 95% CI=0.55–0.57; AUPRC=0.07, 95% CI=0.066–0.073, $n=98,151$, POAG prevalence=5.5%). Nonetheless, when we binned samples by VCDR elastic net PRS, participants in the highest bin (PRS $Z>2.5$, $n=567$) had a considerably higher POAG prevalence (OR=3.4, 95% CI=2.6–4.3; Fig 4b) than those in the lowest bin (PRS $Z<-0.1$, $n=46,136$).

In addition to VCDR, the ML model was trained to predict referable glaucoma risk (Phene et al. 2019); this model output can be interpreted as the probability a specialist would refer an individual for detailed glaucoma evaluation. Because the model output is a continuous value, we can evaluate the contribution of features other than VCDR to referable glaucoma risk by regressing out the VCDR signal. We computed glaucoma risk liability as the logit transform of the ML-based glaucoma probability, which is highly correlated with ML-based VCDR (Fig. 4c, Pearson's $R=0.91$, $n=65,680$, $P<1\times 10^{-300}$). While a large VCDR is the cardinal feature of a glaucomatous optic nerve, there are other features which suggest glaucoma that are difficult to quantify (e.g. bayoneting or barring of blood vessels, and hemorrhages). To examine the genetic associations with glaucomatous optic disc features other than VCDR, we carried out a GWAS of ML-based glaucoma risk conditioned on ML-predicted VCDR, using BOLT-LMM. The observed SNP heritability was 0.062 (s.e.m=0.013) with genomic inflation of 1.04 and S-LDSC-based intercept of 1.01 (s.e.m= 9.8×10^{-3} ; Supplementary Fig. 13) and the GWAS identified eight GWS loci (Supplementary Tables 9 and 10). Interestingly, two of these loci, *OCA2-HERC2* (Fig. 4d; rs12913832, $P=2.2\times 10^{-66}$) and *TYR* (rs1126809, $P=5.8\times 10^{-13}$), have been previously associated with macular inner retinal thickness (retinal nerve fiber layer and ganglion cell inner plexiform layer) as derived from UKB optical coherence tomography images (Currant et al. 2020). These inner retinal parameters have diagnostic utility for glaucoma that is considered complementary to VCDR, and may be particularly efficacious at detecting early glaucoma (Khawaja et al. 2020). Moreover, it is not currently possible to ascertain the thickness of the inner retina from fundus images, which are two-dimensional. Together, this suggests that ML-based phenotyping has the potential to identify glaucoma-related features from fundus images that are complementary to VCDR and not typically gradable by humans.

Glaucoma prediction in the EPIC-Norfolk cohort

To further assess the utility of the ML-based elastic net VCDR PRS for prediction of glaucoma, we classified the status of EPIC-Norfolk participants ($n=5,868$) for POAG (175 cases and 5,693 controls) using previously described criteria (Methods). We additionally sub-categorized POAG cases into high-tension glaucoma (HTG; 98 cases) and normal-tension glaucoma (NTG; 77 cases; see Methods). Given the enrichment of the VCDR PRS for variants associated with neuronal development and function, we hypothesized that the PRS would be particularly associated with NTG. We fit a logistic regression model to predict POAG status using age, sex,

and ML-based elastic net VCDR PRS as its three predictors.

The ML-based elastic net VCDR PRS was strikingly associated with POAG, and particularly NTG, in EPIC-Norfolk (Fig. 5). The ORs (95% CI) comparing the top risk decile with the bottom decile were 9.7 (3.4–27.6) for POAG, 7.4 (2.2–25.2) for HTG, and 16.5 (2.2–125.9) for NTG (Fig. 5). The overall prediction metrics were (AUC=0.74, 95% CI=0.70–0.77; AUPRC=0.08, 95% CI=0.06–0.11; prevalence=3.0%) for POAG, (AUC=0.73, 95% CI=0.68–0.78; AUPRC=0.05, 95% CI=0.03–0.08; prevalence=1.7%) for HTG, and (AUC=0.76, 95% CI=0.71–0.80; AUPRC=0.04, 95% CI=0.03–0.06; prevalence=1.3%) for NTG. The AUC and AUPRC show nominally significant improvements over those from an analogous model using the Craig *et al.* elastic net VCDR PRS for POAG (Δ AUC=0.014, 95% CI=0.0–0.03, $P=0.03$; Δ AUPRC=0.008, 95% CI=0.0–0.02, $P=0.03$, paired bootstrap test) and HTG (Δ AUC=0.014, 95% CI=0.0–0.03, $P=0.04$; Δ AUPRC=0.006, 95% CI=0.0–0.02, $P=0.04$, paired bootstrap test).

Discussion

Large cohorts of genotyped and phenotyped individuals have enabled researchers to identify genetic influences of many traits. As methods to ascertain genetic variants in large cohorts continue to improve, we anticipate the major challenge for cohort generation to be accurate and deep phenotyping (Delude 2015) at scale. Here we demonstrated that ML-based phenotyping shows promise for improving both scalability to biobank-sized datasets and phenotyping accuracy. We predicted VCDR from all 175,337 UKB fundus images in less than one hour on a distributed computing system. Multiple lines of evidence indicate that the model-based VCDR predictions improve accuracy over manual labeling, including the reproduction of known VCDR-related biology, identification of plausible novel genetic associations, and generation of polygenic risk scores that better predict VCDR in multiple held-out datasets. Additional advantages of ML-based phenotyping over manual labeling are improved joint prediction accuracy for multiple correlated phenotypes and predicting liabilities instead of binary labels for binary phenotypes. By regressing out predicted VCDR from the predicted referable glaucoma risk (i.e., whether the individual should seek further ophthalmologist care), we identified residual referable risk not attributable to variation in VCDR.

The improvement of our model-based VCDR GWAS over the recent expert-labeled VCDR GWAS by Craig *et al.* is consistent with improved phenotyping accuracy by our model. The expert labels may include more noise or measurement error than the ML-based labels, as suggested by the inter-grader variability; the inter-grader Pearson's correlation between the two ophthalmologists as reported by Craig *et al.* for images graded multiple times was 0.75 (95% CI=0.72–0.77), whereas the ML model achieves a Pearson's correlation of 0.89 between the model predictions and adjudicated expert labels (95% CI=0.88–0.90). Noise or variability in human grading of VCDR can arise from difficulty in defining the cup-rim border of the optic disc. If the cup-rim border is sloping, rather than having vertical edges, defining it is challenging using two-dimensional images. In this situation, the average VCDR of multiple graders may be considered more accurate than a single grader's score. Our ML-based model was trained and tuned on images that were assessed by multiple graders, and may therefore be expected to

outperform a single human grader, on average.

The 92 novel VCDR-associated loci discovered by ML-based phenotyping substantially expand our knowledge of the biological processes underlying optic nerve head morphology. While elevated IOP is an established cause of glaucoma (Chan et al. 2017), characterized by a pathologically enlarged VCDR, our results support the role of IOP contributing to variation in VCDR within the healthy range as well. Of particular note were common VCDR-associated variants in genes harboring mutations which cause inherited anterior segment dysgenesis that is well-characterized phenotypically. Our findings suggest these dysgenesis processes may also occur at subclinical levels and contribute to variation in the complex VCDR phenotype. Understanding the genotype-phenotype link in rare single-gene disorders can therefore improve our knowledge of some of the many contributory causes to complex traits. Our results also support an important role of neuronal development processes for VCDR. It remains uncertain whether these processes primarily influence VCDR during optic nerve development in early life, thereby reflecting population variation in baseline optic nerve head anatomy, or act later in life and reflect a pathological, glaucomatous change in VCDR over time. Interestingly, genes involved in developmental processes more broadly, including development of the cardiovascular and urogenital systems, were significantly enriched in our results (Supplementary Table 8). This may suggest early life processes are a major determinant of VCDR variation in adult populations.

This study also showed that a substantial proportion of VCDR variation can be predicted using a polygenic risk score. Improving VCDR prediction produces a concomitant improvement in glaucoma prediction, as we demonstrated by stratifying glaucoma prevalence using the VCDR PRS. While the UK National Screening Committee does not currently recommend population screening for glaucoma due to tests lacking sufficient positive predictive value (UK National Screening Committee 2019), using polygenic prediction to identify subsets of the general population that are at risk for glaucoma may enable effective screening. Notably, we identified a substantially higher POAG prevalence in the top decile of VCDR PRS and it may be that current screening tests would have sufficient positive predictive value if applied to this enriched population subset. Earlier detection and treatment of glaucoma, a disease that causes progressive and irreversible vision loss, is a key strategy outlined by the World Health Organization for the prevention of blindness worldwide (World Health Organization 2019).

While this study demonstrates the potential for ML-based phenotyping to expand our understanding of the genetic variation underlying complex traits, the method has important limitations that must be taken into account. Application of this technique relies on the trained model producing accurate predictions in the genomic discovery set. Here we showed strong generalizability of the model trained on non-UKB fundus images to the UKB fundus images used for genomic discovery by manually labeling a small subset of UKB fundus images and validating model predictions against these ground truth labels. Application to other phenotypes derived from fundus images, or other data modalities such as optical coherence tomography or magnetic resonance imaging, would require similar demonstrations of model generalizability. Additionally, the initial model training can be costly and time-intensive, as it requires manual labeling to be performed. While our ablation analysis showed that training on only 10% of the

data still identified the majority of VCDR-associated loci, model performance did not appear to saturate even at the full training set size. Ongoing improvements to transfer learning may reduce future labeled data requirements (Kolesnikov et al. 2019), though the ability to extrapolate consumer imaging improvements to biomedical imaging is unclear (Raghu et al. 2019).

In summary, we have proposed a method for performing genomic discovery on biobank-scale datasets using machine learning algorithms for accurate phenotyping. A key benefit of the method is its ability to use a modest-sized biomedical dataset annotated with reasonable accuracy to train a model that identifies the underlying patterns and yields usable predictions. Extending the method to additional phenotypes and data modalities in large-scale biobanks could further expand our understanding of disease etiology and improve genetic risk modeling.

URLs

1000 Genomes Project Phase 3:

<ftp://ftp.1000genomes.ebi.ac.uk/vol1/ftp/release/20130502>

AREDS dataset:

https://www.ncbi.nlm.nih.gov/projects/gap/cgi-bin/study.cgi?study_id=phs000001.v3.p1

BOLT-LMM software:

<https://data.broadinstitute.org/alkesgroup/bolt-lmm>

BaselineLD annotations:

<https://data.broadinstitute.org/alkesgroup/ldscore>

EPIC-Norfolk Study:

<https://www.epic-norfolk.org.uk>

EyePACS dataset:

<http://www.eyepacs.com/research>

FUMA:

<https://fuma.ctglab.nl>

GenomicRanges:

<https://bioconductor.org/packages/release/bioc/html/genomicranges.html>

GREAT:

<http://great.stanford.edu>

ImageNet dataset:

<http://www.image-net.org>

Inoveon:

<http://www.inoveon.com>

LocusZoom:

<http://locuszoom.org>

Meta-Soft:

http://genetics.cs.ucla.edu/meta_jemdoc

PLINK software:

<https://www.cog-genomics.org/plink1.9>

QCtools:

https://www.well.ox.ac.uk/~gav/qctool_v1

Scikit-learn:

<https://scikit-learn.org/stable>

Springelkamp *et al.* summary statistics:

<https://academic.oup.com/hmg/article/26/2/438/2970289>

TensorFlow:

<https://www.tensorflow.org>

TwoSampleMR:

<https://github.com/mrcieu/twosamplemr>

The UK Biobank Study:

<https://www.ukbiobank.ac.uk>

Methods

Model training and validation

We followed the procedure described previously by (Phene et al. 2019), modifying only to remove all UKB images. Briefly, we used 81,830 color fundus images from AREDS (Age-Related Eye Disease Study Research Group 1999), EyePACS (see URLs), Inoveon (see URLs) from United States, and two eye hospitals in India (Narayana Nethralaya and Sankara Nethralaya). We trained 10 independent multi-task Inception V3 (Szegedy et al. 2016) deep convolutional neural networks on the fundus images, using weights learned from the Image Net dataset (Deng et al. 2009) as pre-trained weights for the convolutional layers. Furthermore, we performed image augmentation (Shorten and Khoshgoftaar 2019) and early stopping (Prechelt 1998) based on mean squared error (MSE) for predicting VCDR on the tune dataset for picking the best model. The final prediction model is the average prediction of the 10 models in the ensemble.

Phenotype calling in UK Biobank cohort

We included UK Biobank participants with color fundus images. After making predictions for 175,337 images, 21,400 were predicted to be ungradable and were removed. Individual-level VCDR values were computed as the average per-eye VCDR within a single visit, with preference for the initial visit (Supplementary Note).

Genome-wide association study

We used BOLT-LMM v3.2 (Loh et al. 2018, 2015) to examine associations between genotype and ML-based VCDR in European individuals in UK Biobank, using the `--lmm` parameter to compute the Bayesian mixed model statistics. We used all genotyped variants with minor allele frequency > 0.001 to perform model-fitting and heritability estimation. ML-based VCDR was rank-based inverse normal (INT) transformed to increase the power for association discovery (McCaw et al. 2019). Finally, in our association study, we used sex, age at visit, visit number (i.e., 1 or 2 to indicate visit 1 or visit 2), number of eyes used to compute VCDR, genotyping array indicator, refractive error, average gradability scores of all fundus images included for each participant, and the top 15 genetic principal components as covariates.

Detecting independent genome-wide significant loci

Genome-wide significant (GWS; $P \leq 5 \times 10^{-8}$) lead SNPs, independent at $R^2=0.1$, were identified using PLINK's `--clump` command (see URLs). The reference panel for LD calculation contained 10,000 unrelated subjects of European ancestry from the UK Biobank. Loci were formed around lead SNPs based on the span of reference panel SNPs in LD with the lead SNPs at $R^2 \geq 0.1$. Loci separated by fewer than 250 kb were subsequently merged.

SNP-heritability estimates for ML-based VCDR

We computed the SNP heritability for ML-based VCDR by applying stratified LD score regression (Bulik-Sullivan et al. 2015) on the VCDR GWAS summary statistics while using the 75 baseline LD annotations provided by S-LDSC authors (see URLs).

Replication of existing loci

Loci for ML-based VCDR and comparator studies were formed as described above, and the common reference panel of 10k randomly selected unrelated subjects from the UK Biobank. Replication was assessed via the proportion of ML-based VCDR loci that overlapped with comparators, and the proportion of comparator loci that overlapped with the ML-based VCDR loci. Thus, replication required that both studies had a GWS variant within a common genomic region, although not necessarily the same variant.

Mendelian randomization and mediation analyses

We performed two sample Mendelian randomization analysis, implemented via TwoSampleMR (see URLs), to examine the causal association between IOP, as assessed by Khawaja *et al* (Khawaja et al. 2018), and ML-based VCDR. Per-SNP associations were meta-analyzed using Egger regression (Egger et al. 1997).

We performed mediation analysis to estimate the association between ML-based VCDR and glaucoma, as assessed by Gharakhani *et al.* (Gharakhani et al. 2020). Mendelian randomization is in fact a special case of mediation analysis in which the instrumental variables (here, SNPs) have no effect on the outcome (here, glaucoma) other than through the mediator (here, ML-based VCDR). Our mediation analysis differs from Mendelian randomization in that, due to limited availability of summary statistics from Gharakhani *et al*, the SNP set was defined based on association with the mediator (ML-based VCDR) rather than the outcome (glaucoma). Among the 118 independent, significant glaucoma SNPs identified by Gharakhani *et al*, 116 remained after harmonizing with VCDR. To account for probable direct effects of the candidate SNPs on glaucoma odds, for example via IOP, the per-SNP associations were again meta-analyzed via Egger regression.

VCDR polygenic risk score

We developed two PRS using the pruning and thresholding (P+T) (Chatterjee, Shi, and García-Closas 2016) and Elastic Net (Zou and Hastie 2005) methods. The UKB test cohort was graded using the same guidelines used in grading other datasets used in this study. The HRT-derived VCDR was examined and, for participants with good quality scans in both eyes, the mean value of right and left eyes was considered, as previously described (Khawaja et al. 2013). Genotyping was carried out on the Affymetrix UK Biobank Axiom array, as previously described (Khawaja et al. 2019).

In the P+T model, we used a set of variants common to the UKB and EPIC Norfolk cohorts. EPIC-Norfolk's imputation was performed using the HRC v1 panel and excludes indels (McCarthy et al. 2016); thus, to harmonize the variants we filtered out variants from Craig *et al.* and our ML-based GWAS not present in EPIC-Norfolk. This resulted in 58 variants from the 76 reported variants from Craig *et al.* GWAS (i.e., 18 variants were dropped) and 282 of the 299 variants from our ML-based GWAS (i.e., 17 fewer variants).

In the Elastic model, we used the ML-predicted VCDR as the target label from the 62,969 UKB training samples to train the elastic model. For Craig *et al*, we used 76 variants that included the

58 variants from the P+T model and 18 additional proxy variants that are in high LD ($R^2 \geq 0.6$) with the 18 variants dropped from Craig *et al.* P+T model. The same set of 282 variants as used in P+T were used for the ML-based model. We performed 5-fold cross validation and used the L1-penalty ratios of [0.1, 0.5, 0.7, 0.9, 0.95, 0.99, 1.0].

Glaucoma liability conditional analysis

We defined glaucoma risk liability as the logit transform of the highest-level of ML-based glaucoma probability ("likely glaucoma"; Supplementary Note) as:

$$g = \log\left(\frac{p}{1-p}\right)$$

where p and g denote ML-based glaucoma risk probability and liability, respectively. We performed conditional analysis on ML-based glaucoma risk liabilities using BOLT-LMM conditional on ML-based VCDR. In this conditional analysis, we additionally adjusted for the same covariates used in the primary ML-based VCDR GWAS.

Glaucoma subtypes prediction in the EPIC-Norfolk cohort

We analyzed 5,868 participants from the EPIC-Norfolk Eye Study cohort who were genotyped using the Affymetrix UK Biobank Axiom Array, met inclusion criteria and quality control, and had scanning laser ophthalmoscopy VCDR measurements (Supplementary Note). Included participants had a mean age of 68 years (SD 7.7, range 48-90), 55% were women, and the mean VCDR was 0.34 (SD 0.23). Of the 5,868 samples, 175 were classified as POAG cases (see Supplementary Note for detailed POAG criteria), of which 98 were classified as high tension glaucoma (HTG; IOP > 21 mmHg) and 77 as normal tension glaucoma (NTG; IOP \leq 21 mmHg) on the basis of the corneal-compensated IOP at the Eye Study assessment. Pre-treatment IOP was imputed by dividing by 0.7 for participants using glaucoma medication at the time of assessment, as previously described (Khawaja *et al.* 2018).

We extracted age, sex, POAG status, NTG status, and HTG status from all 5,868 samples. We fitted independent logistic regression models to predict POAG, HTG, and NTG statuses using VCDR PRS, age, and sex as predictors. We considered both the ML-based elastic net VCDR PRS and the Craig *et al.* elastic net PRS described above.

Acknowledgements

We acknowledge and appreciate research participants in all datasets used for their dedication and contributions. We highly appreciate the contributions of members of both the Genomics and Ophthalmology teams in Google Health, and thank the labeling software team in Google Health for their assistance in data labeling. This research has been conducted using the UK Biobank Resource application 17643. We thank Inoveon, Aravind Eye Hospital, Sankara Nethralaya, and Narayana Nethralaya for providing de-identified data; Jorge Cuadros, OD, PhD, from EyePACS, for data access and helpful conversations; and the National Eye Institute Study of Age-Related Macular Degeneration Research Group and study participants for their valuable contribution to this research. The EPIC-Norfolk study (DOI 10.22025/2019.10.105.00004) has received funding from the Medical Research Council (MR/N003284/1 and MC-UU_12015/1) and Cancer Research UK (C864/A14136). The genetics work in the EPIC-Norfolk study was funded by the Medical Research Council (MC_PC_13048). We are grateful to all the participants who have been part of the project and to the many members of the study teams at the University of Cambridge who have enabled this research. Anthony Khawaja, MD, PhD was supported by a Moorfields Eye Charity Career Development Fellowship and a UK Research and Innovation Future Leaders Fellowship. Lastly, we highly appreciate all glaucoma specialists, ophthalmologists and optometrists who helped in labeling fundus images.

Author contributions

BA, AWC, and CYM conceived the study. BA, FH, APK and CYM designed the study. BA, FH, BB, JC, ZRM, ES, APK and CYM performed experiments and analyzed results. LD, DS, SP, NH contributed to methodology and data collection. BA, FH, BB, ZRM, APK and CYM wrote the manuscript. All authors contributed to the final version of the manuscript.

Competing interests

A.P.K. is an employee of the UCL Institute of Ophthalmology, London, UK. The remaining authors are employees of Google LLC and own Alphabet stock as part of the standard compensation package. This study was funded by Google LLC.

Data availability

The UKB data are available through the UK Biobank Access Management System <https://www.ukbiobank.ac.uk/>. We will deposit the derived data fields and model predictions following UKB policy, which will be available through the UK Biobank Access Management System. The summary statistics, associated loci, and polygenic risk score coefficients will be made publicly available.

Tables

Table 1. Replicated loci of ML-based VCDR GWAS and meta-analysis at GWS level. "ML-based 10% (VCDR)" denotes the GWAS performed on VCDR predictions of the ML model trained using only 10% of the training data. "ML-based + IGGC (VCDR)" denotes meta-analysis of ML-based and IGGC VCDR GWAS. Likewise, "Craig *et al.* + IGGC (VCDR)" denotes meta-analysis of Craig *et al.* VCDR and IGGC VCDR GWAS. Genetic correlation was only computed when the full set of summary statistics were available.

Discovery GWAS details			Number of loci replicated in ML-based VCDR GWAS	Number of loci replicated in ML-based + IGGC VCDR GWAS	S-LDSC-based genetic correlation with ML-based VCDR
Study (phenotype)	Number of participants	Loci			
ML-based (VCDR)	65,680	156	–	151	–
ML-based 10% (VCDR)	65,044	131	123	125	0.99 (2.1x10 ⁻³)
ML-based + IGGC (VCDR)	89,579	189	151	–	0.97 (2.6x10 ⁻³)
IGGC (VCDR)	23,899	22	22	22	0.95 (0.03)
Craig <i>et al.</i> (VCDR)	67,040	65	62	63	N/A
Craig <i>et al.</i> + IGGC (VCDR)	90,939	90	82	85	N/A
Khawaja <i>et al.</i> (IOP)	139,555	107	14	22	0.19 (0.02)
Gharahkhani <i>et al.</i> (POAG)	383,500	118	32	40	N/A

Figures

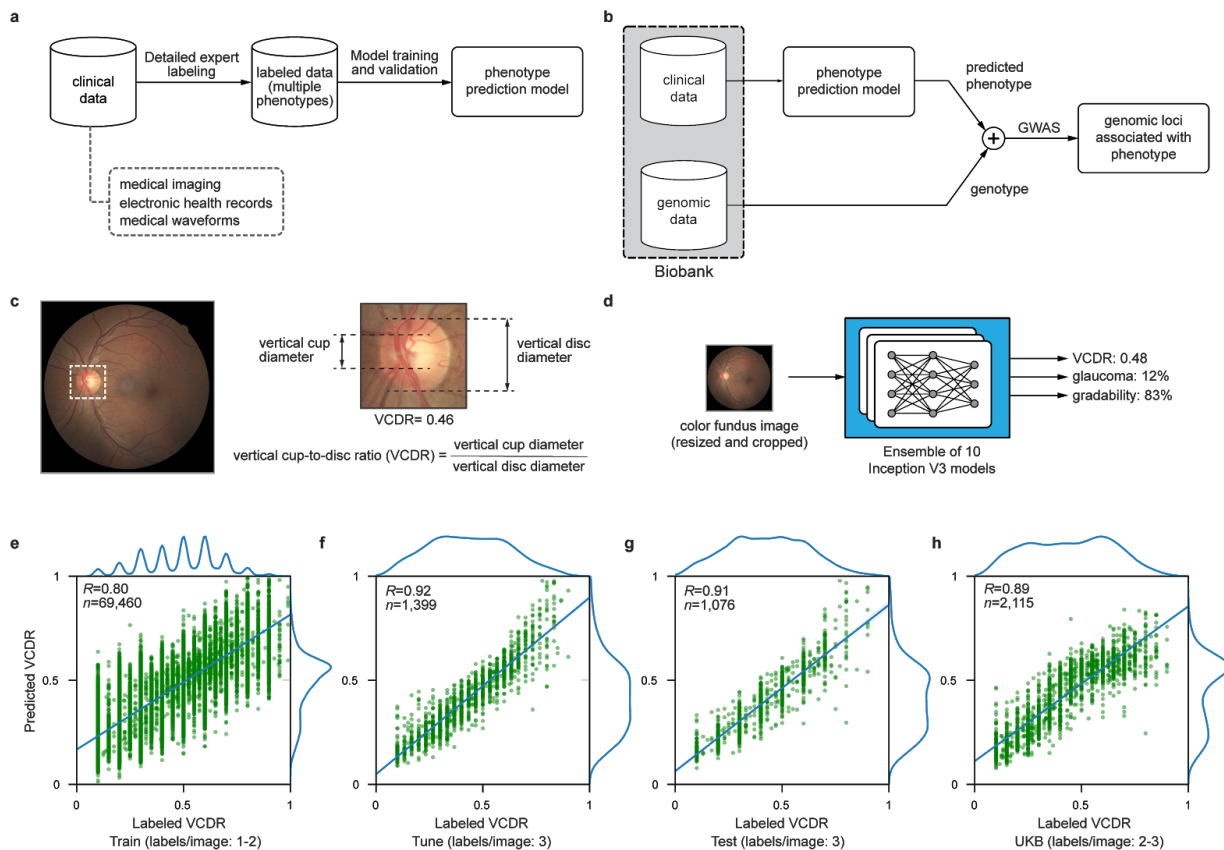


Fig 1. ML-based phenotyping concept and its application to VCDR. **a**, "Model training" phase in which a phenotype prediction model is trained using expert-labelled data. **b**, "Model application" phase in which the validated phenotype prediction model is applied to new, unlabelled data followed by genomic discovery. **c**, Definition of vertical cup-to-disc ratio (VCDR) in a real fundus image. **d**, Schematic of the multi-task ensemble model used in phenotype prediction. **e-h**, Scatter plots of the ML-based VCDR vs expert-labelled VCDR values for the train (**e**), tune (**f**), test (**g**), and UK Biobank (**h**) datasets. Number of grades per image is shown in parentheses.

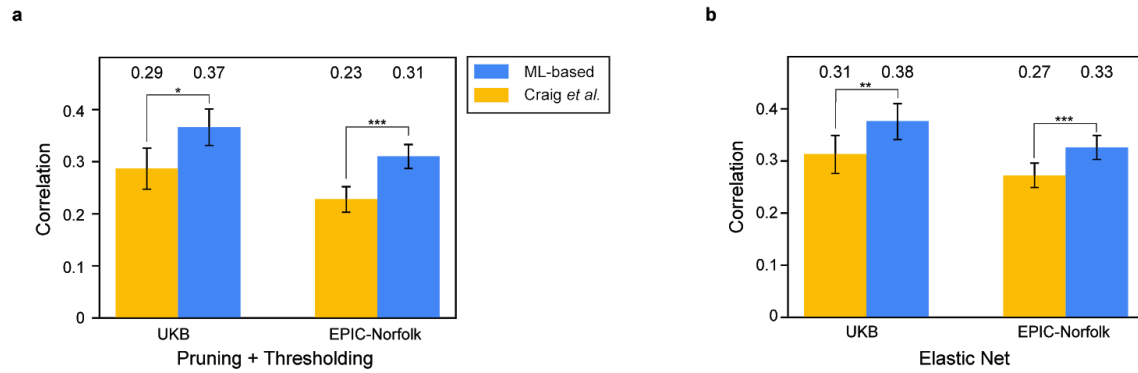


Fig 3. VCDR polygenic risk score performance metrics. Pearson's correlations between measured VCDR values and predictions of the pruning and thresholding (P+T) (a) and the Elastic Net models (b) are shown for the PRS learned from ML-based and Craig *et al.* hits. Error bars depict 95% confidence intervals. Numbers above bars are the observed Pearson's correlations. Indications of P value ranges: * $P \leq 0.05$, ** $P \leq 0.01$, *** $P \leq 0.001$. The Craig *et al.* P+T model uses 58 out of 76 hits. Measured VCDR values were obtained from adjudicated expert labeling of fundus images (UKB, $n=2,076$) and scanning laser ophthalmoscopy (HRT) (EPIC-Norfolk, $n=5,868$).

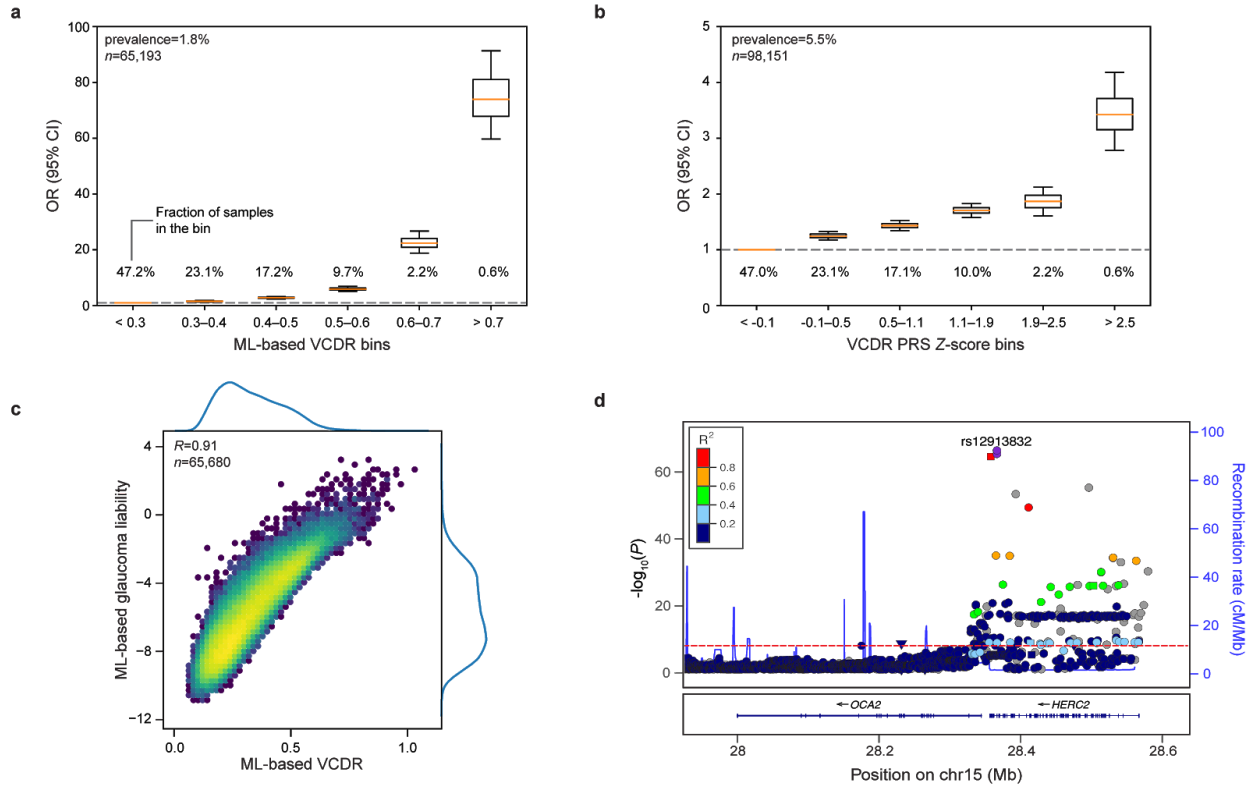


Fig 4. Relationship between glaucoma and VCDR. **a**, Glaucoma odds ratios for each ML-based VCDR bin vs. the bottom bin is shown. The fraction of individuals in each bin is shown ($n=65,193$). **b**, Glaucoma odds ratios for different VCDR elastic net PRS bins vs. the bottom bin for individuals with a glaucoma phenotype not used in the GWAS or developing the PRS ($n=98,151$). The fractions are selected to match those from **a**. **c**, A histogram of ML-based glaucoma liability vs. ML-based VCDR (Pearson's correlation $R=0.91$, $n=65,680$, $P < 1 \times 10^{-300}$). **d**, LocusZoom for the strongest associated variant ($rs12913832$, $P=2.2 \times 10^{-66}$) in the ML-based glaucoma liability GWAS conditioned on the ML-based VCDR.

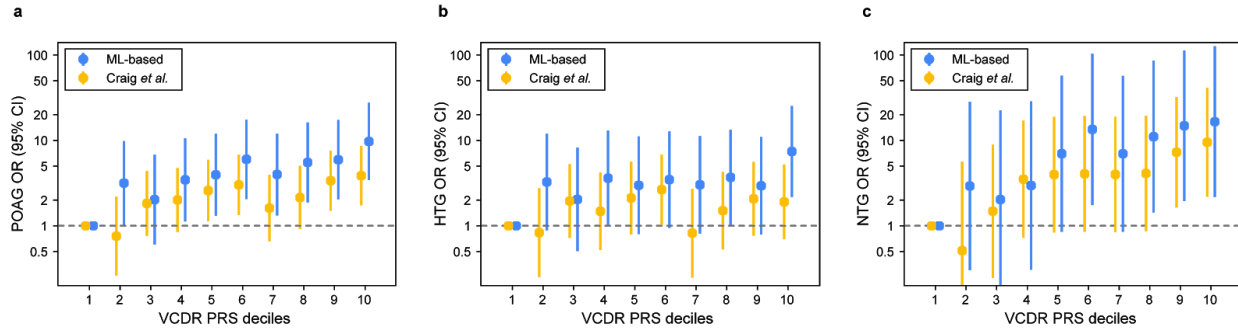


Fig 5. Primary open-angle glaucoma (POAG) prediction in the EPIC-Norfolk cohort. Odds ratios for POAG prevalence by decile of VCDR PRS; reference is decile 1. Results are from logistic regression models adjusted for age and sex for **a**, primary open-angle glaucoma (175 cases, 5,693 controls), **b**, high-tension glaucoma (HTG; 98 cases, 5,693 controls), and **c**, normal-tension glaucoma (NTG; 77 cases, 5,693 controls). Results are presented for the ML-based elastic net VCDR PRS (blue) and the Craig *et al.* elastic net VCDR PRS (yellow). Note the y-axis log scale.

References

- Age-Related Eye Disease Study Research Group. 1999. "The Age-Related Eye Disease Study (AREDS): Design Implications. AREDS Report No. 1." *Controlled Clinical Trials* 20 (6): 573–600.
- Asefa, Nigus Gebremedhin, Anna Neustaeter, Nomdo M. Jansonius, and Harold Snieder. 2019. "Heritability of Glaucoma and Glaucoma-Related Endophenotypes: Systematic Review and Meta-Analysis." *Survey of Ophthalmology* 64 (6): 835–51.
- Azuma, N., A. Hirakiyama, T. Inoue, A. Asaka, and M. Yamada. 2000. "Mutations of a Human Homologue of the Drosophila Eyes Absent Gene (EYA1) Detected in Patients with Congenital Cataracts and Ocular Anterior Segment Anomalies." *Human Molecular Genetics* 9 (3): 363–66.
- Bailey, Jessica N. Cooke, Stephanie J. Loomis, Jae H. Kang, R. Rand Allingham, Puya Gharahkhani, Chiea Chuen Khor, Kathryn P. Burdon, et al. 2016. "Genome-Wide Association Analysis Identifies TXNRD2, ATXN2 and FOXC1 as Susceptibility Loci for Primary Open-Angle Glaucoma." *Nature Genetics* 48 (2): 189–94.
- Bai, Wenjia, Hideaki Suzuki, Jian Huang, Catherine Francis, Shuo Wang, Giacomo Tarroni, Florian Guitton, et al. 2020. "A Population-Based Phenome-Wide Association Study of Cardiac and Aortic Structure and Function." *Nature Medicine*, August. <https://doi.org/10.1038/s41591-020-1009-y>.
- Bowden, Jack, Fabiola Del Greco M, Cosetta Minelli, George Davey Smith, Nuala Sheehan, and John Thompson. 2017. "A Framework for the Investigation of Pleiotropy in Two-Sample Summary Data Mendelian Randomization." *Statistics in Medicine* 36 (11): 1783–1802.
- Bulik-Sullivan, Brendan K., Po-Ru Loh, Hilary K. Finucane, Stephan Ripke, Jian Yang, Schizophrenia Working Group of the Psychiatric Genomics Consortium, Nick Patterson, Mark J. Daly, Alkes L. Price, and Benjamin M. Neale. 2015. "LD Score Regression Distinguishes Confounding from Polygenicity in Genome-Wide Association Studies." *Nature Genetics* 47 (3): 291–95.
- Chan, Michelle P. Y., David C. Broadway, Anthony P. Khawaja, Jennifer L. Y. Yip, David F. Garway-Heath, Jennifer M. Burr, Robert Luben, et al. 2017. "Glaucoma and Intraocular Pressure in EPIC-Norfolk Eye Study: Cross Sectional Study." *BMJ*. <https://doi.org/10.1136/bmj.j3889>.
- Chatterjee, Nilanjan, Jianxin Shi, and Montserrat García-Closas. 2016. "Developing and Evaluating Polygenic Risk Prediction Models for Stratified Disease Prevention." *Nature Reviews. Genetics* 17 (7): 392–406.
- Craig, Jamie E., Xikun Han, Ayub Qassim, Mark Hassall, Jessica N. Cooke Bailey, Tyler G. Kinzy, Anthony P. Khawaja, et al. 2020. "Multitrait Analysis of Glaucoma Identifies New Risk Loci and Enables Polygenic Prediction of Disease Susceptibility and Progression." *Nature Genetics* 52 (2): 160–66.
- Currant, Hannah, Pirro Hysi, Tomas W. Fitzgerald, Puya Gharahkhani, Pieter W. M. Bonnemaier, UK Biobank Eye and Vision Consortium, International Glaucoma Genetics Consortium, et al. 2020. "Genetic Variation Affects Morphological Retinal Phenotypes Extracted from UK Biobank Optical Coherence Tomography Images." *Genetic and Genomic Medicine*. medRxiv. <https://doi.org/10.1101/2020.07.20.20157180>.
- Czudowska, Monika A., Wishal D. Ramdas, Roger C. W. Wolfs, Albert Hofman, Paulus T. V. M. De Jong, Johannes R. Vingerling, and Nomdo M. Jansonius. 2010. "Incidence of

- Glaucomatous Visual Field Loss: A Ten-Year Follow-up from the Rotterdam Study.” *Ophthalmology* 117 (9): 1705–12.
- DeBoever, Christopher, Yosuke Tanigawa, Matthew Aguirre, Greg McInnes, Adam Lavertu, and Manuel A. Rivas. 2020. “Assessing Digital Phenotyping to Enhance Genetic Studies of Human Diseases.” *American Journal of Human Genetics* 106 (5): 611–22.
- D’Elia, Angela Valentina, Lucia Pellizzari, Dora Fabbro, Annalisa Pianta, Maria Teresa Divizia, Rosanna Rinaldi, Barbara Grammatico, Paola Grammatico, Carlo Arduino, and Giuseppe Damante. 2007. “A Deletion 3’ to the PAX6 Gene in Familial Aniridia Cases.” *Molecular Vision* 13 (July): 1245–50.
- Delude, Cathryn M. 2015. “Deep Phenotyping: The Details of Disease.” *Nature* 527 (7576): S14–15.
- Deng, Jia, Wei Dong, Richard Socher, Li-Jia Li, Kai Li, and Li Fei-Fei. 2009. “ImageNet: A Large-Scale Hierarchical Image Database.” *2009 IEEE Conference on Computer Vision and Pattern Recognition*. <https://doi.org/10.1109/cvpr.2009.5206848>.
- Deveza, L. A., L. Melo, T. Yamato, K. Mills, and D. J. Hunter. 2017. “Knee Osteoarthritis Phenotypes and Their Relevance for Outcomes: A Systematic Review of the Literature.” *Osteoarthritis and Cartilage*. <https://doi.org/10.1016/j.joca.2017.02.104>.
- Egger, M., G. Davey Smith, M. Schneider, and C. Minder. 1997. “Bias in Meta-Analysis Detected by a Simple, Graphical Test.” *BMJ* 315 (7109): 629–34.
- Foster, Paul J., Ralf Buhmann, Harry A. Quigley, and Gordon J. Johnson. 2002. “The Definition and Classification of Glaucoma in Prevalence Surveys.” *The British Journal of Ophthalmology* 86 (2): 238–42.
- Gal, Andreas, Isabella Rau, Leila El Matri, Hans-Jürgen Kreienkamp, Susanne Fehr, Karim Baklouti, Ibtissem Chouchane, et al. 2011. “Autosomal-Recessive Posterior Microphthalmos Is Caused by Mutations in PRSS56, a Gene Encoding a Trypsin-Like Serine Protease.” *The American Journal of Human Genetics*. <https://doi.org/10.1016/j.ajhg.2011.02.006>.
- Gao, X. Raymond, Hua Huang, Drew R. Nannini, Fangda Fan, and Heejin Kim. 2018. “Genome-Wide Association Analyses Identify New Loci Influencing Intraocular Pressure.” *Human Molecular Genetics* 27 (12): 2205–13.
- Gharakhani, Puya, Eric Jorgenson, Pirro Hysi, Anthony P. Khawaja, Sarah Pendergrass, Xikun Han, Jue Sheng Ong, et al. 2020. “A Large Cross-Ancestry Meta-Analysis of Genome-Wide Association Studies Identifies 69 Novel Risk Loci for Primary Open-Angle Glaucoma and Includes a Genetic Link with Alzheimer’s Disease.” *bioRxiv*. <https://doi.org/10.1101/2020.01.30.927822>.
- Gordon, Mae O., Julia A. Beiser, James D. Brandt, Dale K. Heuer, Eve J. Higginbotham, Chris A. Johnson, John L. Keltner, et al. 2002. “The Ocular Hypertension Treatment Study: Baseline Factors That Predict the Onset of Primary Open-Angle Glaucoma.” *Archives of Ophthalmology* 120 (6): 714–20; discussion 829–30.
- Hayat, Shabina A., Robert Luben, Victoria L. Keevil, Stephanie Moore, Nichola Dalzell, Amit Bhaniani, Anthony P. Khawaja, et al. 2014. “Cohort Profile: A Prospective Cohort Study of Objective Physical and Cognitive Capability and Visual Health in an Ageing Population of Men and Women in Norfolk (EPIC-Norfolk 3).” *International Journal of Epidemiology* 43 (4): 1063–72.
- Hendee, Kathryn, Lauren Weiping Wang, Linda M. Reis, Gregory M. Rice, Suneel S. Apte, and Elena V. Semina. 2017. “Identification and Functional Analysis of an ADAMTSL1 Variant Associated with a Complex Phenotype Including Congenital Glaucoma, Craniofacial and Other Systemic Features in a Three Generation Human Pedigree.” *Human Mutation* 38

(11): 1485.

- Jonas, Jost B., Tin Aung, Rupert R. Bourne, Alain M. Bron, Robert Ritch, and Songhomitra Panda-Jonas. 2017. "Glaucoma." *The Lancet* 390 (10108): 2183–93.
- Khawaja, Anthony P., Michelle P. Y. Chan, David C. Broadway, David F. Garway-Heath, Robert Luben, Jennifer L. Y. Yip, Shabina Hayat, Kay-Tee Khaw, and Paul J. Foster. 2013. "Laser Scanning Tomography in the EPIC-Norfolk Eye Study: Principal Components and Associations." *Investigative Ophthalmology & Visual Science* 54 (10): 6638–45.
- Khawaja, Anthony P., Sharon Chua, Pirro G. Hysi, Stelios Georgoulas, Hannah Currant, Tomas W. Fitzgerald, Ewan Birney, et al. 2020. "Comparison of Associations with Different Macular Inner Retinal Thickness Parameters in a Large Cohort: The UK Biobank." *Ophthalmology* 127 (1): 62–71.
- Khawaja, Anthony P., Jessica N. Cooke Bailey, Nicholas J. Wareham, Robert A. Scott, Mark Simcoe, Robert P. Igo Jr, Yeunjoo E. Song, et al. 2018. "Genome-Wide Analyses Identify 68 New Loci Associated with Intraocular Pressure and Improve Risk Prediction for Primary Open-Angle Glaucoma." *Nature Genetics* 50 (6): 778–82.
- Khawaja, Anthony P., Karla E. Rojas Lopez, Alison J. Hardcastle, Chris J. Hammond, Petra Liskova, Alice E. Davidson, Daniel M. Gore, et al. 2019. "Genetic Variants Associated With Corneal Biomechanical Properties and Potentially Conferring Susceptibility to Keratoconus in a Genome-Wide Association Study." *JAMA Ophthalmology*, June.
<https://doi.org/10.1001/jamaophthalmol.2019.2058>.
- Kolesnikov, Alexander, Lucas Beyer, Xiaohua Zhai, Joan Puigcerver, Jessica Yung, Sylvain Gelly, and Neil Houlsby. 2019. "Big Transfer (BiT): General Visual Representation Learning." <http://arxiv.org/abs/1912.11370>.
- Lee, Suho, Kyoungwoo Lee, Suha Hwang, Sung Hyun Kim, Woo Keun Song, Zee Yong Park, and Sunghoe Chang. 2006. "SPIN90/WISH Interacts with PSD-95 and Regulates Dendritic Spinogenesis via an N-WASP-Independent Mechanism." *The EMBO Journal* 25 (20): 4983–95.
- Loh, Po-Ru, Gleb Kichaev, Steven Gazal, Armin P. Schoech, and Alkes L. Price. 2018. "Mixed-Model Association for Biobank-Scale Datasets." *Nature Genetics* 50 (7): 906–8.
- Loh, Po-Ru, George Tucker, Brendan K. Bulik-Sullivan, Bjarni J. Vilhjálmsson, Hilary K. Finucane, Rany M. Salem, Daniel I. Chasman, et al. 2015. "Efficient Bayesian Mixed-Model Analysis Increases Association Power in Large Cohorts." *Nature Genetics* 47 (3): 284–90.
- McCarthy, Shane, Sayantan Das, Warren Kretzschmar, Olivier Delaneau, Andrew R. Wood, Alexander Teumer, Hyun Min Kang, et al. 2016. "A Reference Panel of 64,976 Haplotypes for Genotype Imputation." *Nature Genetics* 48 (10): 1279–83.
- McCaw, Zachary R., Jacqueline M. Lane, Richa Saxena, Susan Redline, and Xihong Lin. 2019. "Operating Characteristics of the Rank-Based Inverse Normal Transformation for Quantitative Trait Analysis in Genome-Wide Association Studies." *Biometrics*, December.
<https://doi.org/10.1111/biom.13214>.
- McLean, Cory Y., Dave Bristor, Michael Hiller, Shoa L. Clarke, Bruce T. Schaar, Craig B. Lowe, Aaron M. Wenger, and Gill Bejerano. 2010. "GREAT Improves Functional Interpretation of Cis-Regulatory Regions." *Nature Biotechnology* 28 (5): 495–501.
- Melin, Beatrice S., Jill S. Barnholtz-Sloan, Margaret R. Wrensch, Christoffer Johansen, Dora Il'yasova, Ben Kinnerley, Quinn T. Ostrom, et al. 2017. "Genome-Wide Association Study of Glioma Subtypes Identifies Specific Differences in Genetic Susceptibility to Glioblastoma and Non-Glioblastoma Tumors." *Nature Genetics* 49 (5): 789–94.
- Nagai, Akiko, Makoto Hirata, Yoichiro Kamatani, Kaori Muto, Koichi Matsuda, Yutaka Kiyohara, Toshiharu Ninomiya, et al. 2017. "Overview of the BioBank Japan Project: Study Design

- and Profile.” *Journal of Epidemiology / Japan Epidemiological Association* 27 (3S): S2–8.
- Pascolini, D., and S. P. Mariotti. 2012. “Global Estimates of Visual Impairment: 2010.” *The British Journal of Ophthalmology* 96 (5). <https://doi.org/10.1136/bjophthalmol-2011-300539>.
- Phene, Sonia, R. Carter Dunn, Naama Hammel, Yun Liu, Jonathan Krause, Naho Kitade, Mike Schaekermann, et al. 2019. “Deep Learning and Glaucoma Specialists.” *Ophthalmology* 126 (12): 1627–39.
- Prechelt, Lutz. 1998. “Early Stopping - But When?” In *Neural Networks: Tricks of the Trade*, edited by Genevieve B. Orr and Klaus-Robert Müller, 55–69. Berlin, Heidelberg: Springer Berlin Heidelberg.
- Raghu, Maithra, Chiyuan Zhang, Jon Kleinberg, and Samy Bengio. 2019. “Transfusion: Understanding Transfer Learning for Medical Imaging.” In *Advances in Neural Information Processing Systems*, 3347–57.
- Reim, Kerstin, Hanna Regus-Leidig, Josef Ammermüller, Ahmed El-Kordi, Konstantin Radyushkin, Hannelore Ehrenreich, Johann Helmut Brandstätter, and Nils Brose. 2009. “Aberrant Function and Structure of Retinal Ribbon Synapses in the Absence of Complexin 3 and Complexin 4.” *Journal of Cell Science* 122 (Pt 9): 1352–61.
- Sapir, Tamar, Sivan Sapoznik, Talia Levy, Danit Finkelshtein, Anat Shmueli, Thomas Timm, Eva-Maria Mandelkow, and Orly Reiner. 2008. “Accurate Balance of the Polarity Kinase MARK2/Par-1 Is Required for Proper Cortical Neuronal Migration.” *The Journal of Neuroscience: The Official Journal of the Society for Neuroscience* 28 (22): 5710–20.
- Seifi, M., and M. A. Walter. 2018. “Axenfeld-Rieger Syndrome.” *Clinical Genetics* 93 (6): 1123–30.
- Shorten, Connor, and Taghi M. Khoshgoftaar. 2019. “A Survey on Image Data Augmentation for Deep Learning.” *Journal of Big Data* 6 (1): 60.
- Sinnott-Armstrong, Nasa, Yosuke Tanigawa, David Amar, Nina J. Mars, Matthew Aguirre, Guhan Ram Venkataraman, Michael Wainberg, et al. 2019. “Genetics of 38 Blood and Urine Biomarkers in the UK Biobank.” <https://doi.org/10.1101/660506>.
- Springelkamp, Henriët, Adriana I. Iglesias, Aniket Mishra, René Höhn, Robert Wojciechowski, Anthony P. Khawaja, Abhishek Nag, et al. 2017. “New Insights into the Genetics of Primary Open-Angle Glaucoma Based on Meta-Analyses of Intraocular Pressure and Optic Disc Characteristics.” *Human Molecular Genetics* 26 (2): 438–53.
- Sudlow, Cathie, John Gallacher, Naomi Allen, Valerie Beral, Paul Burton, John Danesh, Paul Downey, et al. 2015. “UK Biobank: An Open Access Resource for Identifying the Causes of a Wide Range of Complex Diseases of Middle and Old Age.” *PLoS Medicine* 12 (3): e1001779.
- Szegedy, Christian, Vincent Vanhoucke, Sergey Ioffe, Jon Shlens, and Zbigniew Wojna. 2016. “Rethinking the Inception Architecture for Computer Vision.” *2016 IEEE Conference on Computer Vision and Pattern Recognition (CVPR)*. <https://doi.org/10.1109/cvpr.2016.308>.
- Tham, Yih-Chung, Xiang Li, Tien Y. Wong, Harry A. Quigley, Tin Aung, and Ching-Yu Cheng. 2014. “Global Prevalence of Glaucoma and Projections of Glaucoma Burden through 2040: A Systematic Review and Meta-Analysis.” *Ophthalmology* 121 (11): 2081–90.
- Tung, Joyce Y., Chuong B. Do, David A. Hinds, Amy K. Kiefer, J. Michael Macpherson, Arnab B. Chowdry, Uta Francke, et al. 2011. “Efficient Replication of over 180 Genetic Associations with Self-Reported Medical Data.” *PLoS One* 6 (8): e23473.
- UK National Screening Committee. 2019. “Screening for Glaucoma - External Review against Programme Appraisal Criteria for the UK National Screening Committee.” UK National Screening Committee. December 2019. https://legacyscreening.phe.org.uk/policydb_download.php?doc=1219.

- Wang, Gao, Abhishek Sarkar, Peter Carbonetto, and Matthew Stephens. 2020. "A Simple New Approach to Variable Selection in Regression, with Application to Genetic Fine Mapping." *Journal of the Royal Statistical Society. Series B, Statistical Methodology* 25 (July): 1.
- Wang, Kanix, Hallie Gaitsch, Hoifung Poon, Nancy J. Cox, and Andrey Rzhetsky. 2017. "Classification of Common Human Diseases Derived from Shared Genetic and Environmental Determinants." *Nature Genetics* 49 (9): 1319–25.
- Watanabe, Kyoko, Erdogan Taskesen, Arjen van Bochoven, and Danielle Posthuma. 2017. "Functional Mapping and Annotation of Genetic Associations with FUMA." *Nature Communications* 8 (1): 1826.
- Wawrocka, Anna, and Maciej R. Krawczynski. 2018. "The Genetics of Aniridia - Simple Things Become Complicated." *Journal of Applied Genetics* 59 (2): 151–59.
- Wheeler, Eleanor, Aaron Leong, Ching-Ti Liu, Marie-France Hivert, Rona J. Strawbridge, Clara Podmore, Man Li, et al. 2017. "Impact of Common Genetic Determinants of Hemoglobin A1c on Type 2 Diabetes Risk and Diagnosis in Ancestrally Diverse Populations: A Transethnic Genome-Wide Meta-Analysis." *PLoS Medicine* 14 (9): e1002383.
- World Health Organization. 2019. "World Report on Vision." October 8, 2019. <https://www.who.int/publications/i/item/world-report-on-vision>.
- Yim, Jason, Reena Chopra, Terry Spitz, Jim Winkens, Annette Obika, Christopher Kelly, Harry Askham, et al. 2020. "Predicting Conversion to Wet Age-Related Macular Degeneration Using Deep Learning." *Nature Medicine* 26 (6): 892–99.
- Zou, Hui, and Trevor Hastie. 2005. "Regularization and Variable Selection via the Elastic Net." *Journal of the Royal Statistical Society. Series B, Statistical Methodology* 67 (2): 301–20.

Supplementary Information -

Large-scale machine learning-based phenotyping significantly improves genomic discovery for optic nerve head morphology

Babak Alipanahi^{1,†,*}, Farhad Hormozdiari^{2,†}, Babak Behsaz^{2,†}, Justin Cosentino^{1,†}, Zachary R. McCaw^{1,†}, Emanuel Schorsch¹, D Sculley², Elizabeth H. Dorfman¹, Sonia Phene¹, Naama Hammel¹, Andrew Carroll¹, Anthony P. Khawaja^{3,4,‡}, Cory Y. McLean^{2,‡,*}

¹Google, Health, Palo Alto, CA

²Google, Health, Cambridge, MA

³NIHR Biomedical Research Centre at Moorfields Eye Hospital & UCL Institute of Ophthalmology, London, UK

⁴Department of Public Health & Primary Care, University of Cambridge, Cambridge, UK

[†]These authors contributed equally to this work.

[‡]These authors contributed equally to this work.

*To whom correspondence should be addressed: cym@google.com or babaka@google.com.

Table of Contents:

Phenotype Prediction Model	3
Data collection	3
Model training and validation	3
Genomic Discovery	4
UK Biobank cohort	4
Phenotype calling	4
Genome-wide association study	5
Identification and comparison of loci	5
Fine-mapping	5
Ablation analysis	6
Genomic discovery power analysis	6
Replication slope analysis	7
Meta-analysis	8
Functional analyses with FUMA and GREAT	8
VCDR-IOP Mendelian Randomization	8
Polygenic VCDR Model	9
Pruning and thresholding	9
Elastic net	9
Permutation P-values	9
Glaucoma Association	10
Mediation Analysis	10
Glaucoma liability conditional analysis	10
UK Biobank glaucoma phenotype	10
EPIC-Norfolk cohort	11
Tables	13
Figures	15
Model hyper-parameters	22
References	23

Phenotype Prediction Model

Data collection

Grading of images has been described in detail previously (Phene et al. 2019). In short, graders assessed each image for gradability, presence of various optic nerve head (ONH) features (including estimation of VCDR; the ratio between the vertical diameter of the cup and the vertical diameter of the disc) and referable glaucomatous optic neuropathy (GON). Gradability was measured based on image quality, blurring, media opacity, or any other confounding reason. If graders selected “ungradable” for a particular feature or referable GON, then no grade was collected for that aspect. To enable systematic training of graders, we developed grading guidelines and iterated on the guidelines with a panel of three fellowship-trained glaucoma specialists to increase inter-rater agreement; please refer to the Supplementary Table 1 in (Phene et al. 2019). Similar to clinical practice, for VCDR graders were asked to provide an estimate as a decimal between 0.0 and 1.0, with 0.1 increments ($0.0 < \text{VCDR} < 1.0$). For referable GON grading we developed guidelines for a four-point GON assessment (“non-glaucomatous”, “low-risk glaucoma suspect”, “high-risk glaucoma suspect”, and “likely glaucoma”) where the “high-risk glaucoma suspect” or “likely glaucoma” levels were considered referable, that is, the ONH appearance was worrisome enough to justify referral for comprehensive examination. Graders were asked to provide a referable GON grade after evaluating the image for the other ONH features.

Model training and validation

Data processing and model training has been described previously (Phene et al. 2019). In short, we first remove all UK Biobank (UKB) samples from the “train”, “tune”, and “test” sets used by (Phene et al. 2019). We use 81,830 color fundus images from AREDS (age-related eye disease study) (Age-Related Eye Disease Study Research Group 1999), EyePACS (<https://www.eyepacs.org/>), Inoveon (<http://www.inoveon.com/>) from United States and two eye hospitals in India (Narayana Nethralaya and Sankara Nethralaya). In total, 69,460 of the 79,355 training images were gradable. All color fundus images are cropped to center the retinal image and resized to 587×587 pixels. The prediction model consists of ten independently trained multi-task Inception V3 (Szegedy et al. 2016) deep convolutional neural networks. To accelerate model training, convolutional layers were initialized using the weights learned from the ImageNet dataset (Deng et al. 2009). We used image augmentation (Shorten and Khoshgoftaar 2019) (randomly changing brightness, hue, contrast, saturation and flipping the image horizontally and vertically) to regularize model training in TensorFlow (Abadi et al. 2016). Full set of hyperparameters is given in the “Model hyper-parameters” section. We used early stopping (Prechelt 1998) based on root mean squared error (RMSE) for predicting VCDR in the tune set for each model. The final prediction was the average prediction of the ten models in the ensemble. Model performance metrics are listed in Supplementary Table 1.

Genomic Discovery

UK Biobank cohort

The UK Biobank is a very large multisite cohort study established by the Medical Research Council, Department of Health, Wellcome Trust medical charity, Scottish Government and Northwest Regional Development Agency. Detailed study protocols are available online (<http://www.ukbiobank.ac.uk/resources/> and <http://biobank.ctsu.ox.ac.uk/crystal/docs.cgi>). A baseline questionnaire, physical measurements, and biological samples were undertaken in 22 assessment centers across the UK between 2006 and 2010. All UK residents aged 40 to 69 years who were registered with the National Health Service (NHS) and living up to 25 miles from a study center were invited to participate. The study was conducted with the approval of the North-West Research Ethics Committee (ref 06/MRE08/65), in accordance with the principles of the Declaration of Helsinki, and all participants gave written informed consent. This research has been conducted using the UK Biobank Resource under Application Number 17643.

Ophthalmic assessment was not part of the original baseline assessment and was introduced as an enhancement in 2009 for 6 assessment centers which are spread across the UK (Liverpool and Sheffield in North England, Birmingham in the Midlands, Swansea in Wales, and Croydon and Hounslow in Greater London). Imaging of both eyes was performed using the Topcon 3D OCT- 1000 Mark II in a dark room without pupil dilation. The instrument takes a color photograph of the retina as well as an optical coherence tomography scan; we used the color photographs in the current study. The right eye was imaged first. Refractive status of both eyes was measured by autorefractometry (Tomey RC5000; Erlangen-Tennenlohe). Spherical equivalent was calculated as the sphere + 0.5 * cylinder and participant-level refractive error was taken as the mean of right and left values.

Phenotype calling

After predicting VCDR for all 175,337 fundus images from 85,665 individuals in UKB, we first remove the 21,400 images which are predicted as ungradable for VCDR. Recall that there are two imaging visits, called visit 1 and 2. We define the phenotype only based on one of these visits, because there is an approximate 5 years difference between the two visits and many factors such as age, medications, eye operations can be materially different between the two visits.

If an individual has any gradable image(s) from visit 1, we define the phenotype based on these images; otherwise, we define it based on visit 2 (a.k.a. first repeat imaging visit). For a specific visit, we first average the VCDRs of each eye and then average these per eye VCDRs if both eyes have gradable images. Moreover, to account for the impact of image gradability on the phenotype, we computed the average gradability score of all images used in defining an individual's phenotype. For the details and statistics of phenotype calling, please refer to Supplementary Fig. 1. To control for the small variations in phenotype calling, we add the visit number used (i.e., 1 or 2) and the number of eyes used in calling the phenotype (i.e., 1 or 2) as covariates. After subsetting to individuals of European ancestry and removing samples with

excess heterozygosity or missingness, putative sex chromosome aneuploidy, and missing refractive error report, we call the VCDR phenotype for 65,680 individuals.

Genome-wide association study

We use linear mixed models as implemented in BOLT-LMM v3.2 (Loh et al. 2015) to account for population structure and cryptic relationships in UK Biobank, and to increase association power. We applied BOLT-LMM to all individuals of European ancestry with available VCDR who passed our sample QC and had non-missing covariates ($n=65,680$). We used sex, age at visit, visit number (i.e., 1 or 2 to indicate visit 1 or visit 2), number of eyes used to compute VCDR (i.e., 1 or 2 to indicate one eye or both eyes are used), genotyping array indicator, refractive error, average gradability scores of all fundus images used in phenotype calling and the top 15 genetic principal components as covariates. To increase association power and make the normality assumption more plausible, ML-based VCDR was rank-based inverse normal (INT; (McCaw et al. 2019)) transformed. We considered the autosomal chromosomes for our GWAS and filtered out variants with minor allele frequency (MAF) < 0.001 , imputation INFO score < 0.8 , or Hardy-Weinberg equilibrium (HWE) $P < 1 \times 10^{-10}$ in Europeans. Using these filters, 13,110,443 variants passed QC. To verify that our association results were not driven by population stratification, we applied LD score regression (Bulik-Sullivan et al. 2015).

Identification and comparison of loci

Genome-wide significant (GWS; $P \leq 5 \times 10^{-8}$) lead SNPs, independent at $R^2=0.1$, were identified using the `plink --clump` command (v1.90b4). The reference panel comprised a random sample of 10,000 unrelated subjects of white European ancestry from the UK Biobank. Around each lead SNP, a locus was defined as the span of reference panel SNPs in LD with the lead SNP at $R^2 \geq 0.1$. For consistency with locus formation as implemented by FUMA (Watanabe et al. 2017), loci separated by fewer than 250 kb were merged, and the most significant, independent SNP in the merged locus was retained as the lead SNP. Gene context annotations were added from the GRCh37 version of GenCode v34 "comprehensive gene annotations." Only protein-coding genes and level 1 long noncoding RNAs (lncRNA) were considered.

For comparing loci across studies, loci were formed for each study using the common reference panel and procedure described above. Locus overlap metrics were calculated using the GenomicRanges package (Lawrence et al. 2013) in R (v3.2.3). In comparing loci from studies A and B, it is possible for a single locus from study A to overlap multiple loci from study B or conversely. To accommodate this, we report the maximum of the number of loci in study B *overlapped by* a locus from study A, and the number of loci in study A *overlapped by* a locus from study B.

Fine-mapping

Fine-mapping of independent significant loci was performed via Sum of Single Effects Regression (SuSiE; v0.9.0) (Wang et al. 2020), as implemented in R. Briefly, SuSiE identifies the likely causal variants in a region using a variational approximation to Bayesian variable

selection regression. A posterior inclusion probability (PIP) is assigned to each SNP in the locus, quantifying the probability that the SNP has a non-zero effect on the outcome. The sum of PIPs for SNPs in a locus is the posterior expectation of the number of causal variants in that locus. To estimate the total number of distinct genetic signals for ML-based VCDR detected in our analysis, PIPs were aggregated across all loci where SuSiE reported no more than the number of GWS variants in the locus. Loci where SuSiE reported more causal variants than GWS variants were considered potentially unreliable. The number of causal variants in such loci was conservatively estimated as the number of GWS variants in the locus, which is potentially an underestimate. Moreover, uncommon SNPs (those with minor allele frequencies below 5%) were removed from the fine-mapping analysis, some of which are likely causal. Nevertheless, the estimated number of genetic signals for VCDR detected by our analysis was 813.

Ablation analysis

In order to assess the dependence of model quality on the training data size, we analyzed model performance when trained on progressively smaller subsets of the full training data. Predicted VCDR vs adjudicated VCDR correlations for different sets are depicted in Supplementary Fig. 3. In particular, when training only on 10% of the data (~7,900 samples), the Pearson's correlations (ratio with regard to the original correlation) were 0.87 (94%), 0.87 (96%) and 0.83 (93%), for the Tune, Test, and UKB Adjudicated cohorts.

We also performed a GWAS using the "10% model" predictions, which identified 131 genome-wide significant loci, replicating 123 of the 156 loci identified by the full model. The scatter plot of P values for the ML-based GWAS and the 10% ablation GWAS are presented in Supplementary Fig. 4.

Genomic discovery power analysis

To assess how the power for genomic discovery varied with phenotyping quality, we followed the "Noisy Measurement Model" (Hormozdiari et al. 2016). Specifically, consider the following:

$$(1) \quad Y = X\beta + \epsilon$$

where Y is the true VCDR, X is genotype, and ϵ is an environmental residual. Suppose Y and X have been standardized to mean zero and variance one. Let h^2 denote the per-SNP heritability, then the residual variance is $1-h^2$. We do not observe the true VCDR, but instead a mismeasured version Y^* , which is related to Y via

$$(2) \quad Y^* = Y + \delta$$

where δ is mean-zero measurement error. Substituting (1) into (2) gives the variance component model

$$(3) \quad Y^* = X\beta + \epsilon + \delta$$

From model (3) we can derive the asymptotic non-centrality parameter (NCP) of the standard Wald χ^2 test of association by considering a sequence of contiguous alternatives (Serfling 1980). The NCP for the χ^2 test based on Y^* takes the simple form

$$NCP = n \cdot \frac{\rho^2 h^2}{1 - \rho^2 h^2}$$

where n is the sample size, ρ^2 is the square of the correlation between the mismeasured Y^* and true Y phenotypes, and h^2 is the true heritability of Y . Power and Non-Centrality Curves as a function of per-SNP heritability, stratified by the correlation between the measured and true phenotypes are shown in Supplementary Fig. 5.

Applying the above model to compare the “10% model” and the model trained on the entire training set, at our GWAS sample size $n=65,680$, the difference in power between a GWAS where the correlation between the observed and true VCDR measurements is 0.89 and a GWAS where the correlation is 0.83 can reach as high as 15%.

Replication slope analysis

To jointly test the ML-based hits for replication of the IGGC VCDR meta-analysis, we first scaled the effect size estimates of the ML-based GWAS results to account for winner’s curse. Winner’s curse correction was performed by fitting a two-component Gaussian mixture model, as described in supplemental section 5.3 of (Turley et al. 2018):

$$f(\hat{\beta}_j | \pi, \tau^2) = \pi \cdot N(\hat{\beta}_j | 0, \sigma_j^2) + (1 - \pi) \cdot N(\hat{\beta}_j | 0, \sigma_j^2 + \tau^2).$$

Here $\hat{\beta}_j$ is the estimated effect size, π is the prior probability of belonging to the null component, σ_j^2 is the sampling variance (i.e., squared standard error) of $\hat{\beta}_j$, and τ^2 is the variance in effect sizes at non-null SNPs. Model parameters (π, τ^2) were estimated by maximum likelihood using the expectation maximization algorithm (McCaw, Julienne, and Aschard 2020; Meng and Rubin 1993). The observed effect sizes were shrunk to their posterior expectation via:

$$E[\beta_j | \hat{\beta}_j] = (1 - \gamma_j) \frac{\tau^2}{\tau^2 + \sigma_j^2} \cdot \hat{\beta}_j$$

where γ_j is the posterior responsibility of the null-component for SNP j :

$$\gamma_i = P[\beta_j = 0 | \hat{\beta}_j] = \frac{\pi \cdot N(\hat{\beta}_j | 0, \sigma_j^2)}{\pi \cdot N(\hat{\beta}_j | 0, \sigma_j^2) + (1 - \pi) \cdot N(\hat{\beta}_j | 0, \sigma_j^2 + \tau^2)}.$$

Winner’s curse correction was performed using all genotyped variants as input, with final model parameter estimates of $(\pi = 0.958, \tau^2 = 0.000427)$. We then identified 214 (of 299) ML-based hits additionally present in the IGGC VCDR meta-analysis and regressed the IGGC effect sizes on the winner’s curse-corrected ML-based GWAS effect size estimates (Supplementary Fig. 7).

Meta-analysis

GWAS summary statistics for ML-based VCDR were combined with summary statistics from a previous meta-analysis of VCDR by the International Glaucoma Genetics Consortium (IGGC) using Meta-Soft (Han and Eskin 2011). The following strategy was adopted for selecting the final P value. At each SNP, the I^2 statistic (Higgins and Thompson 2002) was calculated to quantify the proportion of total variation across studies that was attributable to effect size heterogeneity. For SNPs with $I^2 > 0$, a random effects meta-analysis was performed, using Han and Eskin's "RE2" model (see URLs), whereas for those SNPs with $I^2 = 0$, a fixed effects meta-analysis was performed. Selecting whether to perform random or fixed effects meta-analysis on the basis of I^2 is an effort to apply the most appropriate model for the observed effect sizes. Among the 8.6M SNPs present in both studies, 68% had $I^2 = 0$, while the remaining 32% had $I^2 > 0$. For the 4.5M SNPs present in our analysis but not in IGGC, the original P -value from the ML-based VCDR GWAS was retained. The S-LDSC intercept was 1.06 (s.e.m=0.01) and the SNP-heritability h^2_g was 0.37 (s.e.m=0.02).

Functional analyses with FUMA and GREAT

Functional analyses were performed in FUMA (Watanabe et al. 2017). We assigned each variant to the nearest gene within 10kb using FUMA's "SNP2GENE" functionality, and performed gene-set enrichment analysis using FUMA's "GENE2FUNC" functionality. In both cases, we adopted the default parameter settings. We compared the *relative enrichment* of gene sets that were significant according to both the ML-based and the Craig *et al.* GWAS of VCDR. Specifically, enrichment refers to the odds that a gene in the gene-set was detected in a given GWAS, and relative enrichment is the odds ratio comparing our GWAS with the Craig *et al.* GWAS. Fisher's exact test was applied to determine whether enrichment differed significantly between the two studies. Those sets where the relative enrichment (odds ratio) exceeds 1 represent biologically interesting gene-sets where the ML-based GWAS captured more of the constituent genes.

GREAT enrichment analyses were performed on the human GRCh37 assembly using GREAT v4.0.4 (McLean et al. 2010). The default "basal+extension" region-gene association rule was used with 5 kb upstream, 1 kb downstream, 1000 kb extension, and curated regulatory domains included. Analyses were performed using the same loci as in the FUMA analyses described above; 65 loci from Craig *et al.* and 156 loci from the ML-derived GWAS. Terms were considered statistically significant if the Bonferroni-corrected P -values for both the region-based and gene-based tests were ≤ 0.05 .

VCDR-IOP Mendelian Randomization

Two sample Mendelian randomization (MR) for the association between intraocular pressure (IOP) and ML-based VCDR was performed using the TwoSampleMR (see URLs) package in R (4.0.2). Among the 187 independent significant SNPs for IOP from (Khawaja et al. 2018), 183 remained after harmonizing with ML-based VCDR. This provided 183 candidate instrumental variables for quantifying the association between IOP and ML-based VCDR. Based on

Cochran's Q test, there was significant evidence of pleiotropy ($P < 10^{-16}$). Therefore, per-SNP associations were meta-analyzed using Egger regression (Egger et al. 1997), which is robust to the exclusion restriction (Bowden et al. 2017). The Egger intercept did not differ from zero (intercept=0.001, $P=0.69$). The Egger slope of 0.07 ($P=4 \times 10^{-4}$) provided strong evidence of a directional association between IOP and ML-based VCDR. In a reversed analysis, regarding ML-based VCDR as the mediator and IOP as the outcome, the Egger slope was -0.03 ($P=0.75$), providing no significant evidence of association in the opposite direction.

Polygenic VCDR Model

Pruning and thresholding

Pruning and thresholding-based polygenic risk scores for VCDR were computed as the weighted sum of effect allele counts for independent genome-wide significant variants ($P \leq 5 \times 10^{-8}$), where the weight of each variant was its estimated effect size from the GWAS (Chatterjee, Shi, and García-Closas 2016). To evaluate performance both within the UK Biobank and in the EPIC-Norfolk cohorts, index variants present in both cohorts were used in PRS creation, resulting in 58 of the 76 published variants from Craig *et al.* GWAS and 282 of the 299 index variants from the ML-based GWAS. The UK Biobank evaluation set consisted of adjudicated expert-annotated VCDR measurements in 2,076 individuals of European ancestry. The EPIC-Norfolk evaluation set consisted of scanning laser ophthalmoscopy (HRT)-measured VCDRs in 5,868 individuals.

Elastic net

Elastic net-based polygenic risk scores for VCDR were trained using the ML-predicted VCDR as the target label in 62,969 individuals using scikit-learn (Pedregosa et al. 2011). The Craig *et al.* model used 76 variants (the 58 described in the pruning and thresholding section above, plus 18 proxy variants present in both UK Biobank and EPIC-Norfolk that were in highest linkage disequilibrium ($R^2 \geq 0.6$) with the 18 dropped Craig *et al.* variants) and the ML-based model used the same 282 variants as described above. Each model was trained with 5-fold cross-validation and L1-penalty ratios of [0.1, 0.5, 0.7, 0.9, 0.95, 0.99, 1.0]. Model evaluation was performed in the same evaluation sets as described above. Both the UK Biobank and EPIC-Norfolk test sets were scored using the `plink --score` command and the correlations were computed using the scores in the resulting `*.profile` files.

Permutation P -values

A permutation test was applied to assess whether a polygenic risk score (PRS) trained using summary statistics from the ML-based GWAS significantly outperformed a PRS trained using summary statistics from the Craig *et al.* GWAS for predicting VCDR in the UK Biobank and EPIC-Norfolk cohorts. Phenotypic predictions were generated from both PRS. The test statistic was the difference in Pearson correlations between the observed and predicted phenotypes, comparing ML-based with Craig *et al.* A value exceeding zero indicates better performance by

the ML-based PRS. Under the null hypothesis, the predictions from both PRS are exchangeable. To obtain a realization from the null distribution, for each subject, the predictions of the ML-based and Craig *et al.* PRS were randomly swapped, and the difference in correlations was recalculated. This procedure was repeated 10^5 times to obtain the null distribution. The one-sided P value is given by the proportion of realizations from the null distribution that were as or more extreme than the observed difference in correlations.

Glaucoma Association

Mediation Analysis

A mediation analysis was performed to estimate the association between ML-derived VCDR and glaucoma, as assessed by Gharakhani *et al* (Gharakhani et al. 2020). MR is a special case of mediation analysis in which the SNPs have no direct effect on the outcome; that is, the effect of genotype on the phenotype passes entirely through the mediator. Our mediation analysis differs from MR in that, due to limited availability of summary statistics from Gharakhani *et al*, the SNP set was defined based on association with the mediator (ML-based VCDR) rather than the outcome (glaucoma). Among the 118 independent, significant glaucoma SNPs identified by Gharakhani *et al*, 116 remained after harmonizing with the VCDR summary statistics available from our study. As expected, Cochran's Q test provided strong evidence of pleiotropy ($P < 10^{-16}$), and the Egger intercept of 0.04 ($P = 7 \times 10^{-7}$) suggested that variants with tended to increase VCDR also tended to increase the odds of glaucoma via an alternative pathway. The Egger slope was 5.7 ($P = 3 \times 10^{-3}$; Supplementary Figure 7), which is interpreted as a log odds ratio, provides substantial evidence that increased VCDR was associated with increased glaucoma odds. This estimate of the association between VCDR and glaucoma remains valid, despite the presence of pleiotropy, since Egger regression is robust to the exclusion restriction (Bowden et al. 2017). In a reversed analysis using the same set of candidate SNPs, but regarding glaucoma as the mediator and VCDR as the outcome, the Egger intercept was 0.00 ($P = 0.09$), and the Egger slope was 0.02 ($P = 0.07$), providing no strong evidence of association in the opposite direction.

Glaucoma liability conditional analysis

One of the main advantages of the ML-based model is that we can apply our ML-based model to different phenotypes without additional cost. We computed the glaucoma liability (ML-based glaucoma) for the same set of individuals in UK Biobank for whom we had calculated VCDR as described above. We performed GWAS on glaucoma liability (logit scale of glaucoma probability), using BOLT-LMM, conditional on ML-based VCDR and all covariates included in the ML-based VCDR GWAS. The LD score regression intercept was 1.00 (SE=0.001), with a SNP-heritability of 0.06 (0.01). Moreover, QQ-plot is depicted in Supplementary Figure 9.

UK Biobank glaucoma phenotype

UK Biobank participants who underwent an ophthalmic examination also completed an ophthalmic touchscreen questionnaire and were considered to have POAG if they responded "Glaucoma" to the question "Has a doctor told you that you have any of the following problems with your eyes?". Participants were also considered to have POAG if they had a recorded hospital episode statistic ICD 10 code for POAG (H40.1). Controls were defined as participants who underwent the ophthalmic touchscreen questionnaire but did not meet the criteria to be a case. Additionally, we excluded participants with an ICD 9/10 hospital episode statistic code for types of glaucoma types other than POAG (ICD 9: 365.*; ICD 10: H40.0, H40.2, H40.3, H40.4, H40.5, H40.6, H40.8, H40.9, H42.*), participants meeting the case criteria but reporting an age of glaucoma onset prior to 30 years, and participants reporting glaucoma laser treatment or eye surgery but not reporting glaucoma on the touchscreen questionnaire. Applying these criteria, there were 7,654 cases and 182,726 controls.

EPIC-Norfolk cohort

The European Prospective Investigation into Cancer (EPIC) study is a pan-European prospective cohort study designed to investigate the etiology of major chronic diseases (Riboli and Kaaks 1997). EPIC-Norfolk, one of the UK arms of EPIC, recruited and examined 25,639 participants between 1993 and 1997 for the baseline examination (Day et al. 1999). Recruitment was via general practices in the city of Norwich and the surrounding small towns and rural areas, and methods have been described in detail previously (Hayat et al. 2014). Since virtually all residents in the UK are registered with a general practitioner through the National Health Service, general practice lists serve as population registers. Ophthalmic assessment formed part of the third health examination and this has been termed the EPIC-Norfolk Eye Study (Khawaja et al. 2013).

In total, 8,623 participants were seen for the Eye Study between 2004 and 2011. Ophthalmic examination included tonometry (Ocular Response Analyzer; Reichert, New York, USA; software V.3.01), optic disc photography (Nikon D80 camera; Nikon Corporation, Tokyo, Japan), scanning laser ophthalmoscopy (Heidelberg Retinal Tomograph 3; Heidelberg Engineering, Heidelberg, Germany) and nerve fiber layer assessment (GDx-VCC; Zeiss, Dublin, California, USA). Participants meeting pre-defined criteria and an additional 1:10 participants underwent automated visual field testing (Humphrey 750i Visual Field Analyzer; Carl Zeiss Meditech Ltd, Welwyn Garden City, UK). 99.7% of EPIC-Norfolk are of European descent. The EPIC-Norfolk Eye Study was carried out following the principles of the Declaration of Helsinki and the Research Governance Framework for Health and Social Care. The study was approved by the Norfolk Local Research Ethics Committee (05/Q0101/191) and East Norfolk & Waveney NHS Research Governance Committee (2005EC07L). All participants gave written, informed consent.

Ascertainment of POAG in the EPIC Norfolk third health examination has been described previously (Chan et al. 2017). In brief, participants with study results suspicious of glaucoma (using pre-defined criteria) were referred for further examination by a glaucoma specialist at the

regional University Hospital (Khawaja et al. 2013). Additionally, a diagnosis refinement process was undertaken by a second glaucoma specialist who independently reviewed the test results of all participants classified as glaucoma and a proportion of participants who were not classified as having glaucoma. POAG was defined as the presence of a glaucomatous optic disc together with either a corresponding visual field defect or otherwise unexplained non-specific visual field loss, open angles on gonioscopy, and absence of secondary causes of glaucoma. A glaucomatous disc was defined as one with focal or diffuse neuro-retinal rim thinning, and may possess, though not necessary for the definition, additional characteristic features such as bared circumlinear vessels, disc hemorrhages or nerve fiber layer defects. Pseudoexfoliative and pigmentary glaucoma were defined as secondary glaucoma in this study and therefore did not contribute to POAG cases. We defined controls as participants not meeting referral criteria for glaucoma on initial ophthalmic assessment and participants who attended the University Hospital for further examination and were not classified as having or being suspect for any type of glaucoma or ocular hypertension.

Initial genotyping on a small subset of EPIC-Norfolk was undertaken using the Affymetrix GeneChip Human Mapping 500K Array Set and 1,096 of these participants contributed to the IGGC meta-analysis (Springelkamp et al. 2017). Subsequently, the rest of the EPIC-Norfolk cohort were genotyped using the Affymetrix UK Biobank Axiom Array (the same array as used in UK Biobank); it is 5,868 of these participants (which includes no overlap with the 1,096 participants contributing to the IGGC meta-analysis) that contributed to the EPIC-Norfolk analyses in the current study. SNP exclusion criteria included: call rate < 95%, abnormal cluster pattern on visual inspection, plate batch effect evident by significant variation in minor allele frequency, and/or Hardy-Weinberg equilibrium $P < 10^{-7}$. Sample exclusion criteria included: DishQC < 0.82 (poor fluorescence signal contrast), sex discordance, sample call rate < 97%, heterozygosity outliers (calculated separately for SNPs with minor allele frequency >1% and <1%), rare allele count outlier, and impossible identity-by-descent values. We removed individuals with relatedness corresponding to third-degree relatives or closer across all genotyped participants. Following these exclusions, there were no ethnic outliers. Imputation was carried out using the HRC v1.

Quality control for HRT3 images included requiring a topography SD > 40 μm and checking of the manually drawn optic disc margin contours by an ophthalmologist (with redrawing if necessary). The mean HRT3 VCDR of right and left eyes was considered as the participant's VCDR if good quality scans were available for both eyes. If a good quality scan was only available for one eye, the VCDR value for that eye was considered for the participant.

Tables

Supplementary Table 1. Phenotype prediction model performance metrics. For VCDR Pearson's correlation is reported. AUC, area under ROC curve; AUPRC, area under precision-recall curve, RMSE, root mean square error. The numbers in parentheses are 95% confidence intervals.

Shared nomenclature for all GWAS results:

CHR, chromosome; POS, base-pair variant position; EA, effect allele; NEA, non-effect allele; EAF, effect allele frequency; BETA, estimated effect size; SE, standard error; P, GWAS *P*-value; NUM_INDV, sample size for the variant; SRC, imputed or genotyped variant; INFO, imputation INFO score (set to 1 for genotyped variants); CRAIG, locus replicated in Craig *et al.* GWAS, CRAIG_META, locus replicated in Craig *et al.* meta-analysis; GENE_CONTEXT: genomic context of the variant, as explained below.

- Overlapping gene(s)
 - [A]: variant overlaps gene A
 - [A,B]: variant overlaps genes A and B
- Downstream genes
 - []A: variant position is $0 < p \leq 10^3$ bp upstream of closest downstream gene A
 - []-A: variant position is $10^3 < p \leq 10^4$ bp upstream of closest downstream gene A
 - []--A: variant position is $10^4 < p \leq 10^5$ bp upstream of closest downstream gene A
 - []---A: variant position is $10^5 < p \leq 10^6$ bp upstream of closest downstream gene A
 - []: closest downstream gene is further than 10^6 bp
- Upstream genes
 - The notation for upstream genes is similar, but gene A is on the left side, e.g., B-[] means variant position is $10^3 < p \leq 10^4$ bp downstream of closest gene B

For example, **FOXD2-- []---TRABD2B** indicates the variant is $10^4 < p \leq 10^5$ downstream of *FOXD2* and $10^5 < p \leq 10^6$ upstream of *TRABD2B*.

Supplementary Table 2. ML-based VCDR GWAS independent GWS hits ($R^2 \leq 0.1$, $P \leq 5 \times 10^{-8}$).

Supplementary Table 3. ML-based VCDR GWAS independent GWS loci ($R^2 \leq 0.1$, $P \leq 5 \times 10^{-8}$, distance between top hits > 250k).

Supplementary Table 4. SuSiE per-SNP results for all fine-mapped SNPs. PIP is the posterior probability the SNP is causal, higher being more likely; and LOCUS_IDX is a locus identifying index (as defined in Supplementary Table 3). SNPs with PIP = 0 are not shown. Not included due to large size; available upon request.

Supplementary Table 5. SuSiE results summarized per-locus. N_FINEMAPPED is the number of SNPs in loci with PIPs available. N_GWS is the number of genome-wide significant SNPs with $MAF > 0.05$. N_CAUSAL is the sum of PIPs across SNPs in the locus. The estimated number of causal SNPs for a locus is $\min(N_GWS, N_CAUSAL)$.

Supplementary Table 6. ML-based + IGGC VCDR meta-analysis independent GWS hits ($R^2 \leq 0.1$, $P \leq 5 \times 10^{-8}$).

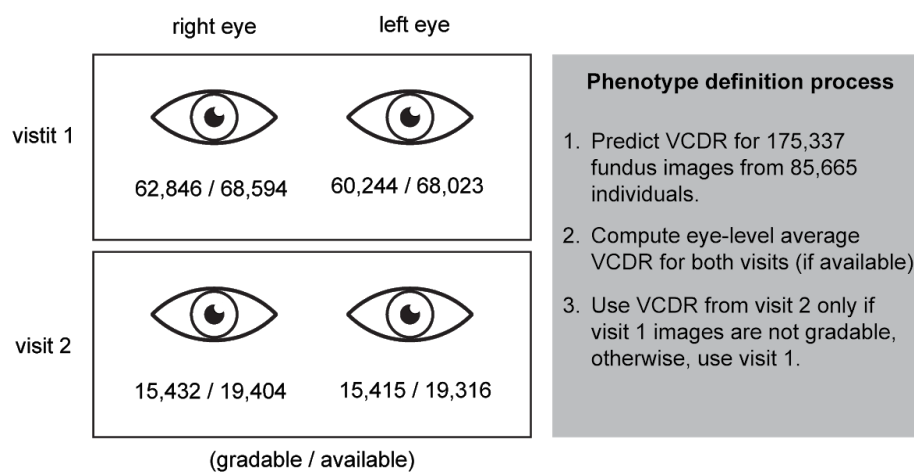
Supplementary Table 7. ML-based + IGGC VCDR meta-analysis independent GWS loci ($R^2 \leq 0.1$, $P \leq 5 \times 10^{-8}$, distance between top hits > 250k).

Supplementary Table 8. All GREAT ontology terms significant for at least one of the two sets of loci. All terms in the ontologies of Supplementary Figure 7 were tested. Abbreviations: ML *P-val*, the Bonferroni-corrected *P* value for the region-based test with the ML-based GWAS loci; Craig *P-val*, the Bonferroni-corrected *P* value for the region-based test with the Craig *et al.* GWAS loci; GOBP, Gene Ontology Biological Process; MP1KO, Mouse Phenotype Single Knockout; HP, Human Phenotype.

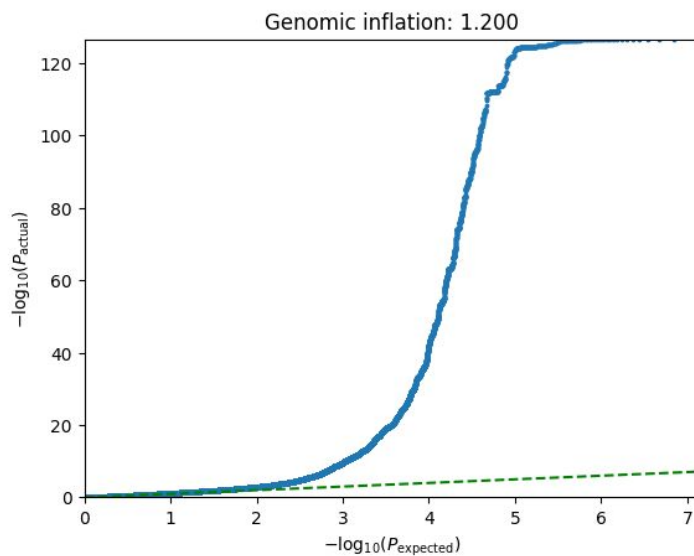
Supplementary Table 9. ML-based glaucoma risk conditioned on ML-based VCDR independent GWS hits ($R^2 \leq 0.1$, $P \leq 5 \times 10^{-8}$).

Supplementary Table 10. ML-based glaucoma risk conditioned on ML-based VCDR independent GWS loci ($R^2 \leq 0.1$, $P \leq 5 \times 10^{-8}$, distance between top hits > 250k).

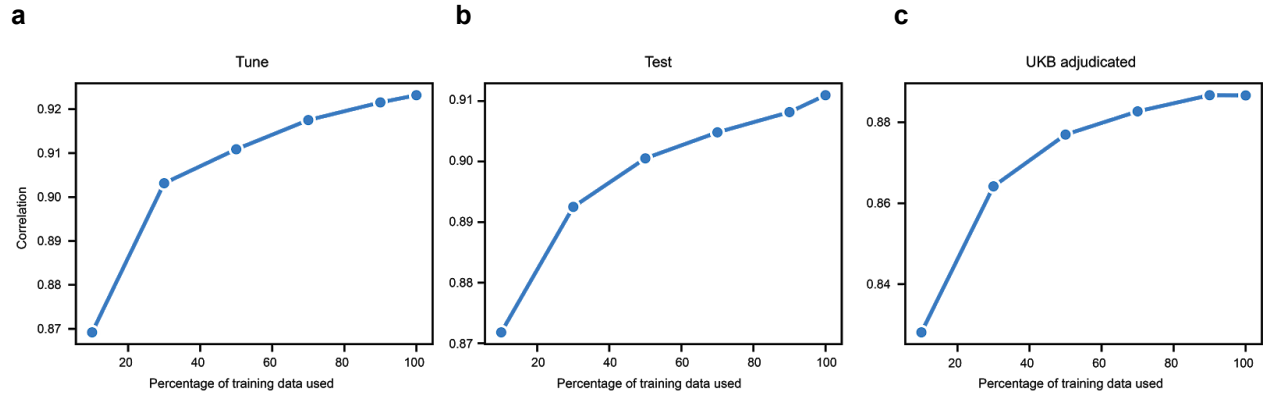
Figures



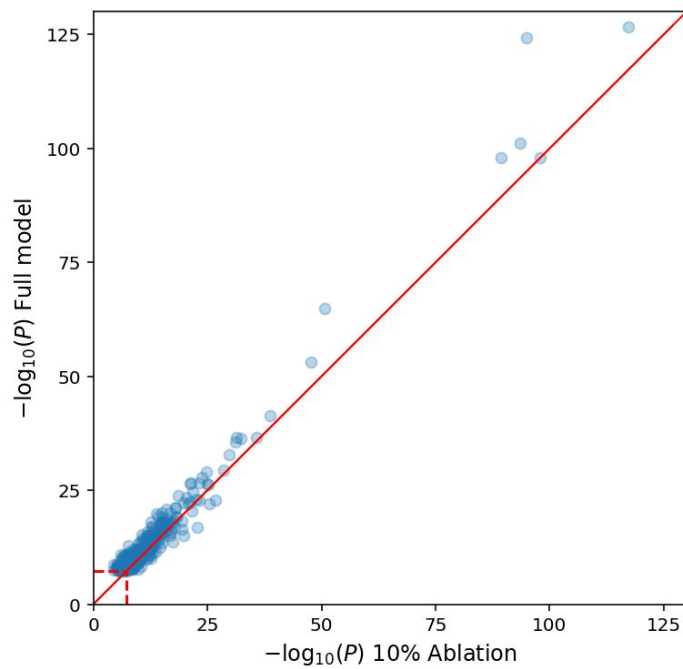
Supplementary Figure 1. VCDR phenotype calling process. The numbers below each eye indicate gradable / available images.



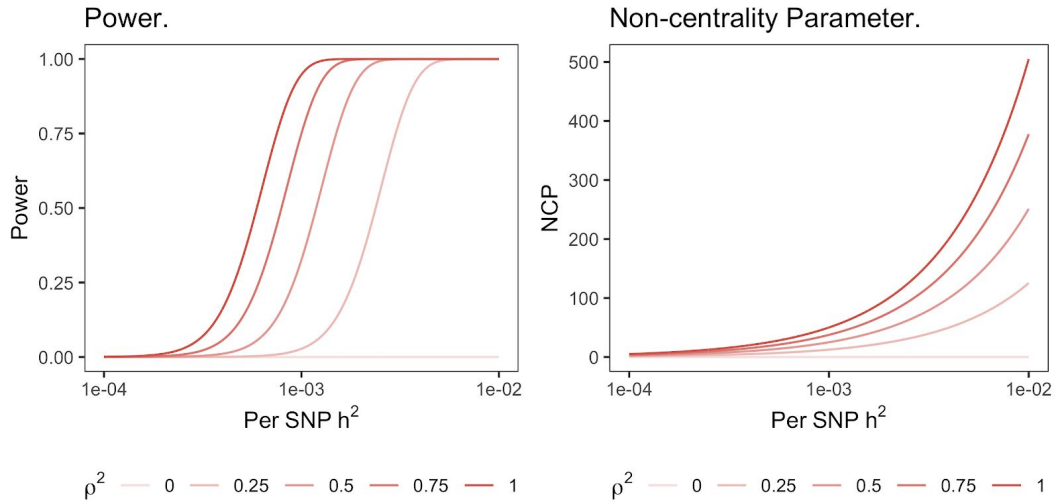
Supplementary Figure 2. QQ-plot for the ML-based VCDR GWAS. The expected P values are based on a uniform distribution.



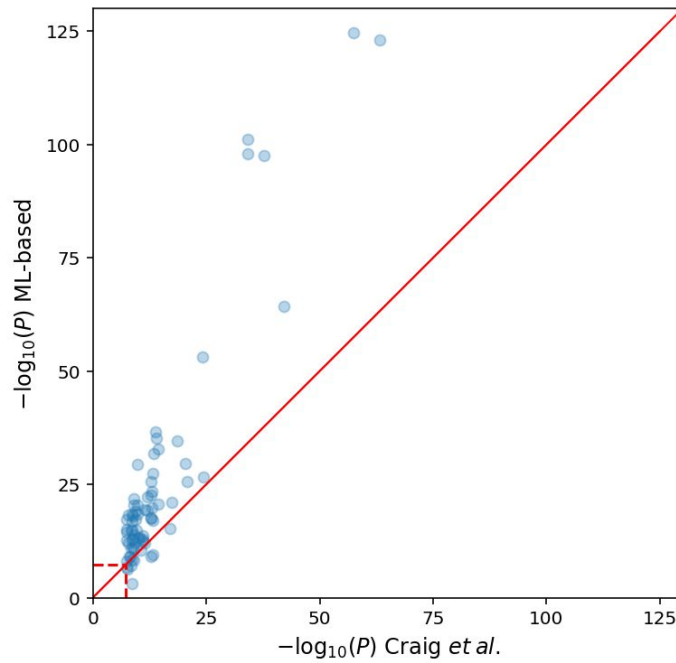
Supplementary Figure 3. VCDR model performance as a function of the percentage of training data samples used to train the model. Pearson's correlation between the model-predicted VCDR and the expert-labeled VCDR at training data percentages from 10% to 100% for **a**, the tune dataset, **b**, the test dataset, and **c**, the UKB adjudicated dataset. See **Model Training and Evaluation** section for detailed dataset definitions.



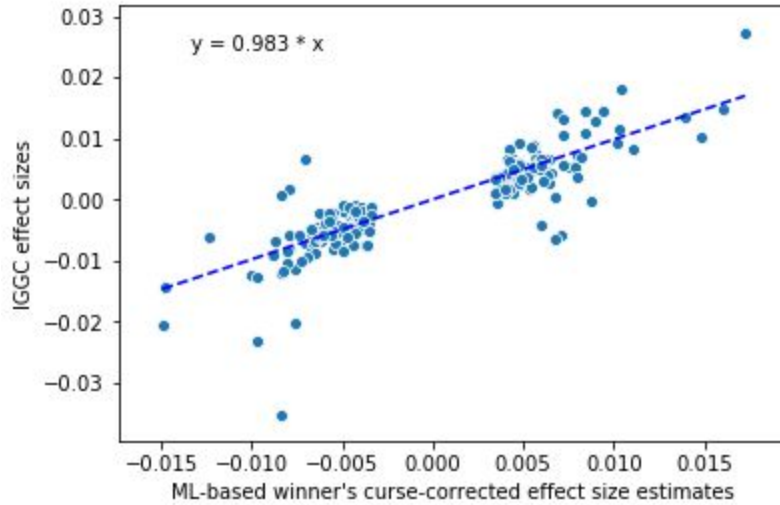
Supplementary Figure 4. Comparison of the Full model P values with the 10% Ablation P values for 299 Full model hits. The dashed red horizontal and vertical lines indicate the GWS level ($P < 5 \times 10^{-8}$).



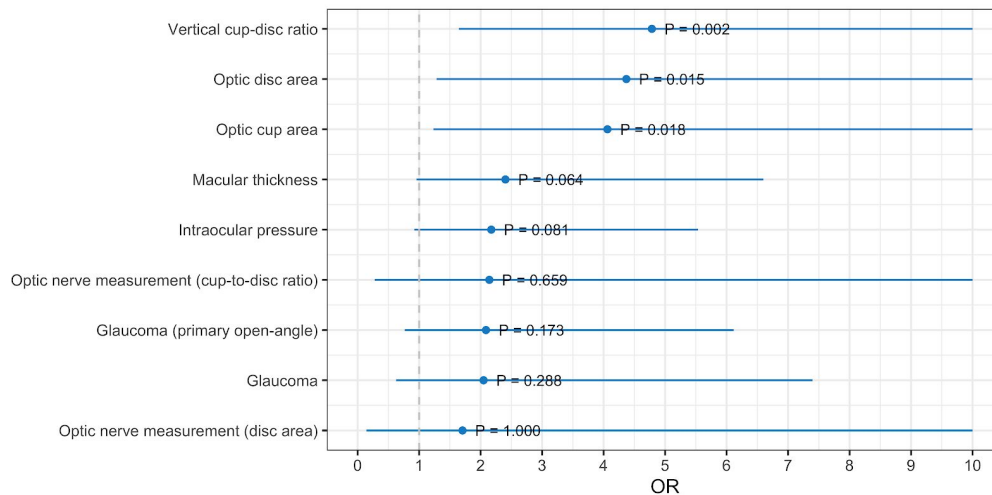
Supplementary Figure 5. Power and non-centrality curves as a function of per-SNP heritability. The curves are stratified by the correlation between the mismeasured and true phenotypes. Sample size was set to $n=50,000$; changing the sample sizes amounts to horizontally shifting the power curves. The range of per-SNP heritabilities was selected to demonstrate the inflection points of the power curves.



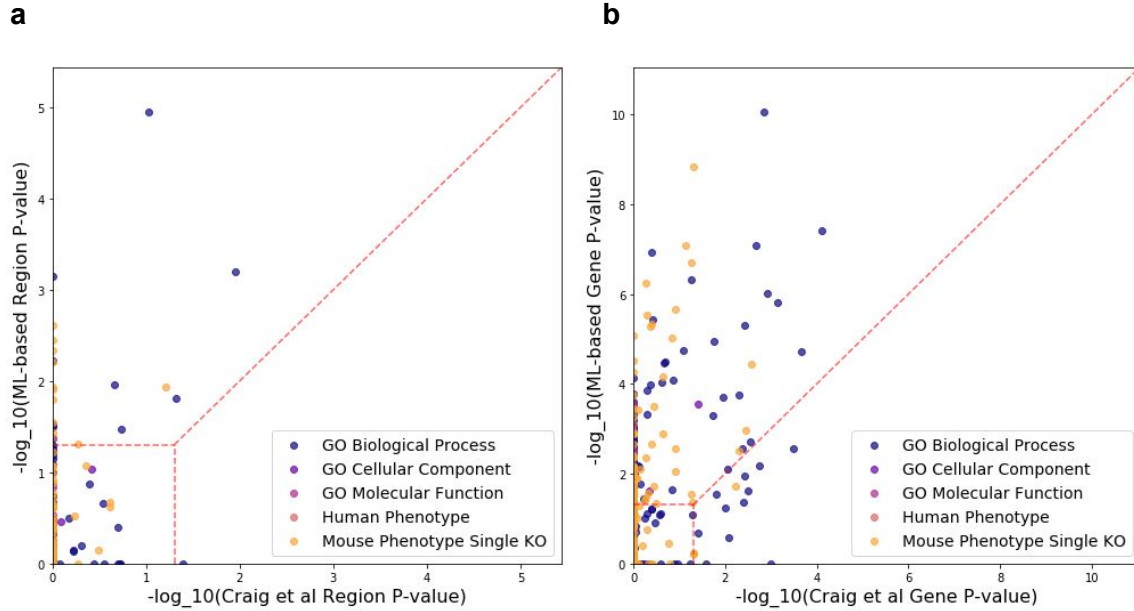
Supplementary Figure 6. Comparison of ML-based VCDR P values with the Craig *et al.* P values for 73 Craig *et al.* hits. The dashed red horizontal and vertical lines indicate the GWS level ($P < 5 \times 10^{-8}$).



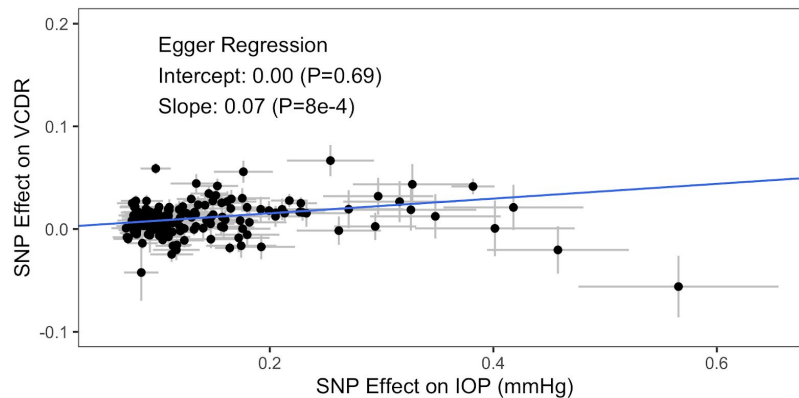
Supplementary Figure 7. Regression of IGGC VCDR meta-analysis effect sizes on winner's curse-corrected ML-based VCDR effect size estimates. Of 299 independent GWS hits, 214 were present in IGGC. Regression slope was computed with intercept fixed to zero. The dotted blue line shows the line of best fit.



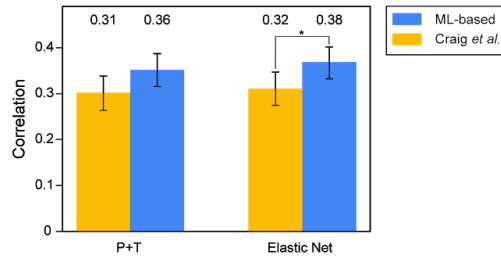
Supplementary Figure 8. FUMA enrichment of eye-related gene sets from the ML-based VCDR GWAS versus the VCDR GWAS of Craig *et al.* Enrichment is quantified via the odds ratio, with confidence interval and *P* value provided by Fisher's exact test.



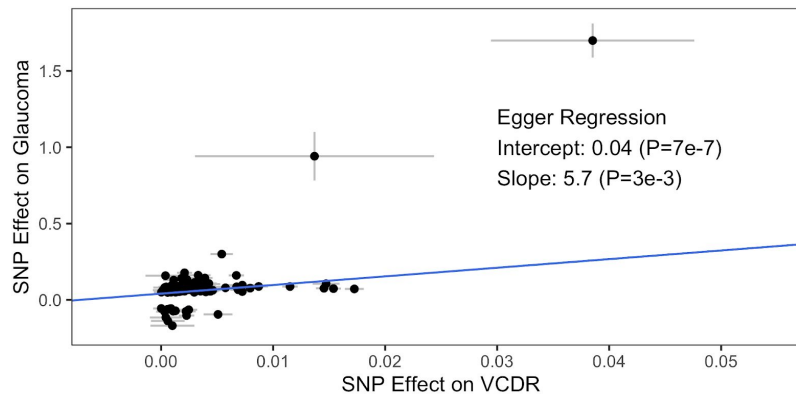
Supplementary Figure 9. GREAT enrichment of loci from the ML-based VCDR GWAS vs the VCDR GWAS of Craig *et al.* **a**, Comparison of Bonferroni-corrected P values for the region-based test reported by GREAT for the five listed ontologies. Dashed horizontal and vertical lines show the threshold for statistical significance at a Bonferroni-corrected $P \leq 0.05$, and the diagonal line indicates $y=x$. More ontology terms are statistically significant for the ML-derived GWAS than Craig *et al.* **b**, Comparison analogous to that in **a**, for the gene-based test.



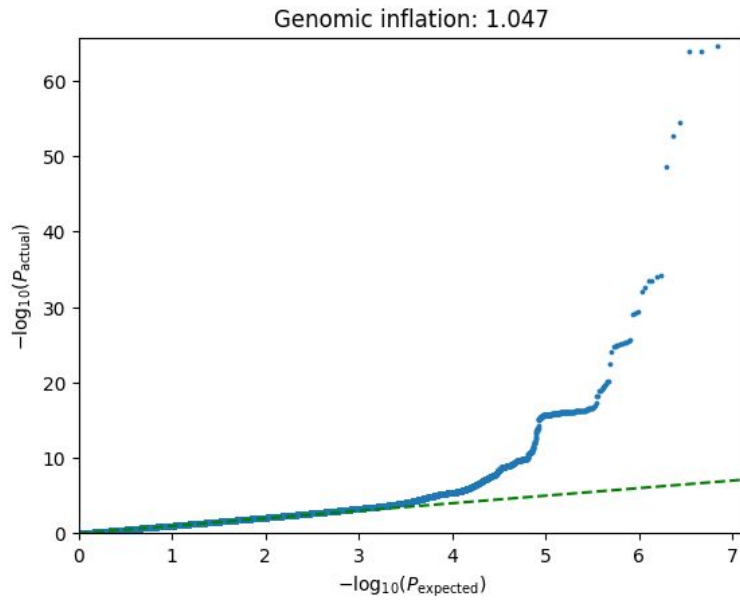
Supplementary Figure 10. Egger Regression for Mendelian Randomization of the effect of IOP on ML-based VCDR. Independent, significant IOP-associated SNPs were ascertained from Khawaja *et al.* and harmonized with GWAS results for ML-based VCDR.



Supplementary Figure 11. VCDR polygenic risk score performance metrics on the UKB imputation panel. Pearson's correlations between measured VCDR values and predictions of the pruning and thresholding (P+T) and the Elastic Net models are shown for the PRS learned from ML-based and Craig *et al.* hits. Error bars depict 95% confidence intervals. Numbers above bars are the observed Pearson's correlations. Indications of P value ranges: * $P \leq 0.05$, ** $P \leq 0.01$, *** $P \leq 0.001$. Measured VCDR values were obtained from adjudicated expert labeling of CFPs (UKB, n=2,076).



Supplementary Figure 12. Egger Regression for Mendelian Randomization of the Effect of VCDR on Glaucoma log Odds. Independent, significant Glaucoma risk SNPs were ascertained from Gharahkhani *et al.* and harmonized with GWAS results from ML-based VCDR.



Supplementary Figure 13. QQ-plot for the ML-based glaucoma liability GWAS conditional on ML-based VCDR. The expected P values are based on a uniform distribution.

Model hyper-parameters

The hyper-parameters used very closely follow (Krause et al. 2018; Phene et al. 2019):

- Inception V3 architecture
- Input image resolution: 587 x 587
- Learning rate: 0.001
- Batch size: 16
- Data augmentation:
 - Random horizontal reflections
 - Random vertical reflections
 - Random brightness changes (with a max delta of 0.1147528) [TensorFlow function `tf.image.random_brightness`]
 - Random saturation changes between 0.5597273 and 1.2748845 [`tf.image.random_saturation`]
 - Random hue changes (with a max delta of 0.0251488) [`tf.image.random_hue`]
 - Random contrast changes between 0.9996807 and 1.7704824 [`tf.image.random_contrast`]

References

- Abadi, Martín, Ashish Agarwal, Paul Barham, Eugene Brevdo, Zhifeng Chen, Craig Citro, Greg S. Corrado, et al. 2016. "TensorFlow: Large-Scale Machine Learning on Heterogeneous Distributed Systems." *arXiv [cs.DC]*. arXiv. <http://arxiv.org/abs/1603.04467>.
- Age-Related Eye Disease Study Research Group. 1999. "The Age-Related Eye Disease Study (AREDS): Design Implications. AREDS Report No. 1." *Controlled Clinical Trials* 20 (6): 573–600.
- Bulik-Sullivan, Brendan K., Po-Ru Loh, Hilary K. Finucane, Stephan Ripke, Jian Yang, Schizophrenia Working Group of the Psychiatric Genomics Consortium, Nick Patterson, Mark J. Daly, Alkes L. Price, and Benjamin M. Neale. 2015. "LD Score Regression Distinguishes Confounding from Polygenicity in Genome-Wide Association Studies." *Nature Genetics* 47 (3): 291–95.
- Chan, Michelle P. Y., David C. Broadway, Anthony P. Khawaja, Jennifer L. Y. Yip, David F. Garway-Heath, Jennifer M. Burr, Robert Luben, et al. 2017. "Glaucoma and Intraocular Pressure in EPIC-Norfolk Eye Study: Cross Sectional Study." *BMJ* 358 (September): j3889.
- Chatterjee, Nilanjan, Jianxin Shi, and Montserrat García-Closas. 2016. "Developing and Evaluating Polygenic Risk Prediction Models for Stratified Disease Prevention." *Nature Reviews. Genetics* 17 (7): 392–406.
- Day, N., S. Oakes, R. Luben, K. T. Khaw, S. Bingham, A. Welch, and N. Wareham. 1999. "EPIC-Norfolk: Study Design and Characteristics of the Cohort. European Prospective Investigation of Cancer." *British Journal of Cancer* 80 Suppl 1 (July): 95–103.
- Deng, Jia, Wei Dong, Richard Socher, Li-Jia Li, Kai Li, and Li Fei-Fei. 2009. "ImageNet: A Large-Scale Hierarchical Image Database." *2009 IEEE Conference on Computer Vision and Pattern Recognition*. <https://doi.org/10.1109/cvpr.2009.5206848>.
- Gharakhani, Puya, Eric Jorgenson, Pirro Hysi, Anthony P. Khawaja, Sarah Pendergrass, Xikun Han, Jue Sheng Ong, et al. 2020. "A Large Cross-Ancestry Meta-Analysis of Genome-Wide Association Studies Identifies 69 Novel Risk Loci for Primary Open-Angle Glaucoma and Includes a Genetic Link with Alzheimer's Disease." *bioRxiv*. <https://doi.org/10.1101/2020.01.30.927822>.
- Han, Buhm, and Eleazar Eskin. 2011. "Random-Effects Model Aimed at Discovering Associations in Meta-Analysis of Genome-Wide Association Studies." *American Journal of Human Genetics* 88 (5): 586–98.
- Hayat, Shabina A., Robert Luben, Victoria L. Keevil, Stephanie Moore, Nichola Dalzell, Amit Bhaniani, Anthony P. Khawaja, et al. 2014. "Cohort Profile: A Prospective Cohort Study of Objective Physical and Cognitive Capability and Visual Health in an Ageing Population of Men and Women in Norfolk (EPIC-Norfolk 3)." *International Journal of Epidemiology* 43 (4): 1063–72.
- Higgins, Julian P. T., and Simon G. Thompson. 2002. "Quantifying Heterogeneity in a Meta-Analysis." *Statistics in Medicine* 21 (11): 1539–58.
- Hormozdiari, Farhad, Eun Yong Kang, Michael Bilow, Eyal Ben-David, Chris Vulpe, Stela McLachlan, Aldons J. Lusis, Buhm Han, and Eleazar Eskin. 2016. "Imputing Phenotypes for Genome-Wide Association Studies." *American Journal of Human Genetics* 99 (1): 89–103.
- Khawaja, Anthony P., Michelle P. Y. Chan, Shabina Hayat, David C. Broadway, Robert Luben, David F. Garway-Heath, Justin C. Sherwin, et al. 2013. "The EPIC-Norfolk Eye Study:

- Rationale, Methods and a Cross-Sectional Analysis of Visual Impairment in a Population-Based Cohort." *BMJ Open* 3 (3). <https://doi.org/10.1136/bmjopen-2013-002684>.
- Krause, Jonathan, Varun Gulshan, Ehsan Rahimy, Peter Karth, Kasumi Widner, Greg S. Corrado, Lily Peng, and Dale R. Webster. 2018. "Grader Variability and the Importance of Reference Standards for Evaluating Machine Learning Models for Diabetic Retinopathy." *Ophthalmology* 125 (8): 1264–72.
- Lawrence, Michael, Wolfgang Huber, Hervé Pagès, Patrick Aboyoun, Marc Carlson, Robert Gentleman, Martin T. Morgan, and Vincent J. Carey. 2013. "Software for Computing and Annotating Genomic Ranges." *PLoS Computational Biology* 9 (8): e1003118.
- Loh, Po-Ru, George Tucker, Brendan K. Bulik-Sullivan, Bjarni J. Vilhjálmsson, Hilary K. Finucane, Rany M. Salem, Daniel I. Chasman, et al. 2015. "Efficient Bayesian Mixed-Model Analysis Increases Association Power in Large Cohorts." *Nature Genetics* 47 (3): 284–90.
- McCaw, Zachary R., Hanna Julienne, and Hugues Aschard. 2020. "MGMM: An R Package for Fitting Gaussian Mixture Models on Incomplete Data." *Cold Spring Harbor Laboratory*. <https://doi.org/10.1101/2019.12.20.884551>.
- McCaw, Zachary R., Jacqueline M. Lane, Richa Saxena, Susan Redline, and Xihong Lin. 2019. "Operating Characteristics of the Rank-Based Inverse Normal Transformation for Quantitative Trait Analysis in Genome-Wide Association Studies." *Biometrics*, December. <https://doi.org/10.1111/biom.13214>.
- McLean, Cory Y., Dave Bristor, Michael Hiller, Shoa L. Clarke, Bruce T. Schaar, Craig B. Lowe, Aaron M. Wenger, and Gill Bejerano. 2010. "GREAT Improves Functional Interpretation of Cis-Regulatory Regions." *Nature Biotechnology* 28 (5): 495–501.
- Meng, Xiao-Li, and Donald B. Rubin. 1993. "Maximum Likelihood Estimation via the ECM Algorithm: A General Framework." *Biometrika* 80 (2): 267–78.
- Pedregosa, Fabian, Gaël Varoquaux, Alexandre Gramfort, Vincent Michel, Bertrand Thirion, Olivier Grisel, Mathieu Blondel, et al. 2011. "Scikit-Learn: Machine Learning in Python." *Journal of Machine Learning Research: JMLR* 12 (85): 2825–30.
- Phene, Sonia, R. Carter Dunn, Naama Hammel, Yun Liu, Jonathan Krause, Naho Kitade, Mike Schaekermann, et al. 2019. "Deep Learning and Glaucoma Specialists." *Ophthalmology* 126 (12): 1627–39.
- Prechelt, Lutz. 1998. "Early Stopping - But When?" In *Neural Networks: Tricks of the Trade*, edited by Genevieve B. Orr and Klaus-Robert Müller, 55–69. Berlin, Heidelberg: Springer Berlin Heidelberg.
- Riboli, E., and R. Kaaks. 1997. "The EPIC Project: Rationale and Study Design. European Prospective Investigation into Cancer and Nutrition." *International Journal of Epidemiology* 26 Suppl 1: S6–14.
- Serfling, Robert J. 1980. *Approximation Theorems of Mathematical Statistics*. Wiley.
- Shorten, Connor, and Taghi M. Khoshgoftaar. 2019. "A Survey on Image Data Augmentation for Deep Learning." *Journal of Big Data* 6 (1): 60.
- Springelkamp, Henriët, Adriana I. Iglesias, Aniket Mishra, René Höhn, Robert Wojciechowski, Anthony P. Khawaja, Abhishek Nag, et al. 2017. "New Insights into the Genetics of Primary Open-Angle Glaucoma Based on Meta-Analyses of Intraocular Pressure and Optic Disc Characteristics." *Human Molecular Genetics* 26 (2): 438–53.
- Szegedy, Christian, Vincent Vanhoucke, Sergey Ioffe, Jon Shlens, and Zbigniew Wojna. 2016. "Rethinking the Inception Architecture for Computer Vision." *2016 IEEE Conference on Computer Vision and Pattern Recognition (CVPR)*. <https://doi.org/10.1109/cvpr.2016.308>.
- Turley, Patrick, Raymond K. Walters, Omeed Maghizian, Aysu Okbay, James J. Lee, Mark Alan Fontana, Tuan Anh Nguyen-Viet, et al. 2018. "Multi-Trait Analysis of Genome-Wide

Association Summary Statistics Using MTAG.” *Nature Genetics* 50 (2): 229–37.

Wang, Gao, Abhishek Sarkar, Peter Carbonetto, and Matthew Stephens. 2020. “A Simple New Approach to Variable Selection in Regression, with Application to Genetic Fine Mapping.” *Journal of the Royal Statistical Society. Series B, Statistical Methodology* 25 (July): 1.

Watanabe, Kyoko, Erdogan Taskesen, Arjen van Bochoven, and Danielle Posthuma. 2017. “Functional Mapping and Annotation of Genetic Associations with FUMA.” *Nature Communications* 8 (1): 1826.

Supplementary Information - Table 1. Model performance metrics

Dataset	Gradable	Graders	VCDR (RMSE)	VCDR (correlation)	Glaucoma risk (AUC)	Glaucoma risk (AUPRC)	Glaucoma risk prevalence
Train	69,460	1-2	0.106 (0.105-0.106)	0.803 (0.800-0.806)	0.896 (0.894-0.899)	0.734 (0.727-0.741)	22.6%
Tune	1,399	3	0.073 (0.069-0.077)	0.923 (0.915-0.931)	0.964 (0.952-0.975)	0.820 (0.768-0.866)	11.5%
Test	1,076	3	0.079 (0.074-0.085)	0.911 (0.899-0.922)	0.957 (0.944-0.969)	0.860 (0.817-0.898)	18.1%
UKB Adjudicated	2,115	2-3	0.092 (0.088-0.096)	0.886 (0.876-0.896)	0.872 (0.854-0.890)	0.506 (0.446-0.567)	13.3%

Supplementary Information - Table 2. ML-based VCDR (hits)

CHR	POS	SNP	EA	NEA	EAF	BETA	SE	P	NUM_INDV	SRC	INFO	GENE_CONTEXT
1	3049362	rs12024620	C	T	0.936	-1.55E-02	1.38E-03	4.00E-30	65680	Imputed	0.995	[PRDM16]
1	3055876	rs10797380	A	G	0.551	-4.06E-03	6.99E-04	8.30E-10	65680	Imputed	0.936	[PRDM16]
1	8468278	rs301792	A	G	0.662	-4.62E-03	7.13E-04	6.80E-13	65680	Imputed	0.998	[RERE]
1	12614029	rs6541032	T	C	0.424	-5.11E-03	6.82E-04	2.60E-14	65680	Imputed	0.999	VPS13D-[]-DHRS3
1	47923058	rs767682581	C	CT	0.374	-4.27E-03	7.07E-04	1.40E-10	65680	Imputed	0.983	FOXD2-[]-TRABD2B
1	68773910	rs34151819	C	T	0.983	1.78E-02	2.61E-03	4.50E-13	65654	Genotyped	1	WLS-[]-RPE65
1	68840797	rs2209559	A	G	0.601	-7.49E-03	6.91E-04	1.90E-28	65484	Genotyped	1	WLS-[]-RPE65
1	89253357	rs786908	A	G	0.383	-4.31E-03	6.95E-04	3.90E-10	65680	Imputed	0.997	[PKN2]
1	92016934	rs61798047	C	T	0.486	4.77E-03	6.79E-04	6.50E-15	65680	Imputed	0.994	CDC7-[]-TGFBFR3
1	92024124	rs75296423	T	G	0.98	-1.78E-02	2.49E-03	5.20E-14	65680	Imputed	0.942	CDC7-[]-TGFBFR3
1	92030967	rs7536573	C	A	0.675	5.05E-03	7.28E-04	2.30E-15	65680	Imputed	0.984	CDC7-[]-TGFBFR3
1	92070810	rs77291384	G	A	0.986	-1.76E-02	3.04E-03	4.10E-09	65680	Imputed	0.897	CDC7-[]-TGFBFR3
1	92077097	rs1192415	G	A	0.188	1.76E-02	8.63E-04	7.60E-102	65610	Genotyped	1	CDC7-[]-TGFBFR3
1	92089160	rs17569923	G	A	0.799	7.09E-03	8.52E-04	1.70E-18	65680	Imputed	0.981	CDC7-[]-TGFBFR3
1	92114938	rs12046642	A	G	0.82	-7.17E-03	8.81E-04	4.00E-16	65680	Imputed	0.99	CDC7-[]-TGFBFR3
1	110627923	rs10857812	T	A	0.636	4.63E-03	7.03E-04	2.10E-11	65680	Imputed	0.993	STRIP1-[]-UBL4B
1	113045061	rs351364	A	T	0.252	-3.95E-03	7.81E-04	2.40E-08	65680	Imputed	0.984	[WNT2B]
1	155033308	rs11589479	G	A	0.837	4.88E-03	9.17E-04	1.20E-08	65404	Genotyped	1	[ADAM15]
1	169551682	rs6028	T	C	0.709	-4.03E-03	7.44E-04	3.10E-09	65680	Imputed	0.996	[F5]
1	183849739	rs41263652	G	C	0.896	7.20E-03	1.12E-03	4.20E-11	65680	Imputed	0.971	[RGL1]
1	218520995	rs6658835	A	G	0.73	-5.97E-03	7.64E-04	7.60E-16	65680	Imputed	0.992	[TGFB2]
1	219573841	rs796959510	C	CT	0.491	-4.02E-03	6.82E-04	7.40E-09	65680	Imputed	0.979	AL360093.1-[]-ZC3H11B
1	222014897	rs11118873	A	G	0.485	3.74E-03	6.79E-04	4.20E-10	65680	Imputed	0.988	DUSP10-[]-HHIPL2
1	227585983	rs6670351	G	A	0.798	-6.66E-03	8.42E-04	3.30E-17	65680	Imputed	0.993	CDC42BPA-[]-ZNF678
2	5680539	rs7575439	C	A	0.358	4.09E-03	7.27E-04	1.50E-08	62872	Genotyped	1	LINC01249-[]-AC108025.1
2	12891476	rs730126	A	C	0.587	3.98E-03	6.95E-04	9.50E-10	65680	Imputed	0.985	TRIB2-[]
2	19307666	rs76455252	C	G	0.926	-7.80E-03	1.30E-03	1.10E-09	65680	Imputed	0.99	NT5C1B-[]-OSR1
2	19431423	rs72778352	C	T	0.987	2.71E-02	2.97E-03	4.80E-22	65680	Imputed	0.982	NT5C1B-[]-OSR1
2	19472235	rs851359	T	C	0.443	5.55E-03	6.81E-04	8.00E-17	65680	Imputed	0.998	NT5C1B-[]-OSR1
2	56072501	rs1430202	G	A	0.798	8.29E-03	8.51E-04	1.80E-24	65680	Imputed	0.99	PNPT1-[]-EFEMP1
2	56102744	rs11899888	A	G	0.841	-5.44E-03	9.34E-04	9.30E-10	65680	Imputed	0.987	[EFEMP1]
2	56210465	rs11303332	G	C	0.786	-4.83E-03	8.51E-04	6.90E-09	65680	Imputed	0.949	EFEMP1-[]-CCDC85A
2	111658010	rs4849203	A	G	0.652	5.07E-03	7.12E-04	1.30E-13	65575	Genotyped	1	[ACOXL]
2	180196027	rs12620141	C	A	0.636	-4.06E-03	7.18E-04	2.50E-09	65680	Imputed	0.961	AC093911.1-[]-ZNF385B
2	190269957	2:190269957_CTTT_C	CTTT	C	0.308	4.16E-03	7.40E-04	3.00E-09	65680	Imputed	0.99	COL5A2-[]-WDR75
2	233389918	rs2853447	A	G	0.297	-3.75E-03	7.44E-04	3.80E-08	65680	Imputed	0.987	[PRSS56]
3	20061023	rs35057657	A	G	0.327	4.06E-03	7.27E-04	4.30E-08	65680	Imputed	0.991	PP2D1-[]-KAT2B
3	25046463	rs12490228	C	T	0.717	-6.08E-03	7.54E-04	3.50E-17	65680	Imputed	0.996	THR-B-AS1-[]-RARB
3	25187193	rs73048443	A	G	0.822	7.10E-03	8.91E-04	1.00E-15	65680	Imputed	0.981	THR-B-AS1-[]-RARB
3	25194626	rs143822311	A	AGTGT	0.438	-4.53E-03	7.01E-04	9.50E-11	65680	Imputed	0.956	THR-B-AS1-[]-RARB
3	29493916	rs9822629	T	G	0.626	-3.71E-03	7.02E-04	1.50E-08	65680	Imputed	0.992	[AC098650.1,RBMS3]
3	32879823	rs56131903	A	T	0.679	6.19E-03	7.34E-04	3.90E-18	65680	Imputed	0.983	[TRIM71]
3	48719638	rs7633840	T	C	0.337	4.72E-03	7.39E-04	1.60E-11	65680	Imputed	0.949	[NCKIPSD]
3	57988028	3:57988028_AAAAT_A	AAAAT	A	0.76	-5.33E-03	7.94E-04	1.20E-11	65680	Imputed	0.998	SLMAP-[]-FLNB
3	58130168	rs2362911	A	G	0.771	-5.34E-03	8.06E-04	3.30E-12	65680	Imputed	0.991	[FLNB]
3	70061377	rs190948281	G	C	0.997	4.43E-02	6.00E-03	1.60E-13	65680	Imputed	0.944	MITF-[]-MDFIC2
3	71182447	rs77877421	A	T	0.943	-1.16E-02	1.50E-03	1.60E-15	65680	Imputed	0.964	[FOX P1,AC097634.4]
3	88380417	rs9852080	T	C	0.448	6.19E-03	6.83E-04	3.70E-21	65680	Imputed	0.996	C3orf38-[]-CSNKA2IP
3	89603917	rs373216501	A	ATATT	0.697	4.27E-03	7.72E-04	3.60E-08	65680	Imputed	0.91	EPHA3-[]
3	98943479	rs13076500	C	T	0.461	-6.73E-03	6.87E-04	9.90E-24	65680	Imputed	0.979	DCBLD2-[]-AC107029.1
3	99078606	rs1871794	T	C	0.748	-8.53E-03	7.82E-04	9.40E-30	65680	Imputed	0.996	DCBLD2-[]-AC107029.1
3	99313686	3:99313686_CAG_C	CAG	C	0.953	-1.11E-02	1.61E-03	1.70E-12	65680	Imputed	0.997	AC107029.1-[]-COL8A1
3	99377999	rs34578241	T	C	0.897	9.30E-03	1.11E-03	1.20E-18	65680	Imputed	0.999	[COL8A1]
3	99707371	rs61144932	A	AG	0.322	-3.95E-03	7.53E-04	9.00E-09	65680	Imputed	0.932	[CMSS1,FILIP1L]
3	100625703	rs17398137	G	A	0.82	8.75E-03	8.90E-04	1.20E-23	65523	Genotyped	1	[ABI3BP]
3	106117209	rs12637686	G	A	0.721	-4.14E-03	7.57E-04	3.50E-09	65680	Imputed	0.993	CBLB-[]-LINC00882
3	128196500	rs2713594	G	A	0.583	-3.68E-03	6.94E-04	4.20E-08	65680	Imputed	0.983	DNAJB8-[]-GATA2
3	134089758	rs143351962	C	T	0.99	-2.15E-02	3.40E-03	7.40E-10	65680	Imputed	1	[AMOTL2]
4	7917204	rs34939228	T	TA	0.617	-4.17E-03	7.05E-04	8.30E-09	65680	Imputed	0.984	[AFAP1]
4	54979145	rs1158402	C	T	0.378	5.88E-03	7.03E-04	6.80E-19	65680	Imputed	0.996	[AC058822.1]
4	55095682	rs565335773	G	GA	0.792	5.84E-03	8.48E-04	9.80E-13	65680	Imputed	0.973	[AC058822.1,PDGFRA]
4	79122057	rs372050829	G	GTA	0.775	4.46E-03	8.46E-04	2.40E-08	65680	Imputed	0.933	[FRAS1]
4	79396057	4:79396057_TC_T	TC	T	0.367	4.02E-03	7.10E-04	2.00E-08	65680	Imputed	0.995	[FRAS1]
4	112399511	rs2661764	A	T	0.638	4.03E-03	7.09E-04	7.30E-09	65680	Imputed	0.995	PITX2-[]-FAM241A
4	126239986	rs1039808	C	T	0.547	4.23E-03	6.85E-04	5.90E-10	65550	Genotyped	1	[FAT4]
4	126407298	rs532857051	C	CTT	0.708	6.06E-03	7.51E-04	4.70E-17	65680	Imputed	0.993	[FAT4]
4	128053375	4:128053375_AACAC_A	AACAC	A	0.52	3.51E-03	6.96E-04	1.60E-08	65680	Imputed	0.953	[]-INTU
5	3646121	rs13165326	C	T	0.672	-3.77E-03	7.25E-04	2.40E-08	65680	Imputed	0.991	IRX1-[]-LINC02063

Supplementary Information - Table 2. ML-based VCDR (hits)

CHR	POS	SNP	EA	NEA	EAF	BETA	SE	P	NUM_INDV	SRC	INFO	GENE_CONTEXT
5	31952051	rs72759609	T	C	0.898	1.35E-02	1.13E-03	2.40E-37	65680	Imputed	0.989	[PDZD2]
5	31966417	rs10045838	G	A	0.585	-3.68E-03	6.98E-04	1.80E-08	65680	Imputed	0.974	[PDZD2]
5	55578661	rs158653	G	A	0.477	5.06E-03	6.85E-04	1.30E-14	65680	Imputed	0.992	ANKRD55---[---LINC01948
5	55701667	rs140212185	C	CTTTTTT	0.496	-3.96E-03	6.86E-04	6.40E-10	65680	Imputed	0.983	ANKRD55---[---LINC01948
5	55744230	rs30372	T	C	0.237	-5.15E-03	8.07E-04	9.40E-12	65680	Imputed	0.978	ANKRD55---[---LINC01948
5	55781912	rs12187324	T	G	0.918	-7.70E-03	1.24E-03	8.60E-10	65680	Imputed	0.996	LINC01948-[---C5orf67
5	82770558	rs11746859	A	G	0.539	4.77E-03	6.82E-04	8.90E-13	65680	Imputed	0.995	[VCAN]
5	87810199	rs150221399	G	A	0.919	-9.99E-03	1.28E-03	3.80E-15	65680	Imputed	0.95	TMEM161B---[---MEF2C
5	121765728	rs2570981	T	C	0.401	4.30E-03	6.93E-04	1.10E-09	65680	Imputed	0.994	[SNCAIP]
5	128931357	rs7448395	G	A	0.204	6.62E-03	8.47E-04	8.00E-17	65680	Imputed	0.999	[ADAMTS19]
5	129100923	rs75047204	G	A	0.885	5.54E-03	1.07E-03	4.60E-08	65680	Imputed	0.987	[MINAR2]
5	131466629	rs3843503	T	A	0.55	4.25E-03	6.94E-04	1.90E-11	65680	Imputed	0.979	CSF2-[---AC063976.1
5	133393380	5:133393380_GA_G	GA	G	0.844	7.22E-03	1.01E-03	3.30E-13	65680	Imputed	0.858	VDAC1-[---TCF7
5	172197790	rs34013988	C	T	0.961	1.46E-02	1.75E-03	4.10E-18	65680	Imputed	0.998	[AC022217.4,DUSP1]
6	593289	6:593289_TG_T	TG	T	0.869	-7.47E-03	1.05E-03	2.60E-14	65680	Imputed	0.913	[EXOC2]
6	1548369	rs2745572	A	G	0.666	4.35E-03	7.26E-04	3.10E-09	65680	Imputed	0.99	FOXF2---[---FOXC1
6	1983440	rs6914444	T	C	0.866	9.30E-03	1.01E-03	9.70E-22	65680	Imputed	0.987	[GMD5]
6	7211818	rs1334576	G	A	0.572	-5.94E-03	6.92E-04	1.60E-18	65515	Genotyped	1	[RREB1]
6	11411838	rs7742703	C	T	0.905	6.43E-03	1.16E-03	8.60E-09	65680	Imputed	0.996	NEDD9-[---TMEM170B
6	31133577	rs145919884	A	AAAGCCC	0.35	4.45E-03	7.18E-04	3.40E-10	65680	Imputed	0.996	[TCF19,POU5F1]
6	31158633	rs9263861	A	G	0.879	6.21E-03	1.05E-03	4.40E-09	65680	Imputed	0.998	POU5F1-[---HC627
6	36552592	rs200252984	G	A	0.79	-7.25E-03	8.47E-04	9.90E-21	65680	Imputed	0.973	STK38-[---SRSF3
6	39537880	rs9369128	T	C	0.651	-6.39E-03	7.15E-04	5.30E-20	65680	Imputed	0.998	[KIF6]
6	122392511	rs2684249	T	C	0.593	6.38E-03	6.95E-04	9.00E-19	65680	Imputed	0.995	GJA1---[---HSF2
6	126767600	rs1361108	C	T	0.543	-6.05E-03	6.89E-04	1.60E-17	65542	Genotyped	1	CENPW-[---RSPO3
6	127289089	rs4897198	C	A	0.548	-4.56E-03	6.88E-04	2.70E-11	65680	Imputed	1	CENPW-[---RSPO3
6	148832343	rs139973521	A	ATGAG	0.89	-7.36E-03	1.10E-03	3.80E-13	65680	Imputed	0.987	[SASH1]
6	149989744	6:149989744_AT_A	AT	A	0.648	4.99E-03	7.24E-04	2.10E-12	65680	Imputed	0.988	[LATS1]
6	151295133	rs6900628	A	G	0.708	4.20E-03	7.55E-04	2.20E-08	65475	Genotyped	1	[MTHFD1L]
7	4767112	rs6946034	A	T	0.52	-3.68E-03	6.86E-04	3.00E-09	65680	Imputed	0.983	[FOXK1]
7	14237240	rs10260511	C	A	0.842	-7.78E-03	9.37E-04	5.90E-19	65597	Genotyped	1	[DGKB]
7	19612305	rs2192476	C	T	0.372	4.26E-03	7.06E-04	2.00E-11	65680	Imputed	0.993	FERD3L---[---TWISTNB
7	28393403	rs7805378	A	C	0.559	4.60E-03	6.86E-04	1.20E-11	65680	Imputed	0.994	[CREB5]
7	28844815	rs2282909	T	G	0.269	4.09E-03	7.70E-04	1.40E-08	65680	Imputed	0.999	[CREB5]
7	42108499	rs2237417	C	T	0.593	3.69E-03	6.99E-04	4.00E-08	65680	Imputed	0.987	[GLI3]
7	101808020	rs6976947	A	G	0.604	4.41E-03	6.97E-04	8.70E-12	65680	Imputed	0.997	[CUX1]
8	8254590	rs2945880	A	G	0.113	-9.34E-03	1.08E-03	2.30E-19	65680	Imputed	0.994	PRAG1-[---AC114550.3
8	17526359	rs11203888	C	T	0.335	-4.18E-03	7.24E-04	2.80E-09	65680	Imputed	0.995	[MTUS1]
8	30336017	rs571194397	A	AT	0.817	-5.07E-03	9.12E-04	1.70E-08	65680	Imputed	0.923	[RBPMS]
8	30386291	rs7013873	C	T	0.784	4.49E-03	8.32E-04	7.90E-10	65680	Imputed	0.989	[RBPMS]
8	30510065	8:30510065_TA_T	TA	T	0.578	3.54E-03	6.98E-04	2.30E-08	65680	Imputed	0.977	[GTF2E2]
8	61911070	rs10957177	A	G	0.749	4.57E-03	7.94E-04	6.80E-09	65680	Imputed	0.978	CHD7-[---CLVS1
8	72278010	rs12543430	T	C	0.39	-6.08E-03	7.11E-04	1.10E-17	65680	Imputed	0.962	[EYA1]
8	72392687	rs10093418	A	G	0.893	6.99E-03	1.12E-03	7.40E-11	65680	Imputed	0.977	[EYA1]
8	72579250	rs10453110	C	T	0.874	-9.94E-03	1.04E-03	8.50E-23	65680	Imputed	0.99	EYA1-[---AC104012.2
8	75522500	rs10957731	A	C	0.402	5.12E-03	6.96E-04	3.70E-14	65680	Imputed	0.994	[MIR2052HG]
8	75532622	rs2081498	C	A	0.936	8.58E-03	1.40E-03	2.40E-10	65680	Imputed	0.986	[MIR2052HG]
8	76025955	rs11991447	C	T	0.756	4.78E-03	7.98E-04	2.80E-09	65680	Imputed	0.984	CRISPLD1-[---HNF4G
8	78948855	rs6999835	T	C	0.634	3.93E-03	7.10E-04	2.00E-09	65680	Imputed	0.996	[---PKIA
8	88664409	rs200382882	G	C	0.485	-4.07E-03	6.86E-04	7.60E-11	65680	Imputed	0.997	CNBD1-[---DCAF4L2
8	131606303	8:131606303_CTGTT_C	CTGTT	C	0.647	3.90E-03	7.18E-04	4.20E-08	65680	Imputed	0.986	ASAP1---[---ADCY8
9	15912375	rs10810475	G	C	0.564	3.67E-03	6.87E-04	1.20E-08	65680	Imputed	0.998	[CCDC171]
9	16619529	rs13290470	A	G	0.603	5.52E-03	6.97E-04	7.20E-19	65680	Imputed	0.991	[BNC2]
9	18089275	rs10738500	C	A	0.927	-9.11E-03	1.31E-03	3.90E-12	65680	Imputed	0.99	[ADAMTSL1]
9	21951175	rs117197971	A	G	0.945	-1.03E-02	1.60E-03	1.30E-11	65680	Imputed	0.855	[AL359922.1]
9	22007330	rs3217978	C	A	0.984	1.53E-02	2.84E-03	3.20E-08	65680	Imputed	0.914	[AL359922.1,CDKN2B-AS1,CDKN2B]
9	22044904	rs74744824	A	G	0.984	-1.85E-02	3.00E-03	2.30E-09	65680	Imputed	0.801	[CDKN2B-AS1]
9	22051670	rs944801	G	C	0.428	-1.57E-02	6.90E-04	5.30E-125	65680	Imputed	0.999	[CDKN2B-AS1]
9	22052068	rs62560775	A	G	0.898	-7.81E-03	1.13E-03	1.50E-12	65680	Imputed	0.993	[CDKN2B-AS1]
9	22082375	rs1547705	A	C	0.877	-8.34E-03	1.08E-03	8.50E-16	65680	Imputed	0.923	[CDKN2B-AS1]
9	22090416	rs10965230	C	T	0.949	1.07E-02	1.62E-03	2.20E-11	65680	Imputed	0.903	[CDKN2B-AS1]
9	76622068	rs11143754	C	A	0.573	4.29E-03	6.90E-04	3.40E-10	65680	Imputed	0.994	AL451127.1---[---AL355674.1
9	89252706	rs10512176	T	C	0.722	-6.49E-03	7.76E-04	1.70E-17	65680	Imputed	0.985	TUT7---[---GAS1
9	89380805	rs1111066	C	G	0.516	3.70E-03	6.85E-04	7.80E-09	65680	Imputed	0.989	TUT7---[---GAS1
9	134563185	rs11793533	G	A	0.719	5.28E-03	7.58E-04	2.80E-12	65419	Genotyped	1	[RAPGEF1]
9	136145414	rs587611953	C	A	0.836	-6.71E-03	1.02E-03	4.80E-13	65680	Imputed	0.824	[ABO]
10	14086579	rs7099081	A	G	0.663	3.85E-03	7.20E-04	2.00E-08	65680	Imputed	0.993	[FRMD4A]

Supplementary Information - Table 2. ML-based VCDR (hits)

CHR	POS	SNP	EA	NEA	EAF	BETA	SE	P	NUM_INDV	SRC	INFO	GENE_CONTEXT
10	21462896	10:21462896_GGC_G	GGC	G	0.987	-2.40E-02	3.08E-03	1.60E-15	65680	Imputed	0.943	[NEBL]
10	60271824	rs7069916	G	A	0.657	-3.95E-03	7.16E-04	5.50E-09	65680	Imputed	0.997	TFAM--[BICC1
10	69838913	rs117479359	G	T	0.917	8.56E-03	1.24E-03	2.70E-12	65680	Imputed	0.989	HERC4--[MYPN
10	69879366	rs113337354	A	G	0.875	6.12E-03	1.03E-03	8.60E-10	65680	Imputed	0.995	[MYPN]
10	69902549	rs3814180	T	C	0.395	-3.92E-03	7.11E-04	1.40E-08	65680	Imputed	0.953	[MYPN]
10	69926319	rs61854624	C	A	0.84	6.54E-03	9.31E-04	3.80E-14	65680	Imputed	1	[MYPN]
10	69974599	10:69974599_CG_C	CG	C	0.71	-6.42E-03	8.03E-04	9.90E-19	65680	Imputed	0.873	MYPN--[ATO7
10	69991853	rs7916697	A	G	0.24	-1.62E-02	7.98E-04	1.20E-98	65604	Genotyped	1	[ATO7]
10	70026190	rs112652264	G	A	0.977	1.74E-02	2.31E-03	9.90E-16	63682	Genotyped	1	ATO7--[PBLD
10	70041695	rs374085072	G	A	0.99	2.15E-02	3.81E-03	1.80E-09	65680	Imputed	0.828	ATO7--[PBLD
10	70206657	rs367873689	C	CA	0.955	1.46E-02	1.71E-03	1.30E-18	65680	Imputed	0.932	[DNA2]
10	70312849	rs4746777	C	T	0.154	-5.48E-03	9.46E-04	2.00E-09	65680	Imputed	0.989	SLC25A16--[TET1
10	70336105	10:70336105_CAA_C	CAA	C	0.535	-4.16E-03	6.85E-04	5.10E-10	65680	Imputed	0.994	[TET1]
10	70349416	rs546745967	C	T	0.974	1.80E-02	2.35E-03	9.20E-17	65680	Imputed	0.825	[TET1]
10	70467778	rs34117216	C	A	0.784	6.57E-03	8.26E-04	3.70E-18	65618	Genotyped	1	TET1--[CCAR1
10	70775081	rs2429022	T	C	0.833	4.80E-03	9.15E-04	2.00E-09	65680	Imputed	0.995	[KIFBP]
10	94974129	rs6583871	G	T	0.264	-5.05E-03	7.76E-04	1.70E-11	65680	Imputed	0.982	CYP26A1---[MYOF
10	96026184	10:96026184_CA_C	CA	C	0.565	-4.35E-03	6.91E-04	3.10E-10	65680	Imputed	0.995	[PLCE1]
10	96071561	rs2077218	G	A	0.238	5.02E-03	8.02E-04	3.80E-10	65680	Imputed	0.992	[PLCE1]
10	118546046	rs11197820	G	A	0.585	-6.17E-03	6.94E-04	2.90E-19	65680	Imputed	0.985	[HSPA12A]
10	118562571	10:118562571_AT_A	AT	A	0.067	-7.68E-03	1.37E-03	1.20E-08	65680	Imputed	0.978	[HSPA12A]
10	118918956	rs72840231	A	T	0.567	-4.64E-03	6.95E-04	1.80E-11	65680	Imputed	0.975	[MIR3663HG]
11	19960147	rs12807015	G	T	0.528	-3.98E-03	6.97E-04	8.90E-09	65680	Imputed	0.96	[NAV2]
11	31719504	11:31719504_CT_C	CT	C	0.233	7.13E-03	8.10E-04	9.60E-21	65680	Imputed	0.992	[ELP4]
11	57656794	rs35328629	T	TA	0.561	-4.29E-03	6.89E-04	2.00E-10	65680	Imputed	0.987	CTNND1--[OR9Q1
11	58405674	rs12799215	C	T	0.758	4.22E-03	7.96E-04	4.20E-08	65680	Imputed	0.996	CNTF--[GLYAT
11	63678128	rs199826712	T	TA	0.926	6.78E-03	1.34E-03	9.90E-09	65680	Imputed	0.948	[MARK2]
11	65091708	11:65091708_AGTGT_A	AGTGT	A	0.32	4.14E-03	7.57E-04	1.60E-08	65680	Imputed	0.931	[AP000944.5]
11	65240979	11:65240979_TAA_T	TAA	T	0.961	-9.80E-03	1.86E-03	1.30E-08	65680	Imputed	0.883	NEAT1--[SCYL1
11	65343399	rs547193816	C	CCCCGCT	0.797	9.19E-03	8.60E-04	2.00E-27	65680	Imputed	0.97	FAM89B-[EHB1L1
11	86666906	rs3758658	T	C	0.312	3.96E-03	7.36E-04	9.60E-09	65680	Imputed	0.987	FZD4--[TMEM135
11	86748437	rs2445575	T	C	0.807	4.90E-03	8.62E-04	7.30E-10	65680	Imputed	0.997	FZD4--[TMEM135
11	94533444	rs138059525	G	A	0.993	3.10E-02	4.07E-03	2.60E-14	65629	Genotyped	1	[AMOTL1]
11	95308854	rs11021221	T	A	0.831	7.22E-03	9.09E-04	3.60E-15	65680	Imputed	0.994	SES3---[FAM76B
11	130281735	rs10894194	T	C	0.797	5.26E-03	8.54E-04	1.50E-10	65680	Imputed	0.983	[ADAMTS8]
11	130288797	rs34248430	A	ACCT	0.282	-7.71E-03	7.72E-04	4.50E-27	65680	Imputed	0.961	[ADAMTS8]
11	130307542	rs56378410	T	C	0.974	-1.23E-02	2.15E-03	1.30E-09	65680	Imputed	0.979	ADAMTS8--[ADAMTS15
12	3353356	rs73047017	C	T	0.937	-8.15E-03	1.41E-03	6.00E-10	65680	Imputed	0.976	[TSPAN9]
12	26392080	rs16930371	A	G	0.816	4.97E-03	8.80E-04	4.80E-09	65283	Genotyped	1	[SSPN]
12	31067490	rs55710412	C	T	0.845	5.27E-03	9.65E-04	8.10E-09	65680	Imputed	0.948	CAPRIN2---[TSPAN11
12	48157019	rs12818241	C	T	0.84	6.29E-03	9.31E-04	1.10E-12	65680	Imputed	0.984	[RAPGEF3.SLC48A1]
12	76114872	rs6582298	G	A	0.595	5.67E-03	7.23E-04	9.30E-16	65680	Imputed	0.901	[AC078923.1]
12	83762921	12:83762921_CA_C	CA	C	0.358	-5.37E-03	7.31E-04	4.20E-14	65680	Imputed	0.943	TMTC2---[
12	83856540	rs12826083	G	A	0.859	-7.51E-03	1.00E-03	1.20E-14	65680	Imputed	0.948	TMTC2---[
12	83858003	rs76005250	G	A	0.941	1.06E-02	1.49E-03	4.70E-14	65680	Imputed	0.94	TMTC2---[
12	83861261	rs77725841	A	G	0.916	8.51E-03	1.24E-03	5.90E-14	65680	Imputed	0.969	TMTC2---[
12	84076137	rs55667441	A	G	0.558	1.58E-02	6.86E-04	2.50E-127	65680	Imputed	0.995	TMTC2---[
12	84119063	rs76513789	C	A	0.945	9.92E-03	1.50E-03	4.90E-12	65680	Imputed	0.994	TMTC2---[
12	84132842	rs1380758	A	G	0.088	7.41E-03	1.24E-03	2.20E-10	65680	Imputed	0.927	TMTC2---[
12	84135457	rs142121892	C	CA	0.666	7.49E-03	7.40E-04	6.30E-27	65680	Imputed	0.949	TMTC2---[
12	84141754	rs79301152	A	G	0.917	-8.96E-03	1.28E-03	1.80E-13	65680	Imputed	0.924	TMTC2---[
12	84154996	rs71450946	A	G	0.927	-8.72E-03	1.31E-03	9.30E-13	65545	Genotyped	1	TMTC2---[
12	84225935	rs7137822	A	T	0.654	7.24E-03	7.73E-04	8.50E-23	65680	Imputed	0.858	TMTC2---[
12	84234482	rs73154757	T	A	0.962	1.03E-02	1.80E-03	1.40E-09	65680	Imputed	0.97	TMTC2---[
12	84237124	12:84237124_CTAA_C	CTAA	C	0.948	9.14E-03	1.57E-03	4.50E-11	65680	Imputed	0.954	TMTC2---[
12	84359892	rs12423401	C	A	0.906	-9.42E-03	1.19E-03	3.30E-16	65680	Imputed	0.961	TMTC2---[SLC6A15
12	84404719	rs4772012	T	C	0.769	4.64E-03	8.10E-04	2.90E-11	65680	Imputed	0.992	TMTC2---[SLC6A15
12	84890667	rs71445008	C	CT	0.561	-5.27E-03	7.09E-04	4.10E-16	65680	Imputed	0.933	[SLC6A15
12	91816926	rs147377344	C	CTTTTACG	0.4	4.03E-03	7.03E-04	2.10E-08	65680	Imputed	0.977	DCN---[LINC01619
12	107073242	12:107073242_CA_C	CA	C	0.653	5.36E-03	7.17E-04	6.00E-15	65680	Imputed	0.988	[AC079385.1.RFX4]
12	108165360	rs2111281	A	C	0.636	-5.30E-03	7.07E-04	1.30E-13	65680	Imputed	0.995	PRDM4--[ASCL4
12	124665773	rs11057488	A	G	0.435	-4.85E-03	6.87E-04	8.50E-14	65680	Imputed	0.994	[RFLNA]
12	25778093	rs17081940	A	G	0.858	5.44E-03	9.90E-04	2.10E-09	65680	Imputed	0.978	[LINC01076]
13	36683268	rs9546383	T	C	0.754	-5.96E-03	7.95E-04	6.70E-16	65680	Imputed	0.992	[DLCK1]
13	51945741	rs9535652	G	A	0.834	5.41E-03	9.19E-04	4.10E-09	65680	Imputed	0.996	[INTS6]
13	109267985	rs10162202	T	C	0.722	6.97E-03	7.68E-04	6.10E-23	65680	Imputed	0.982	[MYO16]
13	110778747	13:110778747_CCTTTT_C	CCTTTT	C	0.641	-6.06E-03	7.31E-04	9.90E-18	65680	Imputed	0.945	IRS2---[COL4A1

Supplementary Information - Table 2. ML-based VCDR (hits)

CHR	POS	SNP	EA	NEA	EAF	BETA	SE	P	NUM_INDV	SRC	INFO	GENE_CONTEXT
14	23452128	rs3811183	C	G	0.6	-4.45E-03	7.01E-04	1.30E-12	65680	Imputed	0.987	AJUBA]-C14orf93
14	53991705	rs2077940	T	C	0.668	5.45E-03	7.24E-04	1.70E-14	65680	Imputed	0.997	DDHD1---[-AL163953.1
14	60808553	rs10162287	C	G	0.696	-7.65E-03	7.48E-04	2.60E-27	65680	Imputed	0.979	PPM1A---[-C14orf39
14	60914325	rs139811951	G	A	0.874	6.34E-03	1.04E-03	1.60E-10	65680	Imputed	0.976	[C14orf39]
14	61238781	rs12147818	G	A	0.993	2.88E-02	4.26E-03	8.10E-13	65680	Imputed	0.955	[MNAT1]
14	65081054	rs149761305	G	GCT	0.83	-7.31E-03	9.14E-04	7.40E-18	65680	Imputed	0.993	PPP1R36---[-PLEKHG3
14	85668732	rs11626115	G	A	0.949	-1.05E-02	1.58E-03	1.10E-10	65680	Imputed	0.947	[---FLRT2
14	85863058	rs2145865	T	A	0.456	4.32E-03	6.97E-04	3.30E-10	65680	Imputed	0.967	[---FLRT2
14	85922578	rs1289426	A	G	0.767	-6.91E-03	8.15E-04	6.80E-16	65680	Imputed	0.974	[---FLRT2
14	86021748	rs2018653	A	G	0.755	-5.84E-03	8.00E-04	3.90E-13	65680	Imputed	0.986	[FLRT2]
14	95957694	rs11160251	T	G	0.703	4.15E-03	7.47E-04	1.90E-09	65680	Imputed	0.991	SYNE3---[-GLRX5
15	71840327	rs35194812	T	C	0.839	-4.96E-03	9.39E-04	1.50E-09	65680	Imputed	0.975	[THSD4]
15	71882771	rs4776562	A	G	0.554	3.95E-03	7.27E-04	1.10E-09	65680	Imputed	0.892	[THSD4]
15	74230660	rs59755145	G	A	0.712	-4.23E-03	7.57E-04	2.90E-09	65680	Imputed	0.992	[LOXL1]
15	84484384	rs59199978	A	G	0.82	-6.14E-03	8.91E-04	6.00E-14	65680	Imputed	0.995	[ADAMTSL3]
15	99458902	rs28612945	C	T	0.794	6.20E-03	8.46E-04	7.80E-15	65547	Genotyped	1	[IGF1R]
15	101200873	rs34222435	C	T	0.865	-9.55E-03	1.00E-03	1.60E-23	65680	Imputed	0.991	ASB7---[-ALDH1A3
15	101200962	rs11452536	T	TA	0.374	-3.87E-03	7.12E-04	1.50E-09	65680	Imputed	0.98	ASB7---[-ALDH1A3
15	101751698	rs8043304	T	C	0.752	4.35E-03	7.95E-04	1.80E-08	65680	Imputed	0.995	[CHSY1]
16	51183728	rs11643654	C	A	0.389	-4.74E-03	7.00E-04	1.50E-10	65680	Imputed	0.997	[SALL1]
16	51341412	rs117537696	T	G	0.981	-1.73E-02	2.47E-03	2.10E-13	65680	Imputed	1	SALL1---[-HNRNPA1P48
16	51400539	rs57495036	C	G	0.972	-1.57E-02	2.06E-03	1.10E-14	65680	Imputed	0.993	SALL1---[-HNRNPA1P48
16	51416004	rs11111196	A	T	0.263	-9.50E-03	7.80E-04	2.20E-37	65680	Imputed	0.985	SALL1---[-HNRNPA1P48
16	51469726	rs8053277	T	C	0.303	1.11E-02	7.45E-04	6.90E-54	65680	Imputed	0.993	SALL1---[-HNRNPA1P48
16	51470928	rs71386559	C	T	0.96	1.36E-02	1.78E-03	2.10E-16	65680	Imputed	0.954	SALL1---[-HNRNPA1P48
16	51526098	rs12443961	T	C	0.494	5.00E-03	6.90E-04	2.90E-14	65680	Imputed	0.977	SALL1---[-HNRNPA1P48
16	51573106	rs143024692	C	A	0.991	2.24E-02	3.68E-03	1.20E-10	65680	Imputed	0.953	SALL1---[-HNRNPA1P48
16	51590885	rs116257475	C	T	0.915	-1.50E-02	1.22E-03	4.40E-37	65680	Imputed	0.995	[HNRNPA1P48]
16	51649796	16:51649796_CTCTT_C	CTCTT	C	0.644	-4.71E-03	7.46E-04	8.90E-10	65680	Imputed	0.907	[HNRNPA1P48]
16	51667131	rs8057507	T	C	0.533	-6.92E-03	6.85E-04	3.00E-27	65680	Imputed	0.993	[HNRNPA1P48]
16	51855425	rs2892063	G	A	0.371	-4.62E-03	7.19E-04	1.20E-11	65680	Imputed	0.966	HNRNPA1P48---[-TOX3
16	74226221	rs807293	T	C	0.636	-4.41E-03	7.10E-04	7.70E-11	65680	Imputed	0.996	ZFX3---[-PSMD7
16	74404812	rs11865100	C	T	0.869	6.31E-03	1.07E-03	9.30E-10	65680	Imputed	0.875	PSMD7---[-NPIP15
16	74458445	rs77199494	T	G	0.967	-1.09E-02	1.99E-03	3.30E-08	65680	Imputed	0.932	[AC009053.4]
16	86366644	rs3762872	C	T	0.487	3.65E-03	6.86E-04	1.00E-08	65680	Imputed	0.99	IRF8---[-FOXF1
16	86380293	rs1687628	T	C	0.09	1.21E-02	1.19E-03	2.10E-25	65680	Imputed	0.992	IRF8---[-FOXF1
16	86403160	rs17178451	A	G	0.468	-4.12E-03	6.84E-04	1.90E-09	65680	Imputed	0.996	IRF8---[-FOXF1
16	86439374	rs12935509	G	A	0.919	-8.16E-03	1.25E-03	1.50E-11	65680	Imputed	0.992	IRF8---[-FOXF1
16	86465590	rs13332095	G	A	0.899	-6.32E-03	1.13E-03	6.10E-09	65680	Imputed	0.991	IRF8---[-FOXF1
16	86513683	16:86513683_GCA_G	GCA	G	0.224	5.95E-03	8.30E-04	7.00E-14	65680	Imputed	0.975	IRF8---[-FOXF1
17	40867365	rs115818584	C	G	0.984	1.62E-02	2.73E-03	1.70E-09	65680	Imputed	0.984	[EZH1]
17	45438886	rs769594276	C	CAGTG	0.548	-4.05E-03	6.88E-04	4.40E-11	65680	Imputed	0.997	[EFCAB13]
17	48225686	rs4794104	C	G	0.838	-5.48E-03	9.29E-04	9.00E-10	65680	Imputed	0.995	[PPP1R9B]
17	61865670	17:61865670_CT_C	CT	C	0.637	-4.25E-03	7.28E-04	2.40E-10	65680	Imputed	0.947	[DDX42]
17	65073835	rs577377763	C	CA	0.642	-4.45E-03	7.38E-04	4.50E-09	65680	Imputed	0.925	[HELZ]
17	80169426	rs796355894	A	AT	0.592	3.96E-03	7.09E-04	1.60E-08	65680	Imputed	0.956	[CDC57]
18	8797487	rs569735	C	A	0.269	4.57E-03	7.89E-04	1.00E-08	65680	Imputed	0.961	[MTCL1]
18	23063159	rs766791666	T	TATC	0.415	-4.02E-03	7.05E-04	4.00E-10	65680	Imputed	0.971	ZNF521---[-SS18
18	34289285	rs61735998	G	T	0.974	1.37E-02	2.17E-03	1.20E-10	65680	Imputed	1	[FHOD3]
18	56943484	rs77759734	C	T	0.951	-8.73E-03	1.59E-03	1.00E-09	65493	Genotyped	1	[CPLX4]
19	817708	rs7250902	A	G	0.681	5.21E-03	7.45E-04	3.40E-12	65680	Imputed	0.966	[PLPPR3]
19	14616371	rs11882319	C	A	0.851	5.31E-03	9.65E-04	6.00E-09	65680	Imputed	0.982	[GPC1]-[DNAJB1
19	32027330	rs8102936	G	A	0.658	6.80E-03	7.26E-04	1.10E-19	65680	Imputed	0.987	TSHZ3---[-ZNF507
19	33523197	rs73039431	A	G	0.955	-1.04E-02	1.66E-03	3.70E-10	65680	Imputed	0.984	[RHPN2]
19	39146780	rs55876653	G	C	0.508	-4.15E-03	6.84E-04	7.40E-10	65680	Imputed	0.997	[ACTN4]
20	1029686	rs4816177	A	G	0.821	-5.44E-03	9.01E-04	4.10E-10	64868	Genotyped	1	RSP04---[-PSMF1
20	6155721	rs751223591	C	CT	0.287	6.23E-03	7.63E-04	5.80E-17	65680	Imputed	0.984	FERMT1---[-LINC01713
20	6229367	rs55708193	C	A	0.799	-5.76E-03	8.58E-04	8.60E-12	65680	Imputed	0.99	FERMT1---[-LINC01713
20	6420731	rs6117259	T	C	0.812	-6.22E-03	8.75E-04	8.20E-13	65680	Imputed	0.996	FERMT1---[-LINC01713
20	6470094	rs2326788	G	A	0.628	1.17E-02	7.07E-04	1.60E-65	65680	Imputed	0.992	FERMT1---[-LINC01713
20	6474916	rs11483156	C	CT	0.889	-7.26E-03	1.10E-03	4.80E-11	65680	Imputed	0.964	FERMT1---[-LINC01713
20	6514692	rs6038531	G	A	0.016	-1.93E-02	2.72E-03	4.80E-13	65680	Imputed	0.976	FERMT1---[-LINC01713
20	6535065	rs78004679	G	A	0.941	1.16E-02	1.48E-03	1.50E-16	65680	Imputed	0.959	FERMT1---[-LINC01713
20	6544738	rs73077173	C	T	0.959	9.85E-03	1.73E-03	8.70E-10	65593	Genotyped	1	FERMT1---[-LINC01713
20	6631055	rs1358805	A	G	0.825	-5.71E-03	9.02E-04	1.90E-10	65680	Imputed	0.992	FERMT1---[-LINC01713
20	6759115	rs235768	A	T	0.391	-5.08E-03	7.01E-04	2.60E-13	65595	Genotyped	1	[BMP2]
20	31157394	rs4911242	A	T	0.678	4.21E-03	7.35E-04	4.20E-09	65680	Imputed	0.992	[NOL4L]

Supplementary Information - Table 2. ML-based VCDR (hits)

CHR	POS	SNP	EA	NEA	EAF	BETA	SE	P	NUM_INDV	SRC	INFO	GENE_CONTEXT
20	31438954	rs4911268	A	G	0.816	6.64E-03	8.85E-04	1.80E-15	65680	Imputed	0.998	MAPRE1[]-EFCAB8
20	45797259	rs3091590	C	T	0.544	-4.29E-03	6.87E-04	1.10E-10	65680	Imputed	0.991	[EYA2]
22	28208528	rs11704137	C	G	0.745	-6.84E-03	7.84E-04	6.10E-20	65680	Imputed	0.998	MN1-[]-PITPNB
22	28358946	rs5762423	A	G	0.056	-1.27E-02	1.53E-03	1.80E-16	65680	Imputed	0.942	[TTC28-AS1]
22	28501414	rs77885044	C	T	0.985	3.49E-02	2.77E-03	3.70E-42	65624	Genotyped	1	[TTC28]
22	28629713	rs16986177	C	T	0.84	-9.02E-03	9.32E-04	3.80E-23	65680	Imputed	0.996	[TTC28]
22	28653727	22:28653727_CATAT_C	CATAT	C	0.593	4.71E-03	7.37E-04	7.50E-11	65680	Imputed	0.886	[TTC28]
22	28925406	rs34320674	C	A	0.951	9.15E-03	1.61E-03	2.70E-09	65680	Imputed	0.964	[TTC28]
22	28990300	rs117456789	C	T	0.948	9.66E-03	1.59E-03	2.40E-09	65680	Imputed	0.938	[TTC28]
22	29063037	rs542574575	C	T	0.538	4.59E-03	7.21E-04	2.00E-11	65680	Imputed	0.902	[TTC28]
22	29115066	rs4822983	C	T	0.677	1.49E-02	7.29E-04	1.30E-98	65680	Imputed	0.999	[CHEK2]
22	29127402	rs8184952	T	C	0.158	8.04E-03	9.38E-04	9.80E-20	65680	Imputed	0.996	[CHEK2]
22	29162191	rs145346186	A	C	0.955	1.20E-02	1.67E-03	7.30E-15	65680	Imputed	0.956	HSCB-[]-CCDC117
22	29405956	rs4580479	T	G	0.452	-4.89E-03	6.92E-04	9.80E-14	65680	Imputed	0.98	[ZNRF3]
22	30592487	rs713875	C	G	0.446	6.54E-03	6.86E-04	4.50E-24	65568	Genotyped	1	[AC002378.1]
22	30606986	rs9614164	C	T	0.781	4.98E-03	8.29E-04	4.00E-09	65680	Imputed	0.985	AC002378.1-[]-LIF
22	30620627	rs6006405	A	G	0.843	-7.50E-03	9.41E-04	1.70E-16	65680	Imputed	0.995	AC002378.1-[]-LIF
22	37908462	rs113605227	A	AC	0.827	-1.15E-02	9.37E-04	1.40E-33	65680	Imputed	0.917	[CARD10]
22	37911770	rs6000761	T	C	0.301	-4.60E-03	7.54E-04	5.90E-11	65680	Imputed	0.97	[CARD10]
22	37916113	rs143643697	T	C	0.964	-1.15E-02	1.89E-03	2.10E-08	65680	Imputed	0.93	CARD10[]-CDC42EP1
22	37923956	rs372494932	C	T	0.99	-2.16E-02	3.63E-03	4.60E-10	65680	Imputed	0.871	CARD10-[]-CDC42EP1
22	37925332	rs549756240	A	T	0.912	-7.43E-03	1.30E-03	1.90E-08	65680	Imputed	0.859	CARD10-[]-CDC42EP1
22	37939510	rs9610795	G	T	0.652	-6.47E-03	7.19E-04	1.70E-21	65680	Imputed	0.989	CARD10-[]-CDC42EP1
22	38057338	rs9622678	A	G	0.781	-4.98E-03	9.29E-04	1.90E-09	65680	Imputed	0.801	[Z83844.3,PDXP]
22	38123259	rs748088318	G	GT	0.165	4.93E-03	9.31E-04	6.90E-09	65680	Imputed	0.975	[TRIOBP]
22	38180407	22:38180407_CAA_C	CAA	C	0.677	-8.77E-03	7.31E-04	2.70E-36	65680	Imputed	0.992	TRIOBP-[]-H1-0
22	38594126	rs147906180	C	CAAAAA	0.675	-6.61E-03	7.32E-04	1.20E-20	65680	Imputed	0.983	[PLA2G6]
22	38662396	rs12485196	T	C	0.804	-4.63E-03	8.61E-04	3.20E-08	65680	Imputed	0.998	[TMEM184B]
22	46375611	rs62654723	C	T	0.832	-5.54E-03	9.23E-04	5.40E-09	65680	Imputed	0.976	WNT7B-[]-LINC00899
22	46383612	rs73175083	C	T	0.687	6.37E-03	7.39E-04	1.40E-17	65680	Imputed	0.995	WNT7B-[]-LINC00899

Supplementary Information - Table 3. ML-based VCDR (loci)

CHR	POS	SNP	EA	NEA	EAF	BETA	SE	P	NUM_INDV	SRC	INFO	GENE_CONTEXT	CRAIG	CRAIG_META
1	3049362	rs12024620	C	T	0.936	-1.55E-02	1.38E-03	4.00E-30	65680	Imputed	0.995	[PRDM16]	TRUE	TRUE
1	8468278	rs301792	A	G	0.662	-4.62E-03	7.13E-04	6.80E-13	65680	Imputed	0.998	[RERE]	FALSE	TRUE
1	12614029	rs6541032	T	C	0.424	-5.11E-03	6.82E-04	2.60E-14	65680	Imputed	0.999	VPS13D--[]--DHRS3	TRUE	TRUE
1	47923058	rs767682581	C	CT	0.374	-4.27E-03	7.07E-04	1.40E-10	65680	Imputed	0.983	FOXD2-[]--TRABD2B	FALSE	FALSE
1	68840797	rs2209559	A	G	0.601	-7.49E-03	6.91E-04	1.90E-28	65484	Genotyped	1	WLS--[]--RPE65	TRUE	TRUE
1	89253357	rs786908	A	G	0.383	-4.31E-03	6.95E-04	3.90E-10	65680	Imputed	0.997	[PKN2]	FALSE	TRUE
1	92077097	rs1192415	G	A	0.188	1.76E-02	8.63E-04	7.60E-102	65610	Genotyped	1	CDC7-[]--TGFB3	TRUE	TRUE
1	110627923	rs10857812	T	A	0.636	4.63E-03	7.03E-04	2.10E-11	65680	Imputed	0.993	STRIP1-[]--UBL4B	FALSE	FALSE
1	113045061	rs351364	A	T	0.252	-3.95E-03	7.81E-04	2.40E-08	65680	Imputed	0.984	[WNT2B]	FALSE	FALSE
1	155033308	rs11589479	G	A	0.837	4.88E-03	9.17E-04	1.20E-08	65404	Genotyped	1	[ADAM15]	FALSE	FALSE
1	169551682	rs6028	T	C	0.709	-4.03E-03	7.44E-04	3.10E-09	65680	Imputed	0.996	[F5]	FALSE	TRUE
1	183849739	rs41263652	G	C	0.896	7.20E-03	1.12E-03	4.20E-11	65680	Imputed	0.971	[RGL1]	FALSE	FALSE
1	218520995	rs6658835	A	G	0.73	-5.97E-03	7.64E-04	7.60E-16	65680	Imputed	0.992	[TGF2]	TRUE	TRUE
1	219573841	rs796959510	C	CT	0.491	-4.02E-03	6.82E-04	7.40E-09	65680	Imputed	0.979	AL360093.1---[]--ZC3H11B	FALSE	FALSE
1	222014897	rs11118873	A	G	0.485	3.74E-03	6.79E-04	4.20E-10	65680	Imputed	0.988	DUSP10-[]--HHIPL2	FALSE	FALSE
1	227585983	rs6670351	G	A	0.798	-6.66E-03	8.42E-04	3.30E-17	65680	Imputed	0.993	CDC42BPA-[]--ZNF678	TRUE	TRUE
2	5680539	rs7575439	C	A	0.358	4.09E-03	7.27E-04	1.50E-08	62872	Genotyped	1	LINC01249---[]--AC108025.1	FALSE	FALSE
2	12891476	rs730126	A	C	0.587	3.98E-03	6.95E-04	9.50E-10	65680	Imputed	0.985	TRIB2-[]	FALSE	FALSE
2	19431423	rs72778352	C	T	0.987	2.71E-02	2.97E-03	4.80E-22	65680	Imputed	0.982	NT5C1B---[]--OSR1	FALSE	TRUE
2	56072501	rs1430202	G	A	0.798	8.29E-03	8.51E-04	1.80E-24	65680	Imputed	0.99	PNPT1---[]--EFEMP1	TRUE	TRUE
2	111658010	rs4849203	A	G	0.652	5.07E-03	7.12E-04	1.30E-13	65575	Genotyped	1	[ACOXL]	TRUE	TRUE
2	180196027	rs12620141	C	A	0.636	-4.06E-03	7.18E-04	2.50E-09	65680	Imputed	0.961	AC093911.1---[]--ZNF385B	FALSE	FALSE
2	190269957	2:190269957_CTTTTC_C	CTTTT	C	0.308	4.16E-03	7.40E-04	3.00E-09	65680	Imputed	0.99	COL5A2-[]--WDR75	FALSE	FALSE
2	233389918	rs2853447	A	G	0.297	-3.75E-03	7.44E-04	3.80E-08	65680	Imputed	0.987	[PRSS56]	FALSE	FALSE
2	20061023	rs35057657	A	G	0.327	4.06E-03	7.27E-04	4.30E-08	65680	Imputed	0.991	PP2D1-[]--KAT2B	FALSE	FALSE
3	25046463	rs12490228	C	T	0.717	-6.08E-03	7.54E-04	3.50E-17	65680	Imputed	0.996	THR-B-AS1---[]--RARB	TRUE	TRUE
3	29493916	rs9822629	T	G	0.626	-3.71E-03	7.02E-04	1.50E-08	65680	Imputed	0.992	[AC098650.1,RBMS3]	FALSE	FALSE
3	32879823	rs56131903	A	T	0.679	6.19E-03	7.34E-04	3.90E-18	65680	Imputed	0.983	[TRIM71]	TRUE	TRUE
3	48719638	rs7633840	T	C	0.337	4.72E-03	7.39E-04	1.60E-11	65680	Imputed	0.949	[NCKIPSD]	FALSE	FALSE
3	58130168	rs2362911	A	G	0.771	-5.34E-03	8.06E-04	3.30E-12	65680	Imputed	0.991	[FLNB]	FALSE	TRUE
3	71182447	rs77877421	A	T	0.943	-1.16E-02	1.50E-03	1.60E-15	65680	Imputed	0.964	[FOXP1,AC097634.4]	FALSE	FALSE
3	88304417	rs9852080	T	C	0.448	6.19E-03	6.83E-04	3.70E-21	65680	Imputed	0.996	C3orf38---[]--CSNK2IP	TRUE	TRUE
3	99078606	rs1871794	T	C	0.748	-8.53E-03	7.82E-04	9.40E-30	65680	Imputed	0.996	DCBLD2---[]--AC107029.1	TRUE	TRUE
3	106117209	rs12637686	G	A	0.721	-4.14E-03	7.57E-04	3.50E-09	65680	Imputed	0.993	CBLB-[]--LINC00882	FALSE	FALSE
3	128196500	rs2713594	G	A	0.583	-3.68E-03	6.94E-04	4.20E-08	65680	Imputed	0.983	DNAJB8-[]--GATA2	FALSE	FALSE
3	134089758	rs143351962	C	T	0.99	-2.15E-02	3.40E-03	7.40E-10	65680	Imputed	1	[AMOTL2]	TRUE	FALSE
4	7917204	rs34939228	T	TA	0.617	-4.17E-03	7.05E-04	8.30E-09	65680	Imputed	0.984	[AFAP1]	FALSE	FALSE
4	54979145	rs1158402	C	T	0.378	5.88E-03	7.03E-04	6.80E-19	65680	Imputed	0.996	[AC058822.1]	TRUE	TRUE
4	79396057	4:79396057_TC_T	TC	T	0.367	4.02E-03	7.10E-04	2.00E-08	65680	Imputed	0.995	[FRAS1]	FALSE	FALSE
4	112399511	rs2661764	A	T	0.638	4.03E-03	7.09E-04	7.30E-09	65680	Imputed	0.995	PITX2-[]--FAM241A	FALSE	FALSE
4	126407298	rs532857051	C	CTT	0.708	6.06E-03	7.51E-04	4.70E-17	65680	Imputed	0.993	[FAT4]	FALSE	TRUE
4	128053375	4:128053375_AACAC_A	AACAC	A	0.52	3.51E-03	6.96E-04	1.60E-08	65680	Imputed	0.953	[]-INTU	FALSE	FALSE
5	3646121	rs13165326	C	T	0.672	-3.77E-03	7.25E-04	2.40E-08	65680	Imputed	0.991	IRX1-[]--LINC02063	FALSE	TRUE
5	31952051	rs72759609	T	C	0.898	1.35E-02	1.13E-03	2.40E-37	65680	Imputed	0.989	[PDZD2]	TRUE	TRUE
5	55578661	rs158653	G	A	0.477	5.06E-03	6.85E-04	1.30E-14	65680	Imputed	0.992	ANKRD55---[]--LINC01948	TRUE	TRUE
5	82770558	rs11746859	A	G	0.539	4.77E-03	6.82E-04	8.90E-13	65680	Imputed	0.995	[VCAN]	FALSE	TRUE
5	87810199	rs150221399	G	A	0.919	-9.99E-03	1.28E-03	3.80E-15	65680	Imputed	0.95	TMEM161B---[]--MEF2C	FALSE	TRUE
5	121765728	rs2570981	T	C	0.401	4.30E-03	6.93E-04	1.10E-09	65680	Imputed	0.994	[SNCAIP]	FALSE	FALSE
5	128931357	rs7448395	G	A	0.204	6.62E-03	8.47E-04	8.00E-17	65680	Imputed	0.999	[ADAMTS19]	TRUE	TRUE
5	133393380	5:133393380_GA_G	GA	G	0.844	7.22E-03	1.01E-03	3.30E-13	65680	Imputed	0.858	VDAC1-[]--TCF7	TRUE	TRUE
5	172197790	rs34013988	C	T	0.961	1.46E-02	1.75E-03	4.10E-18	65680	Imputed	0.998	[AC022217.4,DUSP1]	TRUE	TRUE
6	593289	6:593289_TG_T	TG	T	0.869	-7.47E-03	1.05E-03	2.60E-14	65680	Imputed	0.913	[EXOC2]	FALSE	TRUE
6	1548369	rs2745572	A	G	0.666	4.35E-03	7.26E-04	3.10E-09	65680	Imputed	0.99	FOXF2---[]--FOXC1	FALSE	FALSE
6	1983440	rs6914444	T	C	0.866	9.30E-03	1.01E-03	9.70E-22	65680	Imputed	0.987	[GMSD]	TRUE	TRUE
6	7211818	rs1334576	G	A	0.572	-5.94E-03	6.92E-04	1.60E-18	65515	Genotyped	1	[RREB1]	TRUE	TRUE
6	11411838	rs7742703	C	T	0.905	6.43E-03	1.16E-03	8.60E-09	65680	Imputed	0.996	NEDD9-[]--TMEM170B	FALSE	FALSE
6	31133577	rs145919884	A	AAAGCCC	0.35	4.45E-03	7.18E-04	3.40E-10	65680	Imputed	0.996	[TCF19,POU5F1]	FALSE	FALSE
6	36552592	rs200252984	G	A	0.79	-7.25E-03	8.47E-04	9.90E-21	65680	Imputed	0.973	STK38-[]--SRSF3	TRUE	TRUE
6	39537880	rs9369128	T	C	0.651	-6.39E-03	7.15E-04	5.30E-20	65680	Imputed	0.998	[KIF6]	FALSE	TRUE
6	122392511	rs2684249	T	C	0.593	6.38E-03	6.95E-04	9.00E-19	65680	Imputed	0.995	GJA1-[]--HSF2	TRUE	TRUE
6	126767600	rs1361108	C	T	0.543	-6.05E-03	6.89E-04	1.60E-17	65542	Genotyped	1	CENPW-[]--RSPO3	FALSE	FALSE
6	148832343	rs139973521	A	ATGAG	0.89	-7.36E-03	1.10E-03	3.80E-13	65680	Imputed	0.987	[SASH1]	FALSE	FALSE
6	149989744	6:149989744_AT_A	AT	A	0.648	4.99E-03	7.24E-04	2.10E-12	65680	Imputed	0.988	[LATS1]	FALSE	FALSE
6	151295133	rs6900628	A	G	0.708	4.20E-03	7.55E-04	2.20E-08	65475	Genotyped	1	[MTHFD1L]	FALSE	FALSE
7	4767112	rs6946034	A	T	0.52	-3.68E-03	6.86E-04	3.00E-09	65680	Imputed	0.983	[FOXK1]	FALSE	FALSE
7	14237240	rs10260511	C	A	0.842	-7.78E-03	9.37E-04	5.90E-19	65597	Genotyped	1	[DGKB]	TRUE	TRUE
7	19612305	rs2192476	C	T	0.372	4.26E-03	7.06E-04	2.00E-11	65680	Imputed	0.993	FERD3L---[]--TWISTNB	TRUE	TRUE
7	28393403	rs7805378	A	C	0.559	4.60E-03	6.86E-04	1.20E-11	65680	Imputed	0.994	[CREB5]	TRUE	TRUE
7	28844815	rs2282909	T	G	0.269	4.09E-03	7.70E-04	1.40E-08	65680	Imputed	0.999	[CREB5]	FALSE	FALSE
7	42108499	rs2237417	C	T	0.593	3.69E-03	6.99E-04	4.00E-08	65680	Imputed	0.987	[GLI3]	FALSE	FALSE
7	101808020	rs6976947	A	G	0.604	4.41E-03	6.97E-04	8.70E-12	65680	Imputed	0.997	[CUX1]	FALSE	TRUE
8	8254590	rs2945880	A	G	0.113	-9.34E-03	1.08E-03	2.30E-19	65680	Imputed	0.994	PRAG1-[]--AC114550.3	TRUE	TRUE
8	17526359	rs11203888	C	T	0.335	-4.18E-03	7.24E-04	2.80E-09	65680	Imputed	0.995	[MTUS1]	FALSE	FALSE
8	30386291	rs7013873	C	T	0.784	4.49E-03	8.32E-04	7.90E-10	65680	Imputed	0.989	[RBPMS]	FALSE	FALSE

Supplementary Information - Table 3. ML-based VCDR (loci)

CHR	POS	SNP	EA	NEA	EAF	BETA	SE	P	NUM_INDV	SRC	INFO	GENE_CONTEXT	CRAIG	CRAIG_META
8	61911070	rs10957177	A	G	0.749	4.57E-03	7.94E-04	6.80E-09	65680	Imputed	0.978	CHD7--[]--CLVS1	FALSE	FALSE
8	72579250	rs10453110	C	T	0.874	-9.94E-03	1.04E-03	8.50E-23	65680	Imputed	0.99	EYA1--[]--AC104012.2	TRUE	TRUE
8	75522500	rs10957731	A	C	0.402	5.12E-03	6.96E-04	3.70E-14	65680	Imputed	0.994	[MIR2052HG]	FALSE	FALSE
8	78948855	rs6999835	T	C	0.634	3.93E-03	7.10E-04	2.00E-09	65680	Imputed	0.996	[]--PKIA	FALSE	FALSE
8	88664409	rs200382882	G	C	0.485	-4.07E-03	6.86E-04	7.60E-11	65680	Imputed	0.997	CNBD1--[]--DCAF4L2	FALSE	FALSE
8	131606303	8:131606303_CTGTT_C	CTGTT	C	0.647	3.90E-03	7.18E-04	4.20E-08	65680	Imputed	0.986	ASAP1--[]--ADCY8	FALSE	FALSE
9	15912375	rs10810475	G	C	0.564	3.67E-03	6.87E-04	1.20E-08	65680	Imputed	0.998	[CCDC171]	FALSE	FALSE
9	16619529	rs13290470	A	G	0.603	5.52E-03	6.97E-04	7.20E-19	65680	Imputed	0.991	[BNC2]	FALSE	FALSE
9	18089275	rs10738500	C	A	0.927	-9.11E-03	1.31E-03	3.90E-12	65680	Imputed	0.99	[ADAMTSL1]	TRUE	TRUE
9	22051670	rs944801	G	C	0.428	-1.57E-02	6.90E-04	5.30E-125	65680	Imputed	0.999	[CDKN2B-AS1]	TRUE	TRUE
9	76622068	rs11143754	C	A	0.573	4.29E-03	6.90E-04	3.40E-10	65680	Imputed	0.994	AL451127.1---[]--AL355674.1	FALSE	FALSE
9	89252706	rs10512176	T	C	0.722	-6.49E-03	7.76E-04	1.70E-17	65680	Imputed	0.95	TUT7--[]--GAS1	FALSE	TRUE
9	134563185	rs11793533	G	A	0.719	5.28E-03	7.58E-04	2.80E-12	65419	Genotyped	1	[RAPGEF1]	FALSE	FALSE
9	136145414	rs587611953	C	A	0.836	-6.71E-03	1.02E-03	4.80E-13	65680	Imputed	0.824	[ABO]	FALSE	TRUE
10	14086579	rs7099081	A	G	0.663	3.85E-03	7.20E-04	2.00E-08	65680	Imputed	0.993	[FRMD4A]	FALSE	FALSE
10	21462896	10:21462896_GGC_G	GGC	G	0.987	-2.40E-02	3.08E-03	1.60E-15	65680	Imputed	0.943	[NEBL]	TRUE	TRUE
10	60271824	rs7069916	G	A	0.657	-3.95E-03	7.16E-04	5.50E-09	65680	Imputed	0.997	TFAM--[]--BICC1	FALSE	FALSE
10	69991853	rs7916697	A	G	0.24	-1.62E-02	7.98E-04	1.20E-98	65604	Genotyped	1	[ATOH7]	TRUE	TRUE
10	94974129	rs6583871	G	T	0.264	-5.05E-03	7.76E-04	1.70E-11	65680	Imputed	0.982	CYP26A1---[]--MYOF	TRUE	TRUE
10	96026184	10:96026184_CA_C	CA	C	0.565	-4.35E-03	6.91E-04	3.10E-10	65680	Imputed	0.995	[PLCE1]	FALSE	TRUE
10	118546046	rs11197820	G	A	0.585	-6.17E-03	6.94E-04	2.90E-19	65680	Imputed	0.985	[HSPA12A]	TRUE	TRUE
11	19960147	rs12807015	G	T	0.528	-3.98E-03	6.97E-04	8.90E-09	65680	Imputed	0.96	[NAV2]	FALSE	FALSE
11	31719504	11:31719504_CT_C	CT	C	0.233	7.13E-03	8.10E-04	9.60E-21	65680	Imputed	0.992	[ELP4]	TRUE	TRUE
11	57656794	rs35328629	T	TA	0.561	-4.29E-03	6.89E-04	2.00E-10	65680	Imputed	0.987	CTNND1--[]--OR9Q1	FALSE	FALSE
11	63678128	rs199826712	T	TA	0.926	-6.78E-03	1.34E-03	9.90E-09	65680	Imputed	0.948	[MARK2]	FALSE	FALSE
11	65343399	rs547193816	C	CCCGCT	0.797	9.19E-03	8.60E-04	2.00E-27	65680	Imputed	0.97	FAM89B-[EHBP1L1]	TRUE	TRUE
11	86748437	rs2445575	T	C	0.807	4.90E-03	8.62E-04	7.30E-10	65680	Imputed	0.997	FZD4-[TMEM135]	TRUE	TRUE
11	94533444	rs138059525	G	A	0.993	3.10E-02	4.07E-03	2.60E-14	65629	Genotyped	1	[AMOTL1]	FALSE	FALSE
11	95308854	rs11021221	T	A	0.831	7.22E-03	9.09E-04	3.60E-15	65680	Imputed	0.994	SES3---[]--FAM76B	TRUE	TRUE
11	130288797	rs34248430	A	ACCT	0.282	-7.71E-03	7.72E-04	4.50E-27	65680	Imputed	0.961	[ADAMT58]	TRUE	TRUE
12	3353356	rs73047017	C	T	0.937	-8.15E-03	1.41E-03	6.00E-10	65680	Imputed	0.976	[TSPAN9]	FALSE	FALSE
12	26392080	rs16930371	A	G	0.816	4.97E-03	8.80E-04	4.80E-09	65283	Genotyped	1	[SSPN]	FALSE	TRUE
12	31067490	rs55710412	C	T	0.845	5.27E-03	9.65E-04	8.10E-09	65680	Imputed	0.948	CAPRIN2---[]--TSPAN11	FALSE	FALSE
12	48157019	rs12818241	C	T	0.84	6.29E-03	9.31E-04	1.10E-12	65680	Imputed	0.984	[RAPGEF3.SLC48A1]	FALSE	TRUE
12	76114872	rs6582298	G	A	0.595	5.67E-03	7.23E-04	9.30E-16	65680	Imputed	0.901	[AC078923.1]	TRUE	FALSE
12	84076137	rs55667441	A	G	0.558	1.58E-02	6.86E-04	2.50E-127	65680	Imputed	0.995	[TMC2---[]]	TRUE	TRUE
12	91816926	rs147377344	C	CTTTTACG	0.4	4.03E-03	7.03E-04	2.10E-08	65680	Imputed	0.977	DCN---[]--LINC01619	FALSE	FALSE
12	107073242	12:107073242_CA_C	CA	C	0.653	6.36E-03	7.17E-04	6.00E-15	65680	Imputed	0.988	[AC079385.1.RFX4]	TRUE	TRUE
12	108165360	rs2111281	A	C	0.636	-5.30E-03	7.07E-04	1.30E-13	65680	Imputed	0.995	PRDM4--[]--ASCL4	FALSE	FALSE
12	124665773	rs11057488	A	G	0.435	-4.85E-03	6.87E-04	8.50E-14	65680	Imputed	0.994	[RFLNA]	TRUE	TRUE
12	25778093	rs17081940	A	G	0.858	5.44E-03	9.90E-04	2.10E-09	65680	Imputed	0.978	[LINC01076]	FALSE	FALSE
13	36683268	rs9546383	T	C	0.754	-5.96E-03	7.95E-04	6.70E-16	65680	Imputed	0.992	[DCLK1]	TRUE	TRUE
13	51945741	rs9535652	G	A	0.834	5.41E-03	9.19E-04	4.10E-09	65680	Imputed	0.996	[INTS6]	FALSE	FALSE
13	109267985	rs10162202	T	C	0.722	6.97E-03	7.68E-04	6.10E-23	65680	Imputed	0.982	[MYO16]	TRUE	TRUE
13	110778747	13:110778747 CCTTTT_C	CCTTTT	C	0.641	-6.06E-03	7.31E-04	9.90E-18	65680	Imputed	0.945	IRS2---[]--COL4A1	TRUE	TRUE
14	23452128	rs3811183	C	G	0.6	-4.45E-03	7.01E-04	1.30E-12	65680	Imputed	0.987	AJUBA-[C14orf93]	TRUE	TRUE
14	53991705	rs2077940	T	C	0.668	5.45E-03	7.24E-04	1.70E-14	65680	Imputed	0.997	DDHD1---[]--AL163953.1	TRUE	TRUE
14	60808553	rs10162287	C	G	0.696	-7.65E-03	7.48E-04	2.60E-27	65680	Imputed	0.979	PPM1A--[]--C14orf39	TRUE	TRUE
14	65081054	rs149761305	A	GCT	0.83	-7.31E-03	9.14E-04	7.40E-18	65680	Imputed	0.993	PPP1R3B--[]--PLEKHG3	FALSE	TRUE
14	85922578	rs1289426	G	G	0.767	-6.91E-03	8.15E-04	6.80E-16	65680	Imputed	0.974	[]-FLRT2	TRUE	TRUE
14	95957694	rs11160251	T	G	0.703	4.15E-03	7.47E-04	1.90E-09	65680	Imputed	0.991	SYNE3--[]--GLRX5	FALSE	FALSE
15	71882771	rs4776562	A	G	0.554	3.95E-03	7.27E-04	1.10E-09	65680	Imputed	0.892	[THSD4]	FALSE	TRUE
15	74230660	rs59755145	G	A	0.712	-4.23E-03	7.57E-04	2.90E-09	65680	Imputed	0.992	[LOXL1]	TRUE	TRUE
15	84484384	rs59199978	A	G	0.82	-6.14E-03	8.91E-04	6.00E-14	65680	Imputed	0.995	[ADAMTSL3]	FALSE	FALSE
15	99458902	rs28612945	C	T	0.794	6.20E-03	8.46E-04	7.80E-15	65547	Genotyped	1	[IGF1R]	FALSE	TRUE
15	101200873	rs34222435	C	T	0.865	-9.55E-03	1.00E-03	1.60E-23	65680	Imputed	0.991	ASB7-[]-ALDH1A3	TRUE	TRUE
15	101751698	rs8043304	T	C	0.752	4.35E-03	7.95E-04	1.80E-08	65680	Imputed	0.995	[CHSY1]	FALSE	FALSE
15	51469726	rs8053277	T	C	0.303	1.11E-02	7.45E-04	6.90E-54	65680	Imputed	0.993	SALL1---[]--HNRNPA1P48	TRUE	TRUE
16	74226221	rs807293	T	C	0.636	-4.41E-03	7.10E-04	7.70E-11	65680	Imputed	0.996	ZFXH3---[]--PSMD7	FALSE	FALSE
16	86380293	rs1687628	T	C	0.09	1.21E-02	1.19E-03	2.10E-25	65680	Imputed	0.992	IRF8--[]--FOXF1	TRUE	TRUE
17	40867365	rs115818584	C	G	0.984	1.62E-02	2.73E-03	1.70E-09	65680	Imputed	0.984	[EZH1]	FALSE	FALSE
17	45438886	rs769594276	C	CAGTG	0.548	-4.05E-03	6.88E-04	4.40E-11	65680	Imputed	0.997	[EFCAB13]	FALSE	FALSE
17	48225686	rs4794104	C	G	0.838	-5.48E-03	9.29E-04	9.00E-10	65680	Imputed	0.995	[PPP1R9B]	TRUE	TRUE
17	61865670	17:61865670_CT_C	CT	C	0.637	-4.25E-03	7.28E-04	2.40E-10	65680	Imputed	0.947	[DDX42]	FALSE	FALSE
17	65073835	rs577377763	C	CA	0.642	-4.45E-03	7.38E-04	4.50E-09	65680	Imputed	0.925	[HELZ]	FALSE	TRUE
17	80169426	rs796355894	A	AT	0.592	3.96E-03	7.09E-04	1.60E-08	65680	Imputed	0.956	[CCDC57]	FALSE	FALSE
18	8797487	rs569735	C	A	0.269	4.57E-03	7.89E-04	1.00E-08	65680	Imputed	0.961	[MTCL1]	FALSE	FALSE
18	23063159	rs766791666	T	TATC	0.415	-4.02E-03	7.05E-04	4.00E-10	65680	Imputed	0.971	ZNF521--[]--SS18	FALSE	FALSE
18	34289285	rs61735998	G	T	0.974	1.37E-02	2.17E-03	1.20E-10	65680	Imputed	1	[FHOD3]	FALSE	FALSE
18	56943484	rs77759734	C	T	0.951	-8.73E-03	1.59E-03	1.00E-09	65493	Genotyped	1	[CPLX4]	FALSE	FALSE
19	817708	rs7250902	A	G	0.681	5.21E-03	7.45E-04	3.40E-12	65680	Imputed	0.966	[PLPPR3]	TRUE	TRUE
19	14616371	rs11882319	C	A	0.851	5.31E-03	9.65E-04	6.00E-09	65680	Imputed	0.982	GIPC1-[]-DNAJB1	FALSE	FALSE
19	32027330	rs8102936	G	A	0.658	6.80E-03	7.26E-04	1.10E-19	65680	Imputed	0.987	TSHZ3---[]--ZNF507	TRUE	TRUE
19	33523197	rs73039431	A	G	0.955	-1.04E-02	1.66E-03	3.70E-10	65680	Imputed	0.984	[RHPN2]	FALSE	FALSE

Supplementary Information - Table 3. ML-based VCDR (loci)

CHR	POS	SNP	EA	NEA	EAF	BETA	SE	P	NUM_INDV	SRC	INFO	GENE_CONTEXT	CRAIG	CRAIG_META
19	39146780	rs55876653	G	C	0.508	-4.15E-03	6.84E-04	7.40E-10	65680	Imputed	0.997	[ACTN4]	FALSE	FALSE
20	1029686	rs4816177	A	G	0.821	-5.44E-03	9.01E-04	4.10E-10	64868	Genotyped	1	RSPO4--[]--PSMF1	FALSE	FALSE
20	6470094	rs2326788	G	A	0.628	1.17E-02	7.07E-04	1.60E-65	65680	Imputed	0.992	FERMT1---[]--LINC01713	TRUE	TRUE
20	31438954	rs4911268	A	G	0.816	6.64E-03	8.85E-04	1.80E-15	65680	Imputed	0.998	MAPRE1[]-EFCAB8	TRUE	TRUE
20	45797259	rs3091590	C	T	0.544	-4.29E-03	6.87E-04	1.10E-10	65680	Imputed	0.991	[EYA2]	FALSE	FALSE
22	29115066	rs4822983	C	T	0.677	1.49E-02	7.29E-04	1.30E-98	65680	Imputed	0.999	[CHEK2]	TRUE	TRUE
22	38180407	22:38180407_CAA_C	CAA	C	0.677	-8.77E-03	7.31E-04	2.70E-36	65680	Imputed	0.992	TRIOBP-[]--H1-0	TRUE	TRUE
22	46383612	rs73175083	C	T	0.687	6.37E-03	7.39E-04	1.40E-17	65680	Imputed	0.995	WNT7B--[]--LINC00899	FALSE	FALSE

Supplementary Information - Table 5. SuSiE fine-mapping (loci)

CHR	POS	SNP	P	LOCUS_IDX	N_FINEMAPPED	N_GWS	N_CAUSAL
1	3049362	rs12024620	4.00E-30	1	141	79	2
1	8468278	rs301792	6.80E-13	2	508	56	1
1	12614029	rs6541032	2.60E-14	3	160	51	1
1	47923058	rs767682581	1.40E-10	4	505	20	1
1	68840797	rs2209559	1.90E-28	5	1028	163	9
1	89253357	rs786908	3.90E-10	6	683	127	1
1	92077097	rs1192415	7.60E-102	7	1292	187	10
1	110627923	rs10857812	2.10E-11	8	317	28	8
1	113045061	rs351364	2.40E-08	9	568	2	7
1	155033308	rs11589479	1.20E-08	10	924	1	9
1	169551682	rs6028	3.10E-09	11	185	76	6
1	183849739	rs41263652	4.20E-11	12	159	4	7
1	218520995	rs6658835	7.60E-16	13	42	5	7
1	219573841	rs796959510	7.40E-09	14	237	1	5
1	222014897	rs11118873	4.20E-10	15	165	4	7
1	227585983	rs6670351	3.30E-17	16	522	133	10
2	5680539	rs7575439	1.50E-08	17	27	1	2
2	12891476	rs730126	9.50E-10	18	155	4	8
2	19431423	rs72778352	4.80E-22	19	445	46	9
2	56072501	rs1430202	1.80E-24	20	1699	190	8
2	111658010	rs4849203	1.30E-13	21	492	165	5
2	180196027	rs12620141	2.50E-09	22	53	6	4
2	190269957	2:190269957_CTTT_C	3.00E-09	23	458	42	4
2	233389918	rs2853447	3.80E-08	24	101	1	9
3	20061023	rs35057657	4.30E-08	25	993	2	6
3	25046463	rs12490228	3.50E-17	26	1530	386	7
3	29493916	rs9822629	1.50E-08	27	392	5	6
3	32879823	rs56131903	3.90E-18	28	217	54	6
3	48719638	rs7633840	1.60E-11	29	2149	170	7
3	58130168	rs2362911	3.30E-12	30	845	139	6
3	71182447	rs77877421	1.60E-15	31	1597	4	8
3	88380417	rs9852080	3.70E-21	32	4860	235	7
3	99078606	rs1871794	9.40E-30	33	3389	909	6
3	106117209	rs12637686	3.50E-09	34	444	4	9
3	128196500	rs2713594	4.20E-08	35	11	0	7
3	134089758	rs143351962	7.40E-10	36	125	1	9
4	7917204	rs34939228	8.30E-09	37	619	64	7
4	54979145	rs1158402	6.80E-19	38	532	225	8
4	79396057	4:79396057_TC_T	2.00E-08	39	1201	29	7
4	112399511	rs2661764	7.30E-09	40	181	6	5
4	126407298	rs532857051	4.70E-17	41	205	39	6
4	128053375	4:128053375_AACAC_A	1.60E-08	42	753	1	2
5	3646121	rs13165326	2.40E-08	43	397	4	7
5	31952051	rs72759609	2.40E-37	44	191	34	5
5	55578661	rs158653	1.30E-14	45	786	124	10
5	82770558	rs11746859	8.90E-13	46	107	28	7
5	87810199	rs150221399	3.80E-15	47	412	26	9
5	121765728	rs2570981	1.10E-09	48	169	3	5
5	128931357	rs7448395	8.00E-17	49	1996	141	10
5	133393380	5:133393380_GA_G	3.30E-13	50	228	37	8

Supplementary Information - Table 5. SuSiE fine-mapping (loci)

CHR	POS	SNP	P	LOCUS_IDX	N_FINEMAPPED	N_GWS	N_CAUSAL
5	172197790	rs34013988	4.10E-18	51	273	82	5
6	593289	6:593289_TG_T	2.60E-14	52	425	39	7
6	1548369	rs2745572	3.10E-09	53	187	1	7
6	1983440	rs6914444	9.70E-22	54	784	48	6
6	7211818	rs1334576	1.60E-18	55	788	49	7
6	11411838	rs7742703	8.60E-09	56	277	7	6
6	31133577	rs145919884	3.40E-10	57	19009	88	10
6	36552592	rs200252984	9.90E-21	58	601	380	7
6	39537880	rs9369128	5.30E-20	59	589	180	7
6	122392511	rs2684249	9.00E-19	60	369	60	9
6	126767600	rs1361108	1.60E-17	61	401	133	5
6	148832343	rs139973521	3.80E-13	62	77	4	6
6	149989744	6:149989744_AT_A	2.10E-12	63	532	297	8
6	151295133	rs6900628	2.20E-08	64	132	5	3
7	4767112	rs6946034	3.00E-09	65	57	12	5
7	14237240	rs10260511	5.90E-19	66	113	51	6
7	19612305	rs2192476	2.00E-11	67	1115	173	5
7	28393403	rs7805378	1.20E-11	68	264	5	6
7	28844815	rs2282909	1.40E-08	69	274	4	8
7	42108499	rs2237417	4.00E-08	70	269	2	8
7	101808020	rs6976947	8.70E-12	71	202	68	6
8	8254590	rs2945880	2.30E-19	72	1543	5	7
8	17526359	rs11203888	2.80E-09	73	738	27	7
8	30386291	rs7013873	7.90E-10	74	917	21	6
8	61911070	rs10957177	6.80E-09	75	114	1	6
8	72579250	rs10453110	8.50E-23	76	906	74	7
8	75522500	rs10957731	3.70E-14	77	1749	55	9
8	78948855	rs6999835	2.00E-09	78	2040	124	9
8	88664409	rs200382882	7.60E-11	79	1189	71	8
8	131606303	8:131606303_CTGTT_C	4.20E-08	80	74	0	7
9	15912375	rs10810475	1.20E-08	81	470	3	6
9	16619529	rs13290470	7.20E-19	82	184	26	10
9	18089275	rs10738500	3.90E-12	83	307	21	6
9	22051670	rs944801	5.30E-125	84	220	58	7
9	76622068	rs11143754	3.40E-10	85	606	9	8
9	89252706	rs10512176	1.70E-17	86	530	32	6
9	134563185	rs11793533	2.80E-12	87	735	111	8
9	136145414	rs587611953	4.80E-13	88	668	78	7
10	14086579	rs7099081	2.00E-08	89	451	4	7
10	21462896	10:21462896_GGC_G	1.60E-15	90	645	0	9
10	60271824	rs7069916	5.50E-09	91	89	15	6
10	69991853	rs7916697	1.20E-98	92	1987	566	5
10	94974129	rs6583871	1.70E-11	93	278	21	3
10	96026184	10:96026184_CA_C	3.10E-10	94	943	22	10
10	118546046	rs11197820	2.90E-19	95	457	59	6
11	19960147	rs12807015	8.90E-09	96	109	1	7
11	31719504	11:31719504_CT_C	9.60E-21	97	1255	555	8
11	57656794	rs35328629	2.00E-10	98	2699	152	8
11	63678128	rs199826712	9.90E-09	99	503	33	7
11	65343399	rs547193816	2.00E-27	100	3174	192	7

Supplementary Information - Table 5. SuSiE fine-mapping (loci)

CHR	POS	SNP	P	LOCUS_IDX	N_FINEMAPPED	N_GWS	N_CAUSAL
11	86748437	rs2445575	7.30E-10	101	173	3	5
11	94533444	rs138059525	2.60E-14	102	259	5	5
11	95308854	rs11021221	3.60E-15	103	85	26	9
11	130288797	rs34248430	4.50E-27	104	119	18	6
12	3353356	rs73047017	6.00E-10	105	26	3	4
12	26392080	rs16930371	4.80E-09	106	32	0	10
12	31067490	rs55710412	8.10E-09	107	183	13	6
12	48157019	rs12818241	1.10E-12	108	657	86	9
12	76114872	rs6582298	9.30E-16	109	54	1	6
12	84076137	rs55667441	2.50E-127	110	5946	2199	6
12	91816926	rs147377344	2.10E-08	111	506	2	8
12	107073242	12:107073242_CA_C	6.00E-15	112	1205	279	8
12	108165360	rs2111281	1.30E-13	113	325	99	9
12	124665773	rs11057488	8.50E-14	114	580	66	6
13	25778093	rs17081940	2.10E-09	115	44	8	7
13	36683268	rs9546383	6.70E-16	116	218	17	7
13	51945741	rs9535652	4.10E-09	117	161	16	9
13	109267985	rs10162202	6.10E-23	118	331	91	7
13	110778747	13:110778747_CCTTTT_	9.90E-18	119	285	30	7
14	23452128	rs3811183	1.30E-12	120	295	119	5
14	53991705	rs2077940	1.70E-14	121	641	120	6
14	60808553	rs10162287	2.60E-27	122	2941	322	9
14	65081054	rs149761305	7.40E-18	123	1229	74	6
14	85922578	rs1289426	6.80E-16	124	1314	119	8
14	95957694	rs11160251	1.90E-09	125	90	4	6
15	71882771	rs4776562	1.10E-09	126	74	1	3
15	74230660	rs59755145	2.90E-09	127	54	2	5
15	84484384	rs59199978	6.00E-14	128	457	11	6
15	99458902	rs28612945	7.80E-15	129	13	0	4
15	101200873	rs34222435	1.60E-23	130	42	5	4
15	101751698	rs8043304	1.80E-08	131	62	3	8
16	51469726	rs8053277	6.90E-54	132	1806	514	6
16	74226221	rs807293	7.70E-11	133	1687	55	5
16	86380293	rs1687628	2.10E-25	134	782	166	8
17	40867365	rs115818584	1.70E-09	135	313	2	6
17	45438886	rs769594276	4.40E-11	136	330	105	4
17	48225686	rs4794104	9.00E-10	137	46	0	7
17	61865670	17:61865670_CT_C	2.40E-10	138	131	13	2
17	65073835	rs577377763	4.50E-09	139	99	17	6
17	80169426	rs796355894	1.60E-08	140	238	5	3
18	8797487	rs569735	1.00E-08	141	59	1	7
18	23063159	rs766791666	4.00E-10	142	128	19	4
18	34289285	rs61735998	1.20E-10	143	492	1	6
18	56943484	rs77759734	1.00E-09	144	62	1	7
19	817708	rs7250902	3.40E-12	145	194	22	6
19	14616371	rs11882319	6.00E-09	146	177	19	8
19	32027330	rs8102936	1.10E-19	147	525	22	7
19	33523197	rs73039431	3.70E-10	148	711	12	7
19	39146780	rs55876653	7.40E-10	149	153	18	9
20	1029686	rs4816177	4.10E-10	150	17	0	4

Supplementary Information - Table 5. SuSiE fine-mapping (loci)

CHR	POS	SNP	P	LOCUS_IDX	N_FINEMAPPED	N_GWS	N_CAUSAL
20	6470094	rs2326788	1.60E-65	151	374	141	2
20	31438954	rs4911268	1.80E-15	152	539	27	5
20	45797259	rs3091590	1.10E-10	153	199	45	2
22	29115066	rs4822983	1.30E-98	154	5927	1583	7
22	38180407	22:38180407_CAA_C	2.70E-36	155	2128	745	8
22	46383612	rs73175083	1.40E-17	156	233	36	8

Supplementary Information - Table 6. ML-based meta VCDR (hits)

CHR	POS	SNP	EA	NEA	BETA	SE	P	GENE_CONTEXT
1	3055876	rs10797380	A	G	-3.06E-02	5.27E-03	1.93E-09	[PRDM16]
1	3056222	rs35271327	A	AT	-1.18E-01	1.08E-02	2.10E-29	[PRDM16]
1	8486131	rs302714	A	C	-3.46E-02	5.37E-03	1.61E-14	[RERE,RERE-AS1]
1	12614029	rs6541032	T	C	-3.85E-02	5.14E-03	2.30E-18	VPS13D--[]--DHRS3
1	47923058	rs767682581	C	CT	-3.22E-02	5.33E-03	1.40E-10	FOXO2--[]--TRABD2B
1	53565054	rs58924052	T	C	-6.34E-02	1.22E-02	3.70E-08	[SLC1A7]
1	56955386	rs4638151	C	T	-2.57E-02	5.51E-03	2.76E-08	[AC119674.2]
1	68773910	rs34151819	C	T	1.34E-01	1.96E-02	6.27E-13	WLS--[]--RPE65
1	68848681	rs1925953	A	T	-5.63E-02	5.20E-03	4.49E-34	WLS--[]--RPE65
1	89295765	rs786914	C	A	-3.23E-02	5.23E-03	1.67E-11	[PKN2]
1	92021464	rs12134245	C	T	3.61E-02	5.10E-03	1.21E-12	CDC7--[]--TGFB3
1	92024124	rs75296423	T	G	-1.34E-01	1.88E-02	3.69E-16	CDC7--[]--TGFB3
1	92039474	rs11587658	G	A	3.74E-02	5.41E-03	1.61E-15	CDC7--[]--TGFB3
1	92070810	rs77291384	G	A	-1.33E-01	2.29E-02	4.10E-09	CDC7--[]--TGFB3
1	92077097	rs1192415	G	A	1.33E-01	6.50E-03	8.55E-110	CDC7--[]--TGFB3
1	92089160	rs17569923	G	A	5.34E-02	6.42E-03	1.26E-20	CDC7--[]--TGFB3
1	92114938	rs12046642	A	G	-5.40E-02	6.64E-03	3.28E-19	CDC7--[]--TGFB3
1	92195601	rs10783002	G	A	-2.44E-02	5.22E-03	4.74E-08	[TGFB3]
1	103441814	rs2061705	A	G	2.31E-02	5.13E-03	2.81E-08	[COL11A1]
1	110466338	rs333970	C	A	-2.79E-02	5.21E-03	3.13E-08	[CSF1]
1	110632536	rs11102052	A	T	3.49E-02	5.32E-03	3.52E-12	STRIP1--[]--UBL4B
1	113046395	rs351365	T	C	-2.96E-02	5.89E-03	4.81E-09	[WNT2B]
1	155033308	rs11589479	G	A	3.67E-02	6.91E-03	2.11E-08	[ADAM15]
1	165715300	rs6426939	C	T	4.10E-02	7.68E-03	4.96E-09	[TMCO1]
1	167691909	rs7548746	A	G	5.22E-02	1.08E-02	1.76E-08	[MPZL1]
1	169551682	rs6028	T	C	-3.04E-02	5.61E-03	1.64E-12	[F5]
1	183849739	rs41263652	G	C	5.42E-02	8.45E-03	1.54E-11	[RGL1]
1	218520995	rs6658835	A	G	-4.50E-02	5.76E-03	5.42E-15	[TGFB2]
1	219451442	rs7536147	A	G	2.89E-02	5.58E-03	3.26E-11	AL360093.1--[]--ZC3H11B
1	219648808	rs2791546	T	G	2.29E-02	5.38E-03	3.92E-09	AL360093.1--[]--ZC3H11B
1	227585983	rs6670351	G	A	-5.02E-02	6.35E-03	6.82E-16	CDC42BPA--[]--ZNF678
2	5680539	rs7575439	C	A	3.08E-02	5.48E-03	5.18E-10	LINC01249--[]--AC108025.1
2	12891476	rs730126	A	C	3.00E-02	5.24E-03	1.58E-09	TRIB2-[]
2	19272693	rs4380183	G	A	-3.48E-02	7.18E-03	8.67E-09	NT5C1B--[]--OSR1
2	19303748	rs6755909	C	T	-3.38E-02	6.20E-03	3.61E-10	NT5C1B--[]--OSR1
2	19306891	rs56202558	C	T	-5.86E-02	9.80E-03	8.64E-11	NT5C1B--[]--OSR1
2	19420060	rs851321	C	T	-1.98E-01	2.21E-02	6.99E-22	NT5C1B--[]--OSR1
2	19479000	rs1727198	C	T	4.16E-02	5.13E-03	2.49E-20	NT5C1B--[]--OSR1
2	28383841	rs10165930	G	A	-2.90E-02	6.03E-03	1.80E-08	[BABAM2]
2	42509829	rs6723361	T	C	-3.00E-02	5.50E-03	8.98E-10	[EML4]
2	56013061	rs17047234	A	C	5.97E-02	6.17E-03	1.34E-24	PNPT1--[]--EFEMP1
2	56095994	rs17278665	C	G	-3.76E-02	6.79E-03	5.84E-11	[EFEMP1]
2	56205280	rs6724872	G	C	-3.09E-02	5.81E-03	1.31E-09	EFEMP1--[]--CCDC85A
2	111680818	rs2880192	A	G	3.84E-02	5.37E-03	1.65E-16	[ACOXL]
2	180196027	rs12620141	C	A	-3.06E-02	5.41E-03	2.50E-09	AC093911.1--[]--ZNF385B
2	190269957	2:190269957_CTTTT_C	CTTTT	C	3.13E-02	5.57E-03	3.00E-09	COL5A2--[]--WDR75
2	239273949	rs56330821	C	T	4.50E-02	9.14E-03	3.34E-09	[TRAF3IP1]
2	241931723	rs12694992	G	A	2.87E-02	5.36E-03	9.14E-11	[CROCC2]
3	20059749	rs2948098	G	A	2.99E-02	5.47E-03	2.00E-08	PP2D1-[]--KAT2B
3	25046477	rs4547662	T	G	-2.83E-02	5.13E-03	4.81E-12	THRB-AS1--[]--RARB
3	25059227	rs1021702	A	G	-3.73E-02	5.17E-03	7.86E-14	THRB-AS1--[]--RARB
3	25159627	rs1604012	A	T	-4.18E-02	5.14E-03	3.01E-20	THRB-AS1--[]--RARB

Supplementary Information - Table 6. ML-based meta VCDR (hits)

CHR	POS	SNP	EA	NEA	BETA	SE	P	GENE_CONTEXT
3	25290905	rs34197182	G	A	4.74E-02	7.18E-03	3.28E-11	[RARB]
3	25381021	rs11920003	C	A	2.60E-02	5.41E-03	1.55E-08	[RARB]
3	29493443	rs1946825	A	G	-2.78E-02	5.29E-03	2.71E-09	[AC098650.1,RBMS3]
3	32851635	rs6773458	G	A	-2.61E-02	5.20E-03	8.71E-09	CNOT10--[]-TRIM71
3	32879823	rs56131903	A	T	4.66E-02	5.53E-03	2.12E-21	[TRIM71]
3	48743342	rs551116669	T	TA	3.29E-02	5.38E-03	2.80E-10	[IP6K2]
3	57990467	3:57990467_CTT_C	CTT	C	-3.09E-02	5.29E-03	2.00E-08	SLMAP--[]-FLNB
3	58035497	rs12494328	G	A	-4.28E-02	6.14E-03	5.89E-16	[FLNB]
3	58154671	rs4681787	T	C	-2.93E-02	5.12E-03	8.04E-10	[FLNB,FLNB-AS1]
3	70061377	rs190948281	G	C	3.33E-01	4.52E-02	1.60E-13	MITF--[]---MDFIC2
3	71182447	rs77877421	A	T	-8.71E-02	1.13E-02	1.06E-13	[FOXP1,AC097634.4]
3	88387796	rs9879264	A	G	4.65E-02	5.15E-03	7.27E-24	[CSNKA2IP]
3	89603917	rs373216501	A	ATATT	3.22E-02	5.81E-03	3.60E-08	EPHA3--[]
3	98943479	rs13076500	C	T	-5.07E-02	5.18E-03	1.89E-27	DCBLD2---[]---AC107029.1
3	98982518	rs114755946	C	T	-8.57E-02	1.68E-02	4.24E-08	DCBLD2---[]---AC107029.1
3	99086375	rs34814291	G	A	-6.42E-02	5.89E-03	2.37E-34	DCBLD2---[]---AC107029.1
3	99324088	rs140565493	G	T	-8.33E-02	1.21E-02	6.11E-14	AC107029.1--[]--COL8A1
3	99378077	rs62281832	G	A	7.00E-02	8.39E-03	8.60E-20	[COL8A1]
3	99667565	rs10936003	G	A	-2.60E-02	5.12E-03	3.95E-09	[CMSS1,FILIP1L]
3	100625703	rs17398137	G	A	6.59E-02	6.70E-03	3.22E-24	[ABI3BP]
3	100841979	rs982312	C	T	-2.38E-02	5.56E-03	1.90E-08	ABI3BP---[]-IMPG2
3	106118371	rs11424801	C	CT	3.08E-02	5.71E-03	5.30E-09	CBLB---[]--LINC00882
3	126717964	rs7644947	A	G	-2.63E-02	5.59E-03	2.79E-08	[PLXNA1]
3	134089758	rs143351962	C	T	-1.62E-01	2.56E-02	2.01E-10	[AMOTL2]
4	7919903	rs4696780	A	G	-3.09E-02	5.32E-03	3.61E-11	[AFAP1]
4	53732586	rs8287	T	C	3.21E-02	5.97E-03	2.29E-10	[RASL11B]
4	54979046	rs1158401	C	T	4.43E-02	5.30E-03	3.68E-20	[AC058822.1]
4	55066077	rs6554158	G	A	4.00E-02	6.05E-03	5.70E-15	[AC058822.1]
4	79122800	rs17003043	G	A	2.89E-02	5.41E-03	4.66E-09	[FRAS1]
4	79396057	4:79396057_TC_T	TC	T	3.03E-02	5.35E-03	2.00E-08	[FRAS1]
4	106911742	rs13112725	G	C	-3.17E-02	5.99E-03	2.96E-08	[NPNT]
4	112399511	rs2661764	A	T	3.04E-02	5.34E-03	2.30E-09	PITX2---[]---FAM241A
4	112825940	rs7677732	A	G	2.65E-02	5.44E-03	4.33E-08	[]--FAM241A
4	126239986	rs1039808	C	T	3.19E-02	5.16E-03	9.71E-12	[FAT4]
4	126399998	rs77531977	A	G	4.48E-02	5.63E-03	2.19E-18	[FAT4]
4	128053375	4:128053375_AACAC_A	AACAC	A	2.64E-02	5.25E-03	1.60E-08	[]--INTU
4	166579647	rs2611206	G	A	-3.61E-02	7.32E-03	4.47E-09	CPE---[]---TLL1
5	3645864	rs13184559	A	G	-2.82E-02	5.46E-03	4.57E-10	IRX1--[]---LINC02063
5	15274048	rs7709148	C	T	2.64E-02	5.20E-03	8.61E-09	LINC02149-[]---FBXL7
5	31952051	rs72759609	T	C	1.02E-01	8.52E-03	1.68E-40	[PDZD2]
5	55578661	rs158653	G	A	3.81E-02	5.16E-03	1.26E-17	ANKRD55--[]--LINC01948
5	55701667	rs140212185	C	CTTTTTT	-2.98E-02	5.17E-03	6.40E-10	ANKRD55---[]--LINC01948
5	55744230	rs30372	T	C	-3.88E-02	6.08E-03	9.60E-14	ANKRD55---[]-LINC01948
5	55783715	rs76051791	C	A	-5.75E-02	9.32E-03	3.15E-11	LINC01948-[]--C5orf67
5	82742118	rs12188947	A	C	3.53E-02	5.23E-03	3.15E-17	XRCC4--[]-VCAN
5	87826536	rs56755309	T	C	-6.74E-02	8.98E-03	1.51E-19	TMEM161B---[]---MEF2C
5	121768585	rs304380	G	A	3.19E-02	5.22E-03	5.47E-10	[SNCAIP]
5	125209500	rs10044084	A	T	-2.72E-02	5.45E-03	2.75E-09	[]--GRAMD2B
5	125345974	rs10075656	A	C	-3.26E-02	6.03E-03	6.52E-10	[]--GRAMD2B
5	128881629	rs4276452	C	T	-3.37E-02	5.43E-03	2.20E-11	[ADAMTS19]
5	129054770	rs32819	A	G	8.94E-02	1.14E-02	2.79E-20	[ADAMTS19]
5	131466629	rs3843503	T	A	3.20E-02	5.23E-03	1.57E-10	CSF2--[]--AC063976.1

Supplementary Information - Table 6. ML-based meta VCDR (hits)

CHR	POS	SNP	EA	NEA	BETA	SE	P	GENE_CONTEXT
5	133384337	rs247463	T	G	3.09E-02	6.16E-03	8.62E-10	VDAC1--[]--TCF7
5	133411871	rs187380	C	T	5.94E-02	8.63E-03	1.73E-15	VDAC1--[]--TCF7
5	146925367	rs7715946	A	G	3.91E-02	6.94E-03	3.11E-12	DPYSL3--[]--JAKMIP2
5	172197790	rs34013988	C	T	1.10E-01	1.32E-02	1.27E-23	[AC022217.4,DUSP1]
6	619600	rs1150856	A	C	-4.61E-02	6.81E-03	7.94E-17	[EXOC2]
6	1548369	rs2745572	A	G	3.28E-02	5.47E-03	1.55E-13	FOXF2---[]--FOXC1
6	1983440	rs6914444	T	C	7.01E-02	7.59E-03	1.77E-22	[GMDS]
6	7205796	rs4960295	G	A	-4.37E-02	5.21E-03	3.53E-24	[RREB1]
6	11411838	rs7742703	C	T	4.85E-02	8.73E-03	1.64E-11	NEDD9--[]---TMEM170B
6	31108306	rs7771067	G	A	3.92E-02	6.82E-03	4.84E-09	PSORS1C1[]--CCHCR1
6	31133577	rs145919884	A	AAAGCC	3.35E-02	5.41E-03	3.40E-10	[TCF19,POU5F1]
6	32627155	rs9273402	G	A	2.87E-02	5.20E-03	3.24E-08	HLA-DQA1--[]--HLA-DQB1
6	36552592	rs200252984	G	A	-5.46E-02	6.38E-03	9.90E-21	STK38--[]--SRSF3
6	39531474	rs9369127	T	A	-4.80E-02	5.42E-03	3.46E-20	[KIF6]
6	74850240	rs7770032	A	C	3.49E-02	6.92E-03	2.34E-08	CD109---[]---COL12A1
6	75348855	rs2485070	A	T	-3.17E-02	7.11E-03	4.65E-09	CD109---[]---COL12A1
6	121939112	rs10457423	C	G	3.71E-02	7.25E-03	8.59E-10	GJA1---[]---HSF2
6	122392511	rs2684249	T	C	4.81E-02	5.24E-03	7.95E-25	GJA1---[]---HSF2
6	126730543	rs576049	T	G	-4.48E-02	5.19E-03	9.04E-19	CENPW--[]---RSPO3
6	127298008	rs769528910	A	ACTG	-3.41E-02	5.19E-03	4.60E-11	CENPW--[]---RSPO3
6	148832343	rs139973521	A	ATGAG	-5.54E-02	8.25E-03	3.80E-13	[SASH1]
6	149979416	rs1125	G	A	3.76E-02	5.47E-03	7.56E-14	[LATS1]
6	151295133	rs6900628	A	G	3.17E-02	5.69E-03	4.82E-09	[MTHFD1L]
7	4780514	rs3087749	G	T	-2.74E-02	5.16E-03	1.13E-08	[FOXK1]
7	14237240	rs10260511	C	A	-5.86E-02	7.06E-03	1.52E-23	[DGKB]
7	19624489	rs574793622	A	AT	-3.24E-02	5.37E-03	2.00E-11	FERD3L---[]---TWISTNB
7	28393403	rs7805378	A	C	3.47E-02	5.17E-03	7.25E-14	[CREB5]
7	28854950	rs6964597	T	A	2.97E-02	5.77E-03	7.04E-09	[CREB5]
7	42117040	rs2072201	A	T	2.82E-02	5.28E-03	9.74E-11	[GLI3]
7	101777382	rs201530	A	G	3.11E-02	5.14E-03	1.90E-14	[CUX1]
7	116140931	rs28503222	G	C	-3.03E-02	6.77E-03	1.64E-08	[CAV2]
7	117635382	rs2188836	C	T	-2.42E-02	5.24E-03	4.02E-08	CTTNBP2---[]--AC003084.1
8	8254590	rs2945880	A	G	-7.03E-02	8.14E-03	1.81E-21	PRAG1--[]---AC114550.3
8	17526359	rs11203888	C	T	-3.15E-02	5.45E-03	4.36E-10	[MTUS1]
8	30276920	rs4338062	C	T	-2.57E-02	5.22E-03	2.79E-08	[RBPMS]
8	30336017	rs571194397	A	AT	-3.82E-02	6.87E-03	1.70E-08	[RBPMS]
8	30445960	rs79527387	T	C	3.95E-02	7.71E-03	9.11E-10	[GTF2E2]
8	61911070	rs10957177	A	G	3.45E-02	5.98E-03	2.83E-12	CHD7---[]--CLVS1
8	72278010	rs12543430	T	C	-4.58E-02	5.36E-03	5.21E-18	[EYA1]
8	72392687	rs10093418	A	G	5.26E-02	8.42E-03	1.50E-11	[EYA1]
8	72579250	rs10453110	C	T	-7.49E-02	7.81E-03	7.27E-24	EYA1--[]---AC104012.2
8	75517928	8:75517928_TC_T	TC	T	5.85E-02	1.00E-02	1.20E-09	[MIR2052HG]
8	75519048	8:75519048_TTAAAA_T	TTAAAA	T	3.73E-02	5.30E-03	1.18E-13	[MIR2052HG]
8	75927930	rs28567420	A	C	-3.21E-02	6.26E-03	2.36E-09	[CRISPLD1]
8	76025955	rs11991447	C	T	3.61E-02	6.01E-03	1.37E-11	CRISPLD1--[]---HNF4G
8	78945804	rs10646223	A	AAC	2.92E-02	5.36E-03	2.50E-09	[]--PKIA
8	88761223	rs12547416	C	T	2.97E-02	5.16E-03	2.53E-13	CNBD1---[]---DCAF4L2
8	131636781	rs4565471	C	T	2.58E-02	5.16E-03	1.30E-10	ASAP1---[]---ADCY8
8	143765414	rs2920293	C	G	2.24E-02	5.16E-03	1.67E-09	PSCA--[]--LY6K
9	16619529	rs13290470	A	G	4.16E-02	5.25E-03	3.34E-16	[BNC2]
9	18089832	rs78542921	T	A	-8.83E-02	1.32E-02	2.43E-13	[ADAMTSL1]
9	21941315	rs74903566	G	A	6.26E-02	1.27E-02	1.56E-08	[AL359922.1]

Supplementary Information - Table 6. ML-based meta VCDR (hits)

CHR	POS	SNP	EA	NEA	BETA	SE	P	GENE_CONTEXT
9	21951175	rs117197971	A	G	-7.73E-02	1.21E-02	2.50E-12	[AL359922.1]
9	22007330	rs3217978	C	A	1.16E-01	2.14E-02	3.06E-09	[AL359922.1,CDKN2B-AS1,CDKN2B]
9	22044904	rs74744824	A	G	-1.39E-01	2.26E-02	2.09E-09	[CDKN2B-AS1]
9	22051670	rs944801	G	C	-1.18E-01	5.20E-03	5.11E-144	[CDKN2B-AS1]
9	22052068	rs62560775	A	G	-5.89E-02	8.52E-03	1.16E-12	[CDKN2B-AS1]
9	22082375	rs1547705	A	C	-6.28E-02	8.12E-03	1.15E-19	[CDKN2B-AS1]
9	22090416	rs10965230	C	T	8.10E-02	1.22E-02	9.25E-11	[CDKN2B-AS1]
9	76020565	rs80355279	G	A	3.19E-02	6.66E-03	1.21E-08	ANXA1---[]---AL451127.1
9	76622068	rs11143754	C	A	3.23E-02	5.20E-03	1.18E-09	AL451127.1---[]---AL355674.1
9	89252706	rs10512176	T	C	-4.89E-02	5.85E-03	3.32E-20	TUT7---[]---GAS1
9	89380805	rs1111066	C	G	2.79E-02	5.16E-03	4.04E-09	TUT7---[]---GAS1
9	89819377	rs11141703	T	C	-3.54E-02	6.66E-03	1.44E-09	GAS1---[]---DAPK1
9	134572638	rs35424590	A	G	3.88E-02	5.69E-03	5.82E-13	[RAPGEF1]
9	136145414	rs587611953	C	A	-5.06E-02	7.69E-03	4.80E-13	[ABO]
10	21437861	rs190927291	C	G	-1.60E-01	2.18E-02	7.04E-16	[NEBL]
10	60338753	rs4141671	T	C	-2.73E-02	5.16E-03	8.71E-11	[BICC1]
10	62074139	rs1471246	G	A	2.28E-02	5.25E-03	1.49E-09	[ANK3]
10	63641670	rs2588924	A	G	-2.32E-02	5.16E-03	2.26E-08	CABCOCO1---[]---ARID5B
10	69264839	rs6480262	C	T	-3.54E-02	8.02E-03	3.32E-08	[CTNNA3]
10	69838913	rs117479359	G	T	6.45E-02	9.33E-03	5.02E-15	HERC4-[]--MYPN
10	69879366	rs113337354	A	G	4.61E-02	7.75E-03	2.27E-09	[MYPN]
10	69902549	rs3814180	T	C	-2.96E-02	5.36E-03	5.79E-12	[MYPN]
10	69926319	rs61854624	C	A	4.93E-02	7.01E-03	7.84E-16	[MYPN]
10	69938965	rs10997980	C	T	8.73E-02	1.08E-02	5.11E-20	[MYPN]
10	69952035	rs10998007	C	A	-3.76E-02	8.98E-03	4.34E-08	[MYPN]
10	69974599	10:69974599_CG_C	CG	C	-4.84E-02	6.05E-03	9.90E-19	MYPN-[]--ATOH7
10	69991853	rs7916697	A	G	-1.22E-01	6.01E-03	2.14E-131	[ATOH7]
10	70007008	rs1900020	A	G	6.20E-02	1.62E-02	8.10E-11	ATOH7--[]--PBLD
10	70019201	rs117897884	C	T	1.34E-01	1.77E-02	3.33E-19	ATOH7--[]--PBLD
10	70041695	rs374085072	G	A	1.62E-01	2.87E-02	1.80E-09	ATOH7--[]PBLD
10	70171957	rs10998137	G	A	6.94E-02	1.32E-02	1.43E-12	RUFY2-[]-DNA2
10	70206657	rs367873689	C	CA	1.10E-01	1.29E-02	1.30E-18	[DNA2]
10	70208719	rs200774593	T	C	7.64E-02	1.50E-02	1.60E-08	[DNA2]
10	70399109	rs7095472	A	G	-4.40E-02	5.14E-03	6.87E-21	[TET1]
10	70774039	rs7078237	A	T	3.47E-02	5.68E-03	7.93E-12	[KIFBP]
10	70794817	rs561566466	G	GAA	-5.57E-02	1.08E-02	1.50E-08	[KIFBP]
10	94950713	rs17108260	A	G	-3.32E-02	5.20E-03	5.30E-15	CYP26A1---[]---MYOF
10	94951081	rs61861121	G	A	4.74E-02	9.24E-03	7.44E-09	CYP26A1---[]---MYOF
10	96012950	rs7080472	G	T	-3.30E-02	5.22E-03	5.86E-17	[PLCE1]
10	96071561	rs2077218	G	A	3.78E-02	6.04E-03	2.79E-13	[PLCE1]
10	98967596	rs4919084	G	A	-2.73E-02	5.21E-03	2.73E-09	[ARHGAP19-SLIT1]
10	112028766	rs7077557	T	C	3.13E-02	6.27E-03	2.56E-10	[MXI1]
10	118562545	rs1637553	T	G	-5.69E-02	1.03E-02	3.62E-10	[HSPA12A]
10	118563329	rs1681739	C	T	-4.57E-02	5.24E-03	2.03E-23	[HSPA12A]
10	118918956	rs72840231	A	T	-3.49E-02	5.24E-03	3.00E-11	[MIR3663HG]
11	19960147	rs12807015	G	T	-3.00E-02	5.25E-03	3.20E-10	[NAV2]
11	31570861	rs34618943	T	A	-5.27E-02	6.07E-03	1.30E-21	[ELP4]
11	31807524	rs3026401	C	T	-2.95E-02	6.31E-03	9.33E-09	[ELP4,PAX6]
11	33406776	rs3898926	T	C	-2.80E-02	5.13E-03	1.60E-09	[KIAA1549L]
11	57544484	rs17455626	T	C	-3.13E-02	5.17E-03	2.81E-11	[AP001931.2,AP001931.1,CTNND1]
11	58413910	rs1938598	T	C	3.14E-02	5.99E-03	4.94E-08	[GLYAT]
11	63678128	rs199826712	T	TA	5.11E-02	1.01E-02	9.90E-09	[MARK2]

Supplementary Information - Table 6. ML-based meta VCDR (hits)

CHR	POS	SNP	EA	NEA	BETA	SE	P	GENE_CONTEXT
11	65091708	11:65091708_AGTGT_A	AGTGT	A	3.12E-02	5.70E-03	1.60E-08	[AP000944.5]
11	65146496	rs585210	G	C	-2.48E-02	5.15E-03	4.30E-09	[SLC25A45]
11	65240979	11:65240979_TAA_T	TAA	T	-7.38E-02	1.40E-02	1.30E-08	NEAT1--[--SCYL1
11	65326154	rs12789028	G	A	6.75E-02	6.45E-03	9.77E-40	[LTBP3]
11	86670842	rs11234891	A	G	3.01E-02	5.54E-03	1.78E-09	FZD4--[--TMEM135
11	86740573	rs4944662	C	T	-3.69E-02	6.70E-03	8.11E-12	FZD4--[--TMEM135
11	94533444	rs138059525	G	A	2.34E-01	3.07E-02	2.60E-14	[AMOTL1]
11	95292922	rs11021217	G	A	4.06E-02	5.40E-03	1.49E-16	SESN3---[--FAM76B
11	100645211	rs7123718	G	C	4.18E-02	7.95E-03	3.66E-09	[ARHGAP42]
11	100650559	rs588615	C	A	2.44E-02	5.19E-03	5.82E-09	[ARHGAP42]
11	130262144	rs12806983	G	A	-6.10E-02	1.08E-02	3.83E-11	ZBTB44--[--ADAMTS8
11	130280725	rs4936099	C	A	-5.33E-02	5.25E-03	7.80E-32	[ADAMTS8]
12	3364640	rs147867843	A	ACTTTCT	-6.95E-02	1.28E-02	3.70E-09	[TSPAN9]
12	26392080	rs16930371	A	G	3.74E-02	6.63E-03	2.20E-11	[SSPN]
12	31065843	rs200103122	A	AAAAT	3.73E-02	7.09E-03	1.80E-08	CAPRIN2---[--TSPAN11
12	43548638	rs1399377	G	A	1.84E-02	5.13E-03	2.34E-08	PRICKLE1---[--ADAMTS20
12	48011244	rs679789	C	T	-2.68E-02	5.29E-03	9.07E-10	PCED1B---[--RPAP3
12	48153944	rs12426774	T	C	4.69E-02	7.02E-03	3.81E-16	[RAPGEF3,SLC48A1]
12	76114872	rs6582298	G	A	4.27E-02	5.44E-03	4.21E-14	[AC078923.1]
12	83589688	rs117090733	C	A	4.95E-02	9.86E-03	2.41E-08	TMTC2--[]
12	83604120	rs61931863	A	G	6.67E-02	1.28E-02	1.70E-08	TMTC2--[]
12	83673711	rs11115686	G	A	3.49E-02	5.15E-03	9.08E-15	TMTC2---[]
12	83856540	rs12826083	G	A	-5.66E-02	7.55E-03	1.26E-15	TMTC2---[]
12	83858003	rs76005250	G	A	8.02E-02	1.12E-02	4.23E-15	TMTC2---[]
12	83861261	rs77725841	A	G	6.41E-02	9.37E-03	4.33E-14	TMTC2---[]
12	83928366	rs17653396	C	T	6.21E-02	1.01E-02	1.38E-10	TMTC2---[]
12	84011749	rs11115933	C	G	-6.53E-02	9.46E-03	1.94E-13	TMTC2---[]
12	84049853	rs10506895	G	A	1.18E-01	5.16E-03	4.41E-133	TMTC2---[]
12	84132842	rs1380758	A	G	5.58E-02	9.38E-03	3.49E-11	TMTC2---[]
12	84135457	rs142121892	C	CA	5.65E-02	5.57E-03	6.30E-27	TMTC2---[]
12	84154996	rs71450946	A	G	-6.57E-02	9.87E-03	1.49E-14	TMTC2---[]
12	84225749	rs200654546	C	CT	9.65E-02	1.83E-02	2.68E-15	TMTC2---[]
12	84225935	rs7137822	A	T	5.46E-02	5.82E-03	8.50E-23	TMTC2---[]
12	84237124	12:84237124_CTAA_C	CTAA	C	6.89E-02	1.18E-02	4.50E-11	TMTC2---[]
12	84359892	rs12423401	C	A	-7.10E-02	8.93E-03	4.02E-16	TMTC2---[--SLC6A15
12	84404719	rs4772012	T	C	3.50E-02	6.11E-03	2.90E-11	TMTC2---[--SLC6A15
12	84890667	rs71445008	C	CT	-3.97E-02	5.34E-03	4.10E-16	[---SLC6A15
12	91816926	rs147377344	C	CTTTTAC	3.04E-02	5.30E-03	2.10E-08	DCN---[--LINC01619
12	106716441	rs17218455	C	T	3.44E-02	6.80E-03	2.46E-08	[TCP11L2]
12	107250252	rs17038814	A	G	5.54E-02	7.59E-03	5.13E-18	[RIC8B]
12	108134273	rs4964616	T	A	-4.00E-02	5.32E-03	2.26E-13	[PRDM4]
12	108988757	rs17040818	G	T	-2.97E-02	6.52E-03	3.21E-08	[TMEM119]
12	109874230	rs2075432	A	G	2.45E-02	5.15E-03	1.82E-09	[MYO1H]
12	111800258	rs3809272	G	A	-2.82E-02	5.59E-03	9.62E-09	[PHETA1]
12	124666527	rs7134138	A	G	-3.64E-02	5.16E-03	3.64E-18	[RFLNA]
13	25766614	rs9507473	G	C	-4.22E-02	7.88E-03	6.88E-09	AMER2--[--LINC01076
13	36683268	rs9546383	T	C	-4.49E-02	5.99E-03	1.50E-19	[DCLK1]
13	51913708	rs9535646	C	T	4.00E-02	6.98E-03	4.01E-11	[SERPINE3]
13	109264870	rs139237435	A	ACATTTA	5.18E-02	5.88E-03	1.20E-21	[MYO16]
13	110718555	rs12875868	A	G	-2.80E-02	6.03E-03	4.37E-08	IRS2---[--COL4A1
13	110778747	13:110778747_CCTTTT_C	CCTTTT	C	-4.57E-02	5.51E-03	9.90E-18	IRS2---[--COL4A1
14	23452128	rs3811183	C	G	-3.35E-02	5.28E-03	7.26E-13	AJUBA[-]C14orf93

Supplementary Information - Table 6. ML-based meta VCDR (hits)

CHR	POS	SNP	EA	NEA	BETA	SE	P	GENE_CONTEXT
14	53989952	rs11623384	C	T	4.10E-02	5.45E-03	4.10E-17	DDHD1---[]--AL163953.1
14	59583906	rs61985994	C	G	3.79E-02	7.39E-03	1.88E-08	DACT1---[]--DAAM1
14	60806759	rs7493429	A	C	-5.70E-02	5.62E-03	2.59E-35	PPM1A---[]--C14orf39
14	60914325	rs139811951	G	A	4.77E-02	7.81E-03	1.43E-11	[C14orf39]
14	61238781	rs12147818	G	A	2.17E-01	3.21E-02	8.10E-13	[MNAT1]
14	65074869	rs8006017	A	G	-5.53E-02	6.90E-03	1.23E-19	PPP1R36---[]--PLEKHG3
14	85668732	rs11626115	G	A	-7.93E-02	1.19E-02	8.52E-10	[]--FLRT2
14	85862281	rs34662716	T	TAC	3.25E-02	5.43E-03	6.30E-10	[]--FLRT2
14	85922578	rs1289426	A	G	-5.21E-02	6.14E-03	2.69E-18	[]--FLRT2
14	86021748	rs2018653	A	G	-4.40E-02	6.03E-03	3.06E-17	[FLRT2]
14	95957694	rs11160251	T	G	3.13E-02	5.63E-03	2.53E-08	SYNE3---[]--GLRX5
15	71840327	rs35194812	T	C	-3.73E-02	7.07E-03	2.81E-11	[THSD4]
15	71886234	rs11632300	T	C	2.92E-02	5.55E-03	1.37E-09	[THSD4]
15	71945128	rs17797245	T	C	2.65E-02	5.52E-03	5.32E-09	[THSD4]
15	74228391	rs4077284	A	G	3.07E-02	5.35E-03	1.41E-11	[LOXL1]
15	84484384	rs59199978	A	G	-4.63E-02	6.71E-03	3.11E-11	[ADAMTSL3]
15	99458902	rs28612945	C	T	4.67E-02	6.38E-03	1.54E-15	[IGF1R]
15	101200962	rs11452536	T	TA	-2.92E-02	5.36E-03	1.50E-09	ASB7-[]---ALDH1A3
15	101201604	rs4299136	G	C	-7.17E-02	7.55E-03	7.59E-29	ASB7-[]---ALDH1A3
15	101753394	rs28623369	T	G	3.27E-02	5.99E-03	5.90E-10	[CHSY1]
16	51188433	rs2052284	T	A	-3.46E-02	5.27E-03	1.20E-11	SALL1-[]---HNRNPA1P48
16	51341412	rs117537696	T	G	-1.30E-01	1.86E-02	1.38E-15	SALL1---[]---HNRNPA1P48
16	51401342	rs58577768	C	T	-1.19E-01	1.55E-02	1.05E-16	SALL1---[]---HNRNPA1P48
16	51416004	rs11111196	A	T	-7.16E-02	5.88E-03	5.35E-42	SALL1---[]---HNRNPA1P48
16	51469726	rs8053277	T	C	8.35E-02	5.61E-03	6.28E-65	SALL1---[]---HNRNPA1P48
16	51470928	rs71386559	C	T	1.02E-01	1.34E-02	1.33E-19	SALL1---[]---HNRNPA1P48
16	51500120	rs1080791	A	G	5.60E-02	6.00E-03	9.00E-22	SALL1---[]---HNRNPA1P48
16	51562293	rs537414151	C	G	1.48E-01	2.50E-02	2.20E-10	SALL1---[]---HNRNPA1P48
16	51568425	rs62039775	G	T	-1.04E-01	8.62E-03	3.41E-40	SALL1---[]---HNRNPA1P48
16	51649796	16:51649796_CTCTT_C	CTCTT	C	-3.55E-02	5.62E-03	8.90E-10	[HNRNPA1P48]
16	51667131	rs8057507	T	C	-5.22E-02	5.16E-03	1.44E-26	[HNRNPA1P48]
16	51854068	rs11861489	T	C	-3.47E-02	5.42E-03	1.60E-09	HNRNPA1P48---[]---TOX3
16	74279778	rs4889487	G	C	3.22E-02	5.72E-03	1.05E-11	ZFH3---[]--PSMD7
16	74456717	rs199895842	T	G	-8.15E-02	1.50E-02	3.60E-08	[AC009053.4]
16	74465514	rs11648326	C	A	3.76E-02	7.46E-03	4.21E-09	[AC009053.4]
16	86382120	rs1687626	A	G	2.95E-02	5.30E-03	2.42E-09	IRF8---[]--FOXF1
16	86386675	rs1728368	C	T	9.05E-02	8.98E-03	4.66E-28	IRF8---[]--FOXF1
16	86439374	rs12935509	G	A	-6.15E-02	9.42E-03	1.42E-11	IRF8---[]--FOXF1
16	86465590	rs13332095	G	A	-4.76E-02	8.54E-03	2.23E-10	IRF8---[]--FOXF1
16	86511858	rs7187191	T	G	4.58E-02	6.67E-03	1.24E-16	IRF8---[]--FOXF1
17	10026855	rs12936070	C	T	2.69E-02	5.93E-03	9.97E-10	[GAS7]
17	40867365	rs115818584	C	G	1.22E-01	2.06E-02	4.01E-11	[EZH1]
17	45703433	rs7220935	C	T	2.81E-02	5.15E-03	1.84E-11	NPEPPS-[]--KPNB1
17	48225686	rs4794104	C	G	-4.13E-02	7.00E-03	6.55E-13	[PPP1R9B]
17	55419687	rs792401	G	A	2.71E-02	5.60E-03	2.91E-08	[MSI2]
17	55564211	rs277065	G	A	3.32E-02	7.30E-03	3.95E-08	[MSI2]
17	61865670	17:61865670_CT_C	CT	C	-3.20E-02	5.48E-03	2.40E-10	[DDX42]
17	65264966	rs12939113	C	T	-3.25E-02	5.70E-03	6.93E-11	HELZ-[]--PSMD12
17	79602063	rs9905786	G	T	-2.52E-02	5.36E-03	2.56E-09	[NPLOC4]
17	80169426	rs796355894	A	AT	2.99E-02	5.34E-03	1.60E-08	[CCDC57]
18	8799828	rs568267	C	T	3.34E-02	5.92E-03	3.69E-10	[MTCL1]
18	23063159	rs766791666	T	TATC	-3.03E-02	5.31E-03	4.00E-10	ZNF521---[]---SS18

Supplementary Information - Table 6. ML-based meta VCDR (hits)

CHR	POS	SNP	EA	NEA	BETA	SE	P	GENE_CONTEXT
18	34289285	rs61735998	G	T	1.03E-01	1.64E-02	7.55E-12	[FHOD3]
18	56943484	rs77759734	C	T	-6.58E-02	1.20E-02	2.92E-08	[CPLX4]
19	817708	rs7250902	A	G	3.93E-02	5.61E-03	3.65E-15	[PLPPR3]
19	14639064	rs112614575	C	CT	3.96E-02	7.30E-03	6.10E-09	[DNAJB1,TECR]
19	32027330	rs8102936	G	A	5.12E-02	5.47E-03	1.85E-21	TSHZ3---[]--ZNF507
19	33477716	19:33477716_AAT_A	AAT	A	-4.52E-02	8.08E-03	1.40E-09	[RHPN2]
19	39195302	rs757940594	A	AGGAG	-3.15E-02	5.16E-03	7.40E-10	[ACTN4]
19	46356548	rs7258364	T	C	-2.64E-02	5.51E-03	2.14E-08	[SYMPK]
19	47455315	rs311384	A	G	2.51E-02	5.66E-03	2.42E-08	[ARHGAP35]
20	1029686	rs4816177	A	G	-4.10E-02	6.79E-03	1.83E-08	RSPO4--[]--PSMF1
20	6137310	rs6076954	A	G	4.62E-02	5.71E-03	1.01E-19	FERMT1---[]---LINC01713
20	6230570	rs6133302	C	T	-4.58E-02	7.33E-03	1.29E-13	FERMT1---[]---LINC01713
20	6292315	rs6076968	C	T	2.78E-02	5.18E-03	7.65E-10	FERMT1---[]---LINC01713
20	6411069	rs4815897	A	G	-4.63E-02	6.57E-03	2.31E-12	FERMT1---[]---LINC01713
20	6470094	rs2326788	G	A	8.85E-02	5.33E-03	1.10E-67	FERMT1---[]---LINC01713
20	6474916	rs11483156	C	CT	-5.47E-02	8.27E-03	4.80E-11	FERMT1---[]---LINC01713
20	6514692	rs6038531	G	A	-1.45E-01	2.05E-02	4.81E-15	FERMT1---[]---LINC01713
20	6535065	rs78004679	G	A	8.75E-02	1.11E-02	1.81E-16	FERMT1---[]---LINC01713
20	6544738	rs73077173	C	T	7.42E-02	1.30E-02	3.44E-08	FERMT1---[]---LINC01713
20	6631055	rs1358805	A	G	-4.30E-02	6.79E-03	1.42E-12	FERMT1---[]---LINC01713
20	6650790	rs6054446	G	C	-7.35E-02	1.38E-02	9.81E-10	FERMT1---[]---LINC01713
20	6759115	rs235768	A	T	-3.83E-02	5.28E-03	1.82E-15	[BMP2]
20	31157394	rs4911242	A	T	3.17E-02	5.54E-03	2.02E-10	[NOL4L]
20	31438954	rs4911268	A	G	5.00E-02	6.67E-03	5.16E-17	MAPRE1[]-EFCAB8
20	45796660	rs2903940	A	G	-3.24E-02	5.16E-03	3.31E-13	[EYA2]
21	29506261	rs6516818	T	A	2.43E-02	5.22E-03	4.48E-08	LINC01673---[]---N6AMT1
22	28208528	rs11704137	C	G	-5.16E-02	5.91E-03	6.91E-22	MN1--[]--PITPNB
22	28324924	rs62235636	C	T	9.94E-02	9.97E-03	3.47E-27	[TTC28-AS1]
22	28629713	rs16986177	C	T	-6.80E-02	7.02E-03	2.75E-31	[TTC28]
22	28653727	22:28653727_CATAT_C	CATAT	C	3.55E-02	5.55E-03	7.50E-11	[TTC28]
22	28990300	rs117456789	C	T	7.28E-02	1.20E-02	1.03E-10	[TTC28]
22	29032115	rs71316851	A	ATT	-3.45E-02	5.19E-03	7.60E-11	[TTC28]
22	29051261	rs73170612	A	C	9.70E-02	1.18E-02	1.16E-20	[TTC28]
22	29063037	rs542574575	C	T	3.46E-02	5.43E-03	2.00E-11	[TTC28]
22	29098417	rs112564028	A	G	-7.69E-02	1.85E-02	6.73E-09	[CHEK2]
22	29100301	rs527965516	T	A	2.26E-01	1.79E-02	5.40E-41	[CHEK2]
22	29115066	rs4822983	C	T	1.12E-01	5.49E-03	1.37E-110	[CHEK2]
22	29127402	rs8184952	T	C	6.06E-02	7.06E-03	2.43E-19	[CHEK2]
22	29162191	rs145346186	A	C	9.01E-02	1.26E-02	8.20E-12	HSCB-[]-CCDC117
22	29276230	22:29276230_AT_A	AT	A	4.93E-02	7.76E-03	6.00E-12	Z93930.2--[]-ZNR3
22	29441350	22:29441350_CA_C	CA	C	-3.90E-02	5.63E-03	1.60E-13	[ZNR3]
22	30442880	rs79955051	G	A	-7.92E-02	1.60E-02	9.95E-09	[HORMAD2-AS1]
22	30503827	rs17648370	A	G	9.23E-02	1.91E-02	1.51E-08	[HORMAD2]
22	30570022	rs1003342	A	G	4.80E-02	5.16E-03	3.50E-27	[HORMAD2]
22	30606986	rs9614164	C	T	3.75E-02	6.25E-03	2.87E-10	AC002378.1-[]--LIF
22	30620627	rs6006405	A	G	-5.65E-02	7.09E-03	1.75E-16	AC002378.1-[]--LIF
22	30649229	rs73166584	C	T	-3.85E-02	6.82E-03	1.32E-09	LIF-[]-OSM
22	30653991	rs9620961	C	T	2.83E-02	5.35E-03	1.12E-08	LIF--[]-OSM
22	37819985	rs133726	T	G	-3.82E-02	7.08E-03	8.78E-10	[ELFN2]
22	37872262	rs75110580	G	A	-9.21E-02	1.40E-02	8.60E-12	[MFNG]
22	37904251	rs2235334	T	C	-2.56E-02	5.16E-03	2.40E-08	[CARD10]
22	37907069	rs2092172	G	A	-7.49E-02	6.21E-03	5.81E-40	[CARD10]

Supplementary Information - Table 6. ML-based meta VCDR (hits)

CHR	POS	SNP	EA	NEA	BETA	SE	P	GENE_CONTEXT
22	37925332	rs549756240	A	T	-5.60E-02	9.78E-03	1.90E-08	CARD10-[]--CDC42EP1
22	37939510	rs9610795	G	T	-4.87E-02	5.42E-03	4.03E-21	CARD10-[]--CDC42EP1
22	38057338	rs9622678	A	G	-3.75E-02	7.00E-03	1.90E-09	[Z83844.3,PDXP]
22	38076063	rs62236673	G	A	-2.60E-02	5.48E-03	1.91E-08	LGALS1[]--NOL12
22	38177004	rs12166106	T	C	3.71E-02	7.11E-03	6.65E-09	TRIOBP-[]--H1-0
22	38180407	22:38180407_CAA_C	CAA	C	-6.60E-02	5.51E-03	2.70E-36	TRIOBP-[]--H1-0
22	38594126	rs147906180	C	CAAAAA	-4.98E-02	5.51E-03	1.20E-20	[PLA2G6]
22	38674541	rs8184979	G	A	-3.93E-02	7.24E-03	2.81E-08	TMEM184B-[]--CSNK1E
22	39322264	rs9306330	C	T	-3.43E-02	6.67E-03	2.19E-09	AL022318.1-[]--APOBEC3A
22	46376985	rs77164166	G	A	4.73E-02	5.55E-03	3.90E-17	WNT7B-[]--LINC00899
22	46381414	rs62228064	G	A	-4.09E-02	7.25E-03	1.79E-09	WNT7B-[]--LINC00899

Supplementary Information - Table 7. ML-based meta VCDR (loci)

CHR	POS	SNP	EA	NEA	BETA	SE	P	GENE_CONTEXT	CRAIG	CRAIG_META
1	3056222	rs35271327	A	AT	-1.18E-01	1.08E-02	2.10E-29	[PRDM16]	TRUE	TRUE
1	8486131	rs302714	A	C	-3.46E-02	5.37E-03	1.61E-14	[RERE,RERE-AS1]	FALSE	TRUE
1	12614029	rs6541032	T	C	-3.85E-02	5.14E-03	2.30E-18	VPS13D--[]--DHRS3	TRUE	TRUE
1	47923058	rs767682581	C	CT	-3.22E-02	5.33E-03	1.40E-10	FOXD2--[]---TRABD2B	FALSE	FALSE
1	53565054	rs58924052	T	C	-6.34E-02	1.22E-02	3.70E-08	[SLC1A7]	FALSE	FALSE
1	56955386	rs4638151	C	T	-2.57E-02	5.51E-03	2.76E-08	[AC119674.2]	FALSE	FALSE
1	68848681	rs1925953	A	T	-5.63E-02	5.20E-03	4.49E-34	WLS---[]--RPE65	TRUE	TRUE
1	89295765	rs786914	C	A	-3.23E-02	5.23E-03	1.67E-11	[PKN2]	FALSE	TRUE
1	92077097	rs1192415	G	A	1.33E-01	6.50E-03	8.55E-110	CDC7--[]--TGFB3	TRUE	TRUE
1	103441814	rs2061705	A	G	2.31E-02	5.13E-03	2.81E-08	[COL11A1]	FALSE	FALSE
1	110632536	rs11102052	A	T	3.49E-02	5.32E-03	3.52E-12	STRIP1--[]--UBL4B	FALSE	FALSE
1	113046395	rs351365	T	C	-2.96E-02	5.89E-03	4.81E-09	[WNT2B]	FALSE	FALSE
1	155033308	rs11589479	G	A	3.67E-02	6.91E-03	2.11E-08	[ADAM15]	FALSE	FALSE
1	165715300	rs6426939	C	T	4.10E-02	7.68E-03	4.96E-09	[TMCO1]	FALSE	FALSE
1	167691909	rs7548746	A	G	5.22E-02	1.08E-02	1.76E-08	[MPZL1]	FALSE	FALSE
1	169551682	rs6028	T	C	-3.04E-02	5.61E-03	1.64E-12	[F5]	FALSE	TRUE
1	183849739	rs41263652	G	C	5.42E-02	8.45E-03	1.54E-11	[RGL1]	FALSE	FALSE
1	218520995	rs6658835	A	G	-4.50E-02	5.76E-03	5.42E-15	[TGFB2]	TRUE	TRUE
1	219451442	rs7536147	A	G	2.89E-02	5.58E-03	3.26E-11	AL360093.1--[]--ZC3H11B	FALSE	FALSE
1	227585983	rs6670351	G	A	-5.02E-02	6.35E-03	6.82E-16	CDC42BPA--[]--ZNF678	TRUE	TRUE
2	5680539	rs7575439	C	A	3.08E-02	5.48E-03	5.18E-10	LINC01249---[]--AC108025.1	FALSE	FALSE
2	12891476	rs730126	A	C	3.00E-02	5.24E-03	1.58E-09	TRIB2-[]	FALSE	FALSE
2	19420060	rs851321	C	T	-1.98E-01	2.21E-02	6.99E-22	NT5C1B---[]--OSR1	FALSE	TRUE
2	28383841	rs10165930	G	A	-2.90E-02	6.03E-03	1.80E-08	[BABAM2]	FALSE	FALSE
2	42509829	rs6723361	T	C	-3.00E-02	5.50E-03	8.98E-10	[EML4]	FALSE	FALSE
2	56013061	rs17047234	A	C	5.97E-02	6.17E-03	1.34E-24	PNPT1--[]--EFEMP1	TRUE	TRUE
2	111680818	rs2880192	A	G	3.84E-02	5.37E-03	1.65E-16	[ACOXL]	TRUE	TRUE
2	180196027	rs12620141	C	A	-3.06E-02	5.41E-03	2.50E-09	AC093911.1--[]--ZNF385B	FALSE	FALSE
2	190269957	2:190269957_CTTT_C	CTTTT	C	3.13E-02	5.57E-03	3.00E-09	COL5A2---[]--WDR75	FALSE	FALSE
2	239273949	rs56330821	C	T	4.50E-02	9.14E-03	3.34E-09	[TRAF3IP1]	FALSE	TRUE
2	241931723	rs12694992	G	A	2.87E-02	5.36E-03	9.14E-11	[CROCC2]	FALSE	FALSE
3	20059749	rs2948098	G	A	2.99E-02	5.47E-03	2.00E-08	PP2D1-[]--KAT2B	FALSE	FALSE
3	25159627	rs1604012	A	T	-4.18E-02	5.14E-03	3.01E-20	THRB-AS1---[]--RARB	TRUE	TRUE
3	29493443	rs1946825	A	G	-2.78E-02	5.29E-03	2.71E-09	[AC098650.1,RBMS3]	FALSE	FALSE
3	32879823	rs56131903	A	T	4.66E-02	5.53E-03	2.12E-21	[TRIM71]	TRUE	TRUE
3	48743342	rs551116669	T	TA	3.29E-02	5.38E-03	2.80E-10	[IP6K2]	FALSE	FALSE
3	58035497	rs12494328	G	A	-4.28E-02	6.14E-03	5.89E-16	[FLNB]	FALSE	TRUE
3	71182447	rs77877421	A	T	-8.71E-02	1.13E-02	1.06E-13	[FOXP1,AC097634.4]	FALSE	FALSE
3	88387796	rs9879264	A	G	4.65E-02	5.15E-03	7.27E-24	[CSNKA2IP]	TRUE	TRUE
3	99086375	rs34814291	G	A	-6.42E-02	5.89E-03	2.37E-34	DCBLD2---[]--AC107029.1	TRUE	TRUE
3	106118371	rs11424801	C	CT	3.08E-02	5.71E-03	5.30E-09	CBLB---[]--LINC00882	FALSE	FALSE
3	126717964	rs7644947	A	G	-2.63E-02	5.59E-03	2.79E-08	[PLXNA1]	FALSE	FALSE
3	134089758	rs143351962	C	T	-1.62E-01	2.56E-02	2.01E-10	[AMOTL2]	TRUE	FALSE
4	7919903	rs4696780	A	G	-3.09E-02	5.32E-03	3.61E-11	[AFAP1]	FALSE	FALSE
4	53732586	rs8287	T	C	3.21E-02	5.97E-03	2.29E-10	[RASL11B]	FALSE	FALSE
4	54979046	rs1158401	C	T	4.43E-02	5.30E-03	3.68E-20	[AC058822.1]	TRUE	TRUE
4	79122800	rs17003043	G	A	2.89E-02	5.41E-03	4.66E-09	[FRAS1]	FALSE	FALSE
4	106911742	rs13112725	G	C	-3.17E-02	5.99E-03	2.96E-08	[NPNT]	FALSE	FALSE
4	112399511	rs2661764	A	T	3.04E-02	5.34E-03	2.30E-09	PITX2---[]--FAM241A	FALSE	FALSE
4	126399998	rs77531977	A	G	4.48E-02	5.63E-03	2.19E-18	[FAT4]	FALSE	TRUE
4	128053375	4:128053375_AACAC_A	AACAC	A	2.64E-02	5.25E-03	1.60E-08	[]--INTU	FALSE	FALSE
4	166579647	rs2611206	G	A	-3.61E-02	7.32E-03	4.47E-09	CPE---[]--TLL1	FALSE	TRUE
5	3645864	rs13184559	A	G	-2.82E-02	5.46E-03	4.57E-10	IRX1--[]--LINC02063	FALSE	TRUE
5	15274048	rs7709148	C	T	2.64E-02	5.20E-03	8.61E-09	LINC02149-[]--FBXL7	FALSE	FALSE
5	31952051	rs72759609	T	C	1.02E-01	8.52E-03	1.68E-40	[PDZD2]	TRUE	TRUE
5	55578661	rs158653	G	A	3.81E-02	5.16E-03	1.26E-17	ANKRD55--[]--LINC01948	TRUE	TRUE
5	82742118	rs12188947	A	C	3.53E-02	5.23E-03	3.15E-17	XRCC4--[]--VCAN	FALSE	TRUE
5	87826536	rs56755309	T	C	-6.74E-02	8.98E-03	1.51E-19	TMEM161B---[]--MEF2C	FALSE	TRUE
5	121768585	rs304380	G	A	3.19E-02	5.22E-03	5.47E-10	[SNCAIP]	FALSE	FALSE
5	125345974	rs10075656	A	C	-3.26E-02	6.03E-03	6.52E-10	[]--GRAMD2B	FALSE	FALSE

Supplementary Information - Table 7. ML-based meta VCDR (loci)

CHR	POS	SNP	EA	NEA	BETA	SE	P	GENE_CONTEXT	CRAIG	CRAIG_META
5	129054770	rs32819	A	G	8.94E-02	1.14E-02	2.79E-20	[ADAMTS19]	TRUE	TRUE
5	133411871	rs187380	C	T	5.94E-02	8.63E-03	1.73E-15	VDAC1--[]--TCF7	TRUE	TRUE
5	146925367	rs7715946	A	G	3.91E-02	6.94E-03	3.11E-12	DPYSL3--[]--JAKMIP2	FALSE	FALSE
5	172197790	rs34013988	C	T	1.10E-01	1.32E-02	1.27E-23	[AC022217.4,DUSP1]	TRUE	TRUE
6	619600	rs1150856	A	C	-4.61E-02	6.81E-03	7.94E-17	[EXOC2]	FALSE	TRUE
6	1548369	rs2745572	A	G	3.28E-02	5.47E-03	1.55E-13	FOXF2--[]--FOXC1	FALSE	FALSE
6	1983440	rs6914444	T	C	7.01E-02	7.59E-03	1.77E-22	[GMDS]	TRUE	TRUE
6	7205796	rs4960295	G	A	-4.37E-02	5.21E-03	3.53E-24	[RREB1]	TRUE	TRUE
6	11411838	rs7742703	C	T	4.85E-02	8.73E-03	1.64E-11	NEDD9--[]--TMEM170B	FALSE	FALSE
6	31133577	rs145919884	A	AAAGCCC	3.35E-02	5.41E-03	3.40E-10	[TCF19,POU5F1]	FALSE	FALSE
6	36552592	rs200252984	G	A	-5.46E-02	6.38E-03	9.90E-21	STK38--[]--SRSF3	TRUE	TRUE
6	39531474	rs9369127	T	A	-4.80E-02	5.42E-03	3.46E-20	[KIF6]	FALSE	TRUE
6	75348855	rs2485070	A	T	-3.17E-02	7.11E-03	4.65E-09	CD109--[]--COL12A1	FALSE	FALSE
6	122392511	rs2684249	T	C	4.81E-02	5.24E-03	7.95E-25	GJA1--[]--HSF2	TRUE	TRUE
6	126730543	rs576049	T	G	-4.48E-02	5.19E-03	9.04E-19	CENPW--[]--RSPO3	FALSE	FALSE
6	148832343	rs139973521	A	ATGAG	-5.54E-02	8.25E-03	3.80E-13	[SASH1]	FALSE	FALSE
6	149979416	rs1125	G	A	3.76E-02	5.47E-03	7.56E-14	[LATS1]	FALSE	FALSE
6	151295133	rs6900628	A	G	3.17E-02	5.69E-03	4.82E-09	[MTHFD1L]	FALSE	FALSE
7	4780514	rs3087749	G	T	-2.74E-02	5.16E-03	1.13E-08	[FOKK1]	FALSE	FALSE
7	14237240	rs10260511	C	A	-5.86E-02	7.06E-03	1.52E-23	[DGKB]	TRUE	TRUE
7	19624489	rs574793622	A	AT	-3.24E-02	5.37E-03	2.00E-11	FERD3L---[]---TWISTNB	TRUE	TRUE
7	28393403	rs7805378	A	C	3.47E-02	5.17E-03	7.25E-14	[CREB5]	TRUE	TRUE
7	28854950	rs6964597	T	A	2.97E-02	5.77E-03	7.04E-09	[CREB5]	FALSE	FALSE
7	42117040	rs2072201	A	T	2.82E-02	5.28E-03	9.74E-11	[GLI3]	FALSE	FALSE
7	101777382	rs201530	A	G	3.11E-02	5.14E-03	1.90E-14	[CUX1]	FALSE	TRUE
7	116140931	rs28503222	G	C	-3.03E-02	6.77E-03	1.64E-08	[CAV2]	FALSE	FALSE
7	117635382	rs2188836	C	T	-2.42E-02	5.24E-03	4.02E-08	CTTNBP2---[]--AC003084.1	FALSE	FALSE
8	8254590	rs2945880	A	G	-7.03E-02	8.14E-03	1.81E-21	PRAG1--[]--AC114550.3	TRUE	TRUE
8	17526359	rs11203888	C	T	-3.15E-02	5.45E-03	4.36E-10	[MTUS1]	FALSE	FALSE
8	30445960	rs79527387	T	C	3.95E-02	7.71E-03	9.11E-10	[GTF2E2]	FALSE	FALSE
8	61911070	rs10957177	A	G	3.45E-02	5.98E-03	2.83E-12	CHD7---[]--CLVS1	FALSE	FALSE
8	72579250	rs10453110	C	T	-7.49E-02	7.81E-03	7.27E-24	EYA1--[]--AC104012.2	TRUE	TRUE
8	75519048	8:75519048_TTAAAA_T	TTAAAA	T	3.73E-02	5.30E-03	1.18E-13	[MIR2052HG]	FALSE	FALSE
8	78945804	rs10646223	A	AAC	2.92E-02	5.36E-03	2.50E-09	[]--PKIA	FALSE	FALSE
8	88761223	rs12547416	C	T	2.97E-02	5.16E-03	2.53E-13	CNBD1---[]--DCAF4L2	FALSE	FALSE
8	131636781	rs4565471	C	T	2.58E-02	5.16E-03	1.30E-10	ASAP1---[]--ADCY8	FALSE	FALSE
8	143765414	rs2920293	C	G	2.24E-02	5.16E-03	1.67E-09	PSCA--[]--LY6K	FALSE	FALSE
9	16619529	rs13290470	A	G	4.16E-02	5.25E-03	3.34E-16	[BNC2]	FALSE	FALSE
9	18089832	rs78542921	T	A	-8.83E-02	1.32E-02	2.43E-13	[ADAMTSL1]	TRUE	TRUE
9	22051670	rs944801	G	C	-1.18E-01	5.20E-03	5.11E-144	[CDKN2B-AS1]	TRUE	TRUE
9	76622068	rs11143754	C	A	3.23E-02	5.20E-03	1.18E-09	AL451127.1---[]--AL355674.1	FALSE	FALSE
9	89252706	rs10512176	T	C	-4.89E-02	5.85E-03	3.32E-20	TUT7--[]--GAS1	FALSE	TRUE
9	134572638	rs35424590	A	G	3.88E-02	5.69E-03	5.82E-13	[RAPGEF1]	FALSE	FALSE
9	136145414	rs587611953	C	A	-5.06E-02	7.69E-03	4.80E-13	[ABO]	FALSE	TRUE
10	21437861	rs190927291	C	G	-1.60E-01	2.18E-02	7.04E-16	[NEBL]	TRUE	TRUE
10	60338753	rs4141671	T	C	-2.73E-02	5.16E-03	8.71E-11	[BICC1]	FALSE	FALSE
10	62074139	rs1471246	G	A	2.28E-02	5.25E-03	1.49E-09	[ANK3]	FALSE	FALSE
10	63641670	rs2588924	A	G	-2.32E-02	5.16E-03	2.26E-08	CABCOCO1---[]--ARID5B	FALSE	FALSE
10	69991853	rs7916697	A	G	-1.22E-01	6.01E-03	2.14E-131	[ATOH7]	TRUE	TRUE
10	94950713	rs17108260	A	G	-3.32E-02	5.20E-03	5.30E-15	CYP26A1---[]--MYOF	TRUE	TRUE
10	96012950	rs7080472	G	T	-3.30E-02	5.22E-03	5.86E-17	[PLCE1]	FALSE	TRUE
10	98967596	rs4919084	G	A	-2.73E-02	5.21E-03	2.73E-09	[ARHGAP19-SLIT1]	FALSE	FALSE
10	112028766	rs7077557	T	C	3.13E-02	6.27E-03	2.56E-10	[MXI1]	FALSE	FALSE
10	118563329	rs1681739	C	T	-4.57E-02	5.24E-03	2.03E-23	[HSPA12A]	TRUE	TRUE
11	19960147	rs12807015	G	T	-3.00E-02	5.25E-03	3.20E-10	[NAV2]	FALSE	FALSE
11	31570861	rs34618943	T	A	-5.27E-02	6.07E-03	1.30E-21	[ELP4]	TRUE	TRUE
11	33406776	rs3898926	T	C	-2.80E-02	5.13E-03	1.60E-09	[KIAA1549L]	TRUE	TRUE
11	57544484	rs17445626	T	C	-3.13E-02	5.17E-03	2.81E-11	[AP001931.2,AP001931.1,CTNND1]	FALSE	FALSE
11	63678128	rs199826712	T	TA	5.11E-02	1.01E-02	9.90E-09	[MARK2]	FALSE	FALSE
11	65326154	rs12789028	G	A	6.75E-02	6.45E-03	9.77E-40	[LTBP3]	TRUE	TRUE

Supplementary Information - Table 7. ML-based meta VCDR (loci)

CHR	POS	SNP	EA	NEA	BETA	SE	P	GENE_CONTEXT	CRAIG	CRAIG_META
11	86740573	rs4944662	C	T	-3.69E-02	6.70E-03	8.11E-12	FZD4--[TMEM135	TRUE	TRUE
11	94533444	rs138059525	G	A	2.34E-01	3.07E-02	2.60E-14	[AMOTL1]	FALSE	FALSE
11	95292922	rs11021217	G	A	4.06E-02	5.40E-03	1.49E-16	SES3--[FAM76B	TRUE	TRUE
11	100645211	rs7123718	G	C	4.18E-02	7.95E-03	3.66E-09	[ARHGAP42]	FALSE	FALSE
11	130280725	rs4936099	C	A	-5.33E-02	5.25E-03	7.80E-32	[ADAMTS8]	TRUE	TRUE
12	3364640	rs147867843	A	ACTTTCT	-6.95E-02	1.28E-02	3.70E-09	[TSPAN9]	FALSE	FALSE
12	26392080	rs16930371	A	G	3.74E-02	6.63E-03	2.20E-11	[SSPN]	FALSE	TRUE
12	31065843	rs200103122	A	AAAAT	3.73E-02	7.09E-03	1.80E-08	CAPRIN2--[TSPAN11	FALSE	FALSE
12	43548638	rs1399377	G	A	1.84E-02	5.13E-03	2.34E-08	PRICKLE1--[ADAMTS20	FALSE	FALSE
12	48153944	rs12426774	T	C	4.69E-02	7.02E-03	3.81E-16	[RAPGEF3,SLC48A1]	FALSE	TRUE
12	76114872	rs6582298	G	A	4.27E-02	5.44E-03	4.21E-14	[AC078923.1]	TRUE	FALSE
12	84049853	rs10506895	G	A	1.18E-01	5.16E-03	4.41E-133	TMTC2--[TRUE	TRUE
12	91816926	rs147377344	C	CTTTTAC	3.04E-02	5.30E-03	2.10E-08	DCN--[LINC01619	FALSE	FALSE
12	107250252	rs17038814	A	G	5.54E-02	7.59E-03	5.13E-18	[RIC8B]	TRUE	TRUE
12	108134273	rs4964616	T	A	-4.00E-02	5.32E-03	2.26E-13	[PRDM4]	FALSE	FALSE
12	108988757	rs17040818	G	T	-2.97E-02	6.52E-03	3.21E-08	[TMEM119]	FALSE	FALSE
12	109874230	rs2075432	A	G	2.45E-02	5.15E-03	1.82E-09	[MYO1H]	FALSE	FALSE
12	111800258	rs3809272	G	A	-2.82E-02	5.59E-03	9.62E-09	[PHETA1]	FALSE	FALSE
12	124666527	rs7134138	A	G	-3.64E-02	5.16E-03	3.64E-18	[RFLNA]	TRUE	TRUE
13	25766614	rs9507473	G	C	-4.22E-02	7.88E-03	6.88E-09	AMER2--[LINC01076	FALSE	FALSE
13	36683268	rs9546383	T	C	-4.49E-02	5.99E-03	1.50E-19	[DCLK1]	TRUE	TRUE
13	51913708	rs9535646	C	T	4.00E-02	6.98E-03	4.01E-11	[SERPINE3]	FALSE	FALSE
13	109264870	rs139237435	A	ACATTTA	5.18E-02	5.88E-03	1.20E-21	[MYO16]	TRUE	TRUE
13	110778747	13:110778747_CCTTTT_C	CCTTTT	C	-4.57E-02	5.51E-03	9.90E-18	IRS2--[COL4A1	TRUE	TRUE
14	23452128	rs3811183	C	G	-3.35E-02	5.28E-03	7.26E-13	AJUBA[C14orf93	TRUE	TRUE
14	53989952	rs11623384	C	T	4.10E-02	5.45E-03	4.10E-17	DDHD1--[AL163953.1	TRUE	TRUE
14	59583906	rs61985994	C	G	3.79E-02	7.39E-03	1.88E-08	DACT1--[DAAM1	FALSE	FALSE
14	60806759	rs7493429	A	C	-5.70E-02	5.62E-03	2.59E-35	PPM1A--[C14orf39	TRUE	TRUE
14	65074869	rs8006017	A	G	-5.53E-02	6.90E-03	1.23E-19	PPP1R36--[PLEKHG3	FALSE	TRUE
14	85922578	rs1289426	A	G	-5.21E-02	6.14E-03	2.69E-18	[FLRT2	TRUE	TRUE
14	95957694	rs11160251	T	G	3.13E-02	5.63E-03	2.53E-08	SYNE3--[GLRX5	FALSE	FALSE
15	71840327	rs35194812	T	C	-3.73E-02	7.07E-03	2.81E-11	[THSD4]	FALSE	TRUE
15	74228391	rs4077284	A	G	3.07E-02	5.35E-03	1.41E-11	[LOXL1]	TRUE	TRUE
15	84484384	rs59199978	A	G	-4.63E-02	6.71E-03	3.11E-11	[ADAMTSL3]	FALSE	FALSE
15	99458902	rs28612945	C	T	4.67E-02	6.38E-03	1.54E-15	[IGF1R]	FALSE	TRUE
15	101201604	rs4299136	G	C	-7.17E-02	7.55E-03	7.59E-29	ASB7--[ALDH1A3	TRUE	TRUE
15	101753394	rs28623369	T	G	3.27E-02	5.99E-03	5.90E-10	[CHSY1]	FALSE	FALSE
15	51469726	rs8053277	T	C	8.35E-02	5.61E-03	6.28E-65	SALL1--[HNRNPA1P48	TRUE	TRUE
16	74279778	rs4889487	G	C	3.22E-02	5.72E-03	1.05E-11	ZFX3--[PSMD7	FALSE	FALSE
16	86386675	rs1728368	C	T	9.05E-02	8.98E-03	4.66E-28	IRF8--[FOXF1	TRUE	TRUE
17	10026855	rs12936070	C	T	2.69E-02	5.93E-03	9.97E-10	[GAS7]	FALSE	FALSE
17	40867365	rs115818584	C	G	1.22E-01	2.06E-02	4.01E-11	[EZH1]	FALSE	FALSE
17	45703433	rs7220935	C	T	2.81E-02	5.15E-03	1.84E-11	NPEPPS--[KPNB1	FALSE	FALSE
17	48225686	rs4794104	C	G	-4.13E-02	7.00E-03	6.55E-13	[PPP1R9B]	TRUE	TRUE
17	55419687	rs792401	G	A	2.71E-02	5.60E-03	2.91E-08	[MSI2]	FALSE	FALSE
17	61865670	17:61865670_CT_C	CT	C	-3.20E-02	5.48E-03	2.40E-10	[DDX42]	FALSE	FALSE
17	65264966	rs12939113	C	T	-3.25E-02	5.70E-03	6.93E-11	HELZ--[PSMD12	FALSE	TRUE
17	79602063	rs9905786	G	T	-2.52E-02	5.36E-03	2.56E-09	[NPLOC4]	FALSE	FALSE
17	80169426	rs796355894	A	AT	2.99E-02	5.34E-03	1.60E-08	[CCDC57]	FALSE	FALSE
18	8799828	rs568267	C	T	3.34E-02	5.92E-03	3.69E-10	[MTCL1]	FALSE	FALSE
18	23063159	rs766791666	T	TATC	-3.03E-02	5.31E-03	4.00E-10	ZNF521--[SS18	FALSE	FALSE
18	34289285	rs61735998	G	T	1.03E-01	1.64E-02	7.55E-12	[FHOD3]	FALSE	FALSE
18	56943484	rs77759734	C	T	-6.58E-02	1.20E-02	2.92E-08	[CPLX4]	FALSE	FALSE
19	817708	rs7250902	A	G	3.93E-02	5.61E-03	3.65E-15	[PLPPR3]	TRUE	TRUE
19	14639064	rs112614575	C	CT	3.96E-02	7.30E-03	6.10E-09	[DNAJB1,TECR]	FALSE	FALSE
19	32027330	rs8102936	G	A	5.12E-02	5.47E-03	1.85E-21	TSHZ3--[ZNF507	TRUE	TRUE
19	33477716	19:33477716_AAT_A	AAT	A	-4.52E-02	8.08E-03	1.40E-09	[RHPN2]	FALSE	FALSE
19	39195302	rs757940594	A	AGGAG	-3.15E-02	5.16E-03	7.40E-10	[ACTN4]	FALSE	FALSE
19	46356548	rs7258364	T	C	-2.64E-02	5.51E-03	2.14E-08	[SYMPK]	FALSE	FALSE
19	47455315	rs311384	A	G	2.51E-02	5.66E-03	2.42E-08	[ARHGAP35]	FALSE	FALSE

Supplementary Information - Table 7. ML-based meta VCDR (loci)

CHR	POS	SNP	EA	NEA	BETA	SE	P	GENE_CONTEXT	CRAIG	CRAIG_META
20	1029686	rs4816177	A	G	-4.10E-02	6.79E-03	1.83E-08	RSPO4--[]--PSMF1	FALSE	FALSE
20	6470094	rs2326788	G	A	8.85E-02	5.33E-03	1.10E-67	FERMT1---[]---LINC01713	TRUE	TRUE
20	31438954	rs4911268	A	G	5.00E-02	6.67E-03	5.16E-17	MAPRE1[]-EFCAB8	TRUE	TRUE
20	45796660	rs2903940	A	G	-3.24E-02	5.16E-03	3.31E-13	[EYA2]	FALSE	FALSE
21	29506261	rs6516818	T	A	2.43E-02	5.22E-03	4.48E-08	LINC01673---[]---N6AMT1	FALSE	FALSE
22	29115066	rs4822983	C	T	1.12E-01	5.49E-03	1.37E-110	[CHEK2]	TRUE	TRUE
22	37907069	rs2092172	G	A	-7.49E-02	6.21E-03	5.81E-40	[CARD10]	TRUE	TRUE
22	39322264	rs9306330	C	T	-3.43E-02	6.67E-03	2.19E-09	AL022318.1-[]--APOBEC3A	FALSE	FALSE
22	46376985	rs77164166	G	A	4.73E-02	5.55E-03	3.90E-17	WNT7B-[]--LINC00899	FALSE	FALSE

Supplementary Information - Table 8. GREAT results

Ontology	Term ID	Description	ML-based P-val	Craig <i>et al.</i> P-val
GOBP	GO:0048598	embryonic morphogenesis	1.1x10 ⁻⁵	0.093
GOBP	GO:0007423	sensory organ development	6.4x10 ⁻⁴	0.011
GOBP	GO:0060021	palate development	7.2x10 ⁻⁴	1
MP1KO	MP:0001297	microphthalmia	0.0025	1
MP1KO	MP:0001286	abnormal eye development	0.0036	1
MP1KO	MP:0002697	abnormal eye size	0.0047	1
GOBP	GO:0001655	urogenital system development	0.006	1
MP1KO	MP:0002081	perinatal lethality	0.0062	1
GOBP	GO:0048566	embryonic digestive tract development	0.011	0.22
MP1KO	MP:0004508	abnormal pectoral girdle bone morphology	0.012	1
MP1KO	MP:0003257	abnormal abdominal wall morphology	0.012	0.062
MP1KO	MP:0011087	neonatal lethality, complete penetrance	0.012	1
GOBP	GO:0043010	camera-type eye development	0.015	0.048
MP1KO	MP:0000455	abnormal maxilla morphology	0.016	1
MP1KO	MP:0002058	neonatal lethality	0.028	1
GOBP	GO:0048562	embryonic organ morphogenesis	0.03	1
GOBP	GO:0060537	muscle tissue development	0.032	1
GOBP	GO:0001654	eye development	0.033	0.18
MP1KO	MP:0002925	abnormal cardiovascular development	0.037	1
HP	HP:0008056	Aplasia/Hypoplasia affecting the eye	0.041	1
GOBP	GO:0014706	striated muscle tissue development	0.042	1
MP1KO	MP:0003942	abnormal urinary system development	0.049	0.54
GOBP	GO:0055123	digestive system development	1	0.041

Supplementary Information - Table 9. ML-based glaucoma | VCDR (hits)

CHR	POS	SNP	EA	NEA	EAF	BETA	SE	P	NUM_INDV	SRC	INFO	GENE_CONTEXT
2	19486169	rs1658243	A	G	0.455	-3.57E-03	6.63E-04	4.60E-08	65741	Genotyped	1	NT5C1B---[]--OSR1
6	151296166	rs6906912	A	G	0.71	4.02E-03	7.31E-04	2.90E-08	65896	Imputed	0.996	[MTHFD1L]
7	99939050	rs118119933	C	T	0.827	5.94E-03	8.91E-04	2.00E-11	65896	Imputed	0.963	SPDYE3--[]--PILRB
7	100457578	rs80308281	T	C	0.994	-2.71E-02	4.38E-03	7.50E-10	65774	Genotyped	1	[SLC12A9]
11	89017961	rs1126809	G	A	0.699	-5.32E-03	7.38E-04	5.80E-13	63346	Genotyped	1	[TYR]
13	36663302	rs9315385	T	G	0.805	4.79E-03	8.39E-04	8.00E-09	65192	Genotyped	1	[DCLK1]
15	28337939	rs4778239	C	T	0.01	-2.24E-02	3.35E-03	1.80E-11	65896	Imputed	0.942	[OCA2]
15	28350407	rs111155258	G	A	0.982	1.61E-02	2.53E-03	1.70E-10	65896	Imputed	0.97	OCA2-[]-HERC2
15	28365618	rs12913832	A	G	0.216	-1.38E-02	8.07E-04	2.20E-66	65666	Genotyped	1	[HERC2]
15	28534777	rs117325217	C	T	0.973	1.40E-02	2.19E-03	2.50E-10	65896	Imputed	0.867	[HERC2]
15	28566742	rs2525964	G	A	0.045	-1.44E-02	1.75E-03	1.40E-16	65896	Imputed	0.863	[HERC2]
17	79530993	rs8070929	G	T	0.638	-3.81E-03	6.90E-04	1.50E-08	65896	Imputed	0.987	[NPLOC4]
22	29094084	rs5762750	T	A	0.372	3.93E-03	6.98E-04	9.70E-09	65896	Imputed	0.963	[CHEK2]

Supplementary Information - Table 10. ML-based glaucoma | VCDR (loci)

CHR	POS	SNP	EA	NEA	EA F	BETA	SE	P	NUM_INDV	SRC	INFO	GENE_CONTEXT
2	19486169	rs1658243	A	G	0.455	-3.57E-03	6.63E-04	4.60E-08	65741	Genotyped	1	NT5C1B---[]--OSR1
6	151296166	rs6906912	A	G	0.71	4.02E-03	7.31E-04	2.90E-08	65896	Imputed	0.996	[MTHFD1L]
7	99939050	rs118119933	C	T	0.827	5.94E-03	8.91E-04	2.00E-11	65896	Imputed	0.963	SPDYE3--[]--PILRB
11	89017961	rs1126809	G	A	0.699	-5.32E-03	7.38E-04	5.80E-13	63346	Genotyped	1	[TYR]
13	36663302	rs9315385	T	G	0.805	4.79E-03	8.39E-04	8.00E-09	65192	Genotyped	1	[DCLK1]
15	28365618	rs12913832	A	G	0.216	-1.38E-02	8.07E-04	2.20E-66	65666	Genotyped	1	[HERC2]
17	79530993	rs8070929	G	T	0.638	-3.81E-03	6.90E-04	1.50E-08	65896	Imputed	0.987	[NPLOC4]
22	29094084	rs5762750	T	A	0.372	3.93E-03	6.98E-04	9.70E-09	65896	Imputed	0.963	[CHEK2]